Fakultät für Physik

Lehrstuhl für molekulare und zelluläre Biophysik

Spatial Coordination of Atg8-Lipidation in Selective and Non-selective Autophagy

Benjamin Hofmann

Vollständiger Abdruck der von der Fakultät für Physik der
Technischen Universität München zur Erlangung des akademischen Grades eines
Doktors der Naturwissenschaften (Dr. rer. nat.)
genehmigten Dissertation.

Vorsitzender: Univ.-Prof. Dr. Martin Zacharias

Prüfer der Dissertation:

1. Priv.-Doz. Dr. Günther Woehlke
2. Univ.-Prof. Dr. Friedrich C. Simmel

Die Dissertation wurde am 12.11.2015 bei der Technischen Universität München
eingereicht und durch die Fakultät für Physik am 13.01.2016 angenommen.

Contents

List of Figures

List of Tables

Abbreviations

AFM	**A**tomic **F**orce **M**icroscopy
AIM	**A**tg8-**I**nteraction **M**otif
ALP	**AL**kaline**P**hosphatase
Atg	**Aut**ophag**y** related
ATP	**A**denosine**T**ri**P**osphate
AV	**A**utophagic**V**esicle
CLASP	**CL**athrin-**A**ssociated **S**orting **P**rotein
CP	**C**ore **P**article
CMA	**C**haperone-**M**ediated**A**utophagy
CoIP	**Co**-**I**mmuno**P**recipitation
COP	**CO**at **P**rotein
Cvt	**C**ytoplasm-to-**v**acuole-**t**argeting
DLS	**D**ynamic **L**ight **S**cattering
DMSO	**D**i**M**ethyl**S**ulf**O**xide
DTT	**D**i**T**hio**T**hreitol
EDTA	**E**thylene**D**iamine**T**etra**A**cetic acid
ER	**E**arly **E**ndosome
ESCRT	**E**ndosomal **S**orting **C**omplex **R**equired for **T**ransport
ER	**E**ndoplasmic **R**eticulum
ERES	**ER E**xit **S**ites
ERGIC	**ER G**olgi **I**ntermediate **C**ompartment
FRAP	**F**luorescence **R**ecovery **A**fter **P**hotobleaching
FRET	**F**luorescence **R**esonance **E**nergy **T**ransfer
GAP	**G**TPase **A**ctivating **P**rotein
GDF	**G**DI **D**isplacement **F**actor
GDI	**G**TP **D**issociation **I**nhibitor
GDP	**G**uanosine **D**i**P**hosphate
GEF	**G**uanosine **E**xchange **F**actor
GFP	**G**reen **F**luorescent **P**rotein
GTPase	**G**uanosine**T**ri **P**hosphate hydrol**ase**

GUV	**G**iant **U**nilamellar **V**esicle
HOPS	**HO**motypic fusion and vacuole **P**rotein **S**orting
ILV	**I**ntra**L**uminal **V**esicle
IM	**I**solation **M**embrane
IPTG	**I**so**P**ropyl-β-D-**T**hio**G**alactopyranosid
LB	**L**uria **B**ertani
LC-MS	**L**iquid **C**hromatography **M**ass **S**pectrometry
LUV	**L**arge **U**nilamellar **V**esicle
MLV	**M**altose **B**inding **P**rotein
MLV	**M**ulti**L**amellar **V**esicle
MVB	**M**ulti**V**esicular **B**ody
MTC	**M**ultisubunit **T**ethering **C**omplex
MVB	**M**ulti-**V**esicular **B**ody
NSF	**N**-ethylmaleimide-**S**ensitive **F**actor
ORF	**O**pen **R**eading **F**rame
PAGE	**P**oly-**A**crylamide-**G**el **E**lectrophoresis
PAS	**P**agophore **A**ssembly **S**ite
PCR	**P**olymerase **C**hain **R**eaction
PEG	**P**oly**E**thylene**G**lycol
PIP	**P**hosphatidyl**I**nositol-**P**hosphate
PIPES	1,4-**PIP**erazinedi**E**thane**S**ulfonic acid
PM	**P**lasma**M**embrane
PMN	**P**iece**M**eal **N**ucleophagy
POPC	1-**P**almitoyl-2-**O**leoyl-sn-glycerol-3-**P**hosphatidyl**C**holin
POPE	1-**P**almitoyl-2-**O**leoyl-sn-glycerol-3-**P**hosphatidyl**E**thanolamine
POPS	1-**P**almitoyl-2-**O**leoyl-sn-glycerol-3-**P**hosphatidyl**S**erine
PROPPIN	β-**PROP**eller binding **P**hospho**IN**ositides
PVDF	**P**oly**V**inyli**D**ene**F**luoride
RE	**R**ecycling **E**ndosome
RP	**R**egulatory **P**article
RU	**R**esonance **U**nit
SD	**S**tandard **D**eviation
SE	**S**orting **E**ndosome

SEC	**S**ize **E**xclusion **C**hromatography
SDS	**S**odium **D**odecyl **S**ulfate
SLB	**S**upported **L**ipid **B**ilayer
SLIC	**S**eamless **L**igation **I**ndependent **C**loning
SNARE	**S**oluble **N**SF **A**ttachment protein **RE**ceptor
SPR	**S**urface **P**lasmon **R**esonance
SUV	**S**mall **U**nilamellar **V**esicles
TBS-T	**T**ris **B**uffered **S**aline with **T**ween
TCA	**T**ri**C**hloroacetic **A**cid
TGN	**T**rans **G**olgi **N**etwork
TIRF	**T**otal **I**nternal **R**eflection **F**luorescence
TORC	**T**arget **O**f **R**apamycin **C**omplex
TRAPP	**TRA**nsport **P**rotein **P**article
Ub	**Ub**iquitin
UPS	**U**biquitin-**P**roteasome-**S**ystem
WIPI	**W**D40-repeat protein **I**nteracting with **P**hospho**I**nositides
YPD	**Y**est extract **P**eptone **D**extrose

To my parents

Summary

Autophagy is a highly conserved metabolic pathway delivering cytoplasmic cargo to the vacuole for degradation by a double membrane, termed phagophore. Selective autophagy recycles unwanted or damaged components to maintain cellular homeostasis. In contrast, non-selective autophagy is induced by cytotoxic stress and starvation and sequesters bulk cytoplasm to replenish the cell with building blocks such as amino acids. Atg8, a ubiquitin-like protein, is covalently attached to the phagophore and plays key roles in selective and non-selective autophagy. First, Atg8 functions as cargo adaptor and tightly tethers specific cargo to the phagophore. Second, Atg8 determines the size of autophagosomes, presumably by forming a protein scaffold at the convex face of the membrane. How these different functions are coordinated remains elusive, but Atg18 and Atg21, belonging to the PROPPIN (β-propeller that binds phosphoinositides) family, are likely to be involved. In mammalian cells, an Atg18 homolog has been proposed to promote Atg8-lipidation and in yeast a similar function for Atg21 has been suggested under vegetative conditions. The exact molecular function of yeast PROPPINs during starvation is, however, not well understood.

This thesis aimed at the characterization of both PROPPINs, Atg18 and Atg21. *In vitro* reconstitution of Atg8-conjugation on model membranes demonstrates that Atg18 and Atg21 facilitate Atg8-lipidation by recruiting the E3-like ligase Atg12–Atg5-Atg16 to membranes. To analyse the influence of PROPPINs on scaffold formation AFM- and smTIRF-based methods were established. Extensive biochemical and microscopic analyses *in vivo* reveal that Atg18 and Atg21 cooperate in selective and non-selective autophagy. Both PROPPINs are essential for selective degradation of small specific cargo under vegetative conditions, whereas Atg21 becomes dispensable during starvation. Transport of large specific cargo and bulk cytoplasm is, however, strongly impaired upon *ATG21* deletion. Consistently, Atg21 promotes Atg8-lipidation during starvation and, thereby, controls membrane expansion and autophagosome size. These data show for the first time that Atg21 plays an important role in starvation induced autophagy.

Atg18 overexpression rescues inefficient transport of large specific cargo in *atg21*Δ cells by restoring Atg8-lipidation and membrane expansion at specific cargo. It is proposed that Atg18 has the potential to promote Atg8-lipidation essential for cargo tethering. Fine mapping of PROPPINs suggests that different functions of PROPPINs are regulated by their distinct localization at the phagophore membrane. Taken together this work provides strong evidence that both PROPPINs coordinate Atg8-lipidation at the phagophore to ensure efficient cargo transport. In addition, Atg21 seems to be involved in autophagy-independent pathways delivering cytoplasm to the vacuole for degradation.

Zusammenfassung

Autophagozytose - ein hoch konservierter, metabolischer Prozess - liefert zytoplasmatisches Material, mittels der sogenannten Phagophor-Membran, zum Verdau in die Vakuole. Selektive Autophagozytose erhält die zelluläre Homöostase durch Wiederverwertung ungenutzter Komponenten. Unselektive Autophagozytose dagegen wird durch zytotoxischen Stress oder Nährstoffmangel induziert und führt zu willkürlichem Verdau von Zytoplasma um die Zelle mit Bausteinen wie Aminosäuren zu versorgen. Ubiquitin-ähnliches Atg8 wird kovalent an die Phagophor-Membran gebunden und ist wichtig für selektive und unselektive Autophagozytose. Erstens agiert Atg8 als Adapter, der Ladung spezifisch an die Membran koppelt. Zweitens bestimmt Atg8 die Größe von Autophagosomen, vermutlich durch die Bildung eines Protein-Gerüsts an der äußeren Membran. Atg18 und Atg21, die zur Familie der PROPPINs (β-Proppeller, der Phosphoinositide bindet) gehören, sind wahrscheinlich an der Koordination der verschiedenen Atg8-Funktionen beteiligt. In Säugerzellen verbessert ein Atg18 Homolog die Atg8-Lipidierung. Eine ähnliche Funktion wurde für Atg21 unter vegetativen Bedingungen in Hefen gezeigt. Die molekulare Funktion der Hefe PROPPINs unter Nährstoffmangel ist jedoch unklar.
In dieser Arbeit wurden beide PROPPINs charakterisiert. *In vitro* Rekonstitution der Atg8-Konjugation an Model-Membranen zeigt, dass Atg18 und Atg21 die Atg8-Lipidierung, durch Membranrekrutierung der E3-Ligase Atg12–Atg5-Atg16, vorantreiben. Um den Einfluss von PROPPINs auf die Ausbildung des Protein-Gerüsts zu bestimmen, wurden AFM- und Einzelmolekül-TIRF-Methoden etabliert. Biochemische und mikroskopische *in vivo*-Analysen zeigen, dass PROPPINs in selektiver und unselektiver Autophagozytose kooperieren. Unter vegetativen Bedingungen sind beide PROPPINs für den selektiven Abbau kleiner, spezifischer Ladung essentiell, während Atg21 unter Nährstoffmangel entbehrlich ist. Der Transport von großer, spezifischer Ladung und Zytoplasma ist durch *ATG21* Deletion aber stark vermindert, da Atg21 mittels Atg8-Lipidierung die Membranexpansion und die Größe der Autophagosomen kontrolliert. Diese Daten belegen, dass Atg21 eine entscheidende Rolle in Hunger-induzierter Autophagozytose spielt. Durch Atg18 Überexpression wird die Atg8-Lipidierung und die Membranexpansion an großer, spezifischer Ladung und somit deren effizienter Abbau in *atg21*Δ Zellen erreicht. Dies weist darauf hin, dass Atg18 die Lipidierung von Atg8, das als Ladungs-Adapter agiert, katalysieren kann. Die unterschiedlichen Funktionen der beiden PROPPINs ist wahrscheinlich durch deren verschiedene Lokalisation an der Phagophor-Membran reguliert. Diese Arbeit zeigt, dass beide PROPPINs die Atg8-Lipidierung koordinieren und so effizienten Transport von Ladung sicherstellen. Zudem scheint Atg21 an Autophagozytose-unabhängigem Transport von Zytoplasma zur Vakuole mitzuwirken.

Introduction

1.1 Vesicular Trafficking in Eukaryotic Cells

Eukaryotic cells consist of multiple membrane enclosed organelles with specialized functions, including nucleus, endoplasmic reticulum (ER) and Golgi. A distinct and highly specific protein and membrane composition of organells needs to be maintained. Additionally, newly synthesized proteins need to be transported efficiently to their destined organelles. Furthermore, intercellular communication and adjustments in response to external cues are of vital importance. In order to achieve these goals the cell employs a complex and highly regulated network of vesicular trafficking (Figure 1.1).
The lifecycle of transport vesicles comprises five steps: Cargo sorting and budding from donor membranes; scission to generate transport vesicles; transport to their destination; recognition of vesicle and target membrane; fusion (reviewed in [1, 2]).

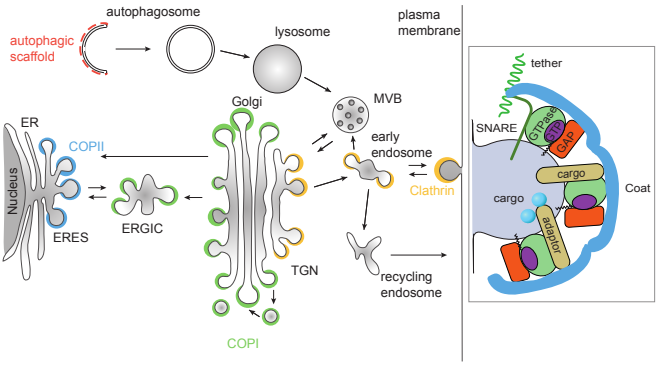

Figure 1.1: Vesicular Trafficking and Cargo Sorting. Three canonical protein coats are involved in distinct trafficking processes. COPII (blue) vesicles mediate anterograde transport in the early secretory pathway. COPI (green) is critical for retrograde transport in the Golgi and from Golgi to ER. Clathrin (yellow) mediates endocytosis and trafficking from the *trans*-Golgi-network (TGN). Protein coats play funcamental roles in cargo sorting and vesicle formation. Additionally, they interact with tethering factors and SNARE proteins to mediate recognition of the correct target membrane (right panel). In addition to canonical membrane trafficking coats, a protein scaffold has been proposed to be involved in autophagy. Similar to transport vesicles, autophagy employs cargo binding to a membrane for efficient degradation. COP = Coat protein complex, ER = endoplasmic reticulum, ERES = ER exit sites, ERGIC = ER-Golgi intermediate compartment, MVB = multi-vesicular body TGN = *trans*-Golgi network. Adapted from [1]

In addition to vesicular trafficking, a highly conserved metabolic pathway, termed autophagy, has evolved. Autophagosomes are double membrane vesicles that transport cytoplasmic material to the lysosome (vacuole in yeast) for degradation and recycling

of building blocks. The formation of the autophagosomal membrane largely depends on specific autophagy-related (Atg) proteins. In addition, some proteins are shared with vesicular trafficking pathways, including soluble N-ethylmaleimide-sensitive factor (NSF) attachment protein receptors (SNAREs), tethering complexes and small GTPases [3, 4]. Therefore, vesicular trafficking and autophagy are interconnected pathways. Consequently, perturbation of trafficking events might have an influence on autophagy and vice versa.

1.1.1 Protein Coats in Vesicular Trafficking

Three types of protein coated vesicles have been identified. Clathrin coated vesicles mediate transport in endocytosis and late secretory pathway, coat protein complex I (COPI) coated vesicles function in retrograde and anterograde transport in the early secretory pathway and COPII vesicles transport proteins from ER to Golgi [1, 5–8]. All canonical coats share two main functions, they concentrate cargo and form a protein scaffold that induces membrane budding and vesicle formation (Figure 1.1 right panel, reviewed in [1, 5–7]).

As apparent from their common functions, coat complexes share substantial structural and functional characteristics, but also possess important differences. Components of clathrin and COPII coats can be subdivided into two subunits, a cargo adaptor and a protein cage (reviewed in [7]). Interactions between the two subcomplexes ensure membrane budding at sites with concentrated cargo [9–11]. In contrast, the heptameric COPI complex is recruited *en bloc* [12]. The recruitment of COPI and COPII depends on a membrane-bound active form of the specific small GTPases Sar1 and Arf1, respectively. In contrast, assembly of clathrin coats is not necessarily initiated by a small GTPase (reviewed in [7]).

Since basic principles of cargo sorting and coat formation are similar for all three coats [1, 7, 13] they are explained for clathrin coated vesicles. Cargo sorting is a central function of coated vesicles. Therefore, cargo concentration needs to be tightly coordinated with vesicle formation. In clathrin-mediated endocytosis a plethora of clathrin-associated sorting proteins (CLASPs) have been identified which mostly comprise binding sites for clathrin, cargo, lipids and accessory proteins (reviewed in [14]). The best characterized example is the heterotetrameric adaptor protein 2 (AP2). This protein complex is recruited to the PM by interaction with phosphatidylinositol-4,5-bisphosphate ($PI(4,5)P_2$) [15] leading to an exposition of its cargo binding site [16]. AP2 specifically recognizes a linear peptide motif found in cytoplasmic domains of cargo proteins [17]. In addition, AP2 binds to a β-propeller in the heavy chain of clathrin [18, 19]. Thereby, AP2 coordinates clathrin recruitment and cargo concentration. Clathrin, consisting of a light and a heavy chain which form triskelia, assembles into a protein coated vesicle. As suggested

by cryo-electron microscopy (EM) studies of *in vitro* reconstituted clathrin cages, the legs of triskelia intertwin to form a hexagonal cage [20]. Membrane buds coated with calthrin are subsequently pinched off the donor membrane.
In autophagy, cargo is transported to the vacuole by vesicles formed *de novo*. Apart from canonical membrane trafficking coats, a protein scaffold has recently been proposed to build on autophagosomes [21] presumably facilitating expansion of autophagosomal membranes. A key component of this scaffold, Atg8, has an additional function as cargo adaptor for selective cargo transport [22]. Therefore, cargo selection and vesicle formation in autophagy is interconnected, similar to canonical membrane trafficking mechanisms.

1.1.2 Membrane Scission

In order to complete vesicle formation efficient membrane scission is needed to pinch off vesicles from the donor compartment. For fission to occur the bud neck of the forming vesicle needs to be constricted to bring the membranes in close proximity. First, the inner layer of phospholipids fuses (hemifusion), followed by fusion of the outer layer which relaxes the high energy state (reviewed in [23]). Since membrane scission is impaired by its high energy state intermediates, several mechanisms are used to lower the transition energy or to provide the energy needed. Proteins like dynamin, acting in endocytosis, constrict membrane necks by changing their conformation after membrane binding. Other proteins such as Arf1 and Sar1 act in COPI- and COPII-mediated vesicle trafficking and insert an amphipathic helix into the membrane and thereby induce curvature, needed for membrane neck formation. Despite external force generation, the lipid composition can be changed with the help of protein kinase D, lysophosphatidic acid acyltransferase or phospholipase D. These lipid alterations take place at the *trans*-Golgi-Network and in COPI vesicle formation and lead to budding and scission by phase-separation (reviewed in [23, 24]).
Dynamin is a large multidomain GTPase that has been shown to function in scission of clathrin-coated endosomal vesicles (reviewed in [25]). It is recruited to the plasmamembrane (PM) by interaction of its pleckstrin-homology (PH) domain with $PI(4,5)P_2$ [26] and by interaction of its prolin rich domain (PRD) with amphiphysin and SNX9 [27, 28]. Dynamin oligomerizes at the membrane to form a right-handed helix [29, 30]. Different models for the scission mechanism have been proposed. All of them depend on conformational change upon GTP hydrolysis (reviewed in [25]), followed by membrane scission through constriction [30], spring-like opening of the right-handed helix [31], twisting the membrane neck [32] or by cycles of binding and dissociation [33].
As opposed to dynamin, Arf1 and Sar1 are small GTPases involved in COPI- and

COPII-mediated vesicle trafficking, respectively [7]. Besides their function in recruiting coat components, both GTPases undergo conformational change upon GDP to GTP exchange and insert an amphipatic helix into the membrane (reviewed in [23]). This insertion induces membrane bending, needed for the membrane bud to form. Using synthetic membranes it has been suggested that Sar1 completes COPII-vesicle fission dependent on insertion of its amphipathic helix resulting in high membrane curvature [34]. The exact mechanism of Sar1- or Arf1-mediated membrane scission remains, however, elusive and it is controversial whether GTP-hydrolysis is required for Sar1- and Arf1-mediated membrane scission [23, 35].
After scission vesicles are transported to the target membrane via microtubules or actin using motor proteins that are recruited by small GTPases [2]. Tethering factors recognize the target membrane and facilitate SNARE-mediated vesicle fusion.

1.1.3 Membrane Tethering

First contact between transport vesicles and target organelle is mediated by membrane tethering complexes. They provide specificity to fusion with the correct target membrane (reviewed in [36]). Most tethering factors are Rab-effectors and can be subdivided in two classes, large homodimeric coiled-coils or multisubunit tehtering complexes (MTCs, reviewed in [2, 36]). Despite structural differences, tethering factors accelerate SNARE-mediated membrane fusion by promoting SNARE-pairing and directly interact with coat components for efficient vesicle target-membrane recognition (reviewed in [36]).
Today, nine conserved MTCs have been identified: TRAPP-I,-II,-III, Dsl1, COG, exocyst, HOPS, CORVET and GRAP/VFT. The transport protein particle-I (TRAPP-I) complex acts in ER-Golgi trafficking while TRAPP-II mediates intra-Golgi and endosome-*trans*-Golgi transport (reviewed in [2]). The most recently identified TRAPP-III is involved in autophagy [4]. While most tethers are Rab effectors, TRAPP-complexes are guanine nucleotide exchange factors (GEFs) for Ypt1 (TRAPP-I,-III) [4, 37] and Ypt31/Ypt32 (TRAPP-II) [38]. According to their specificity, TRAPP-I has been demonstrated to bind to COPII components [39], while TRAPP-II interacts with COPI directly (reviewed in [1]). Tethering of COPII vesicles additionally involves Uso1, a coiled-coil tether, recruited by Ypt1. It has been suggested, that COPII vesicle tethering is a sequential process with the first contact being mediated by TRAPP-I. This activates Ypt1 and thereby enables tethering via Uso1 (reviewed in [1]). Besides initial contact formation TRAPP complexes were suggested to directly regulate membrane fusion. This is achieved by their common subunit SEDL structurally resembling N-terminal regulatory domains of SNARE proteins [40].
The TRAPP-III complex has been shown to be specific for autophagy and is targeted to the site of autophagosome formation (phagophore assembly site = PAS) by its unique

subunit Trs85 [4]. Trs85 has been proposed to interact with the autophagy specific proteins Atg17 or Atg9, which is an integral membrane protein essential for autophagosome formation [41, 42]. Structural characterization of TRAPP-III by electron microscopy revealed that COPII vesicles contribute to autophagosome fromation [43].
Another tethering factor involved in autophagy is the (homotypic fusion and vacuole protein sorting) HOPS complex, which has initially been shown to play a role in endosome-vacuole tethering (reviewed in [2]). In a recent study, it has been revealed that contact between autophagosomal membranes and the HOPS complex is established via a human Atg8 homolog (LC3) that is covalently attached to the autophagosomal membrane [44, 45]. In addition, HOPS was demonstrated to interact with syntaxin17, being involved in autophagosome lysosome fusion. The interaction is likely to be mediated by a HOPS subunit which acts like a Sec18/Munc1 (SM) protein stabilizing cognate SNARE complexes [46, 47]. Taken together it emerges that multiple interactions of tethering factors with different components of vesicular trafficking determine the specificity of membrane trafficking and fusion.
Despite their positive influence on membrane fusion, tethering factors do not facilitate fusion themselves. This final step is mediated by SNARE proteins (reviewed in [48]).

1.1.4 SNARE-mediated membrane fusion

SNARE proteins facilitate membrane fusion and were initially reported to be sufficient for specific targeting of vesicles [49]. Subsequent studies, however, demonstrated a certain ambiguity in SNARE mediated fusion (reviewed in [2]). Consequently, cargo delivery depends on the intricate interplay of SNAREs, tethering complexes and other components of the membrane trafficking machinery.
SNARE proteins mostly consist of two domains. The C-terminal transmembrane domain anchors SNAREs to the membrane. A domain of 60 - 70 amino acids that contains heptad repeats, the SNARE motif, is immediately N-terminal to the transmembrane domain. These motifs can form coiled coils and are used to classify SNAREs into Q_a-, Q_b-, Q_c- and R-SNAREs, according to the amino acid at the central position within the motif [50]. A functional classification divides SNAREs into vesicle (v)-SNAREs and target membrane (t)-SNAREs [49]. N-terminal of the SNARE motif some SNAREs contain regulatory domains (reviewed in [48]).
In most cases a functional SNARE complex contains one SNARE of each class, Q_a, Q_b, Q_c and R (reviewed in [48]). The t-SNAREs pre-assemble to form a template for v-SNARE binding. Subsequently, cognate v- and t-SNAREs assemble into a four-helix bundle in a zipper-like mechanism from the membrane distal to its proximal end. This *trans*-SNARE complex formation drives fusion of two membranes (reviewed in [48]). After membrane fusion the resulting *cis*-SNARE complex is disassembled by the ATPase

NSF [51].

Opposed to the initial hypothesis that SNAREs are sufficient for specific vesicle targeting, SNARE proteins can function in different pathways. SNARE proteins have been shown to be involved in autophagy, but specific SNARE components that drive autophagic fusion events have not been defined, yet. Among these SNAREs are Sso1 and Sec9, which are involved in exocytosis, as well as Sec22 and Ykt6 being endosomal SNAREs [3].

Another layer of specificity and regulation of SNARE assembly is added by SM proteins. Different SM proteins act in distinct pathways (reviewed in [48]). A particularly well studied example is Munc18-1 which has been shown to play a dual role in SNARE complex formation. On the one hand, it inhibits t-SNARE complex formation by interaction with a Q_a-SNARE [52]. On the other hand, Munc18-1 binds the cognate v-SNARE which relieves t-SNARE inhibition and finally stimulates membrane fusion [53].

Taken together SNARE proteins assemble into a four-helix bundle to overcome the energy barrier for membrane fusion and provide limited specificity in membrane trafficking. This specificity is complemented by tethering factors and small GTPases of the Rab family.

1.1.5 Small GTPases and How They Regulate Trafficking

Rab-GTPases, small GTPases of the Ras superfamily, are key regulators of cellular functions including different steps in vesicular trafficking (reviewed in [54]). GTPases are activated and deactivated in a cyclic fashion. In their GDP-bound form Rab-GTPases are dispersed in the cytoplasm, bound to a GTP dissociation inhibitor (GDI). A specific GDI displacement factor (GDF) enables membrane association of the Rab-GTPase. Specific GEFs than catalyze the exchange of GDP to GTP and, thereby, activate the GTPase by a conformational switch (reviewed in [55]). The active Rab can recruit various effector proteins, before it is deactivated by GTPase activating proteins (GAPs) (reviewed in [54]).

In order to obtain highly coordinated actions of Rab-GTPases, Rab signalling employs cascades of GEFs and GAPs as well as Rab-GEF positive feedback loops. Thereby, Rab GTPases seem to built a network coordinating different steps of vesicular trafficking (reviewed in [56]). Well studied examples involve the exchange of Rab5 against Rab7 on membranes during endosome maturation. Rab5 acts on early endosomes and in its GTP-bound form interacts with the tethering factor HOPS. HOPS recruits a GEF for Rab7 resulting in Rab7 membrane recruitment and activation. Once associated with endosomes, Rab7 recruits a Rab5-specific GAP. This GAP deactivates Rab5, which in turn dissociates from the membrane. Thereby, transition from early to late endosomes seems to be coordinated by a GEF cascade and a negative feedback loop leading to the coordinated exchange of small GTPases (reviewed in [56]).

As previously mentioned, small GTPases coordinate different steps of vesicular trafficking: Sar1 and Arf1, for example, coordinate cargo sorting and coat formation [1], whereas uncoating of clathrin coated vesicles is promoted by Rab5 [57]. Moreover, small GTPases such as Ypt11 regulate vesicle transport by direct linkage of myosin V to COPI vesicles [58]. Furthermore, a role in coordinating vesicle tethering has been proposed by direct binding of Sec4 (GTPase) to exocyst (tethering factor) [59].

1.2 Cellular Degradation and Recycling Pathways

Cells constantly recycle their cytoplasmic contents to maintain viability or to respond and adapt to endogenous and exogenous cues. In consequence, cellular degradation and recycling pathways are inevitable for proper function. Three elaborate pathways have evolved to accomplish this task (Figure 1.2), including the Ubiquitin-proteasome system (UPS), multivesicular body-(MVB-)biogenesis and autophagy. Ubiquitin (Ub) attachment to cytoplasmic or PM proteins serves as a marker for degradation by the UPS and MVB-pathway, respectively (reviewed in [60, 61]). Cytoplasmic components that are not degraded by the UPS are transported to and degraded in the vacuole by autophagy. Therefore, autophagy transports the most complex set of cargo using selective and non-selective subforms (Figure 1.2, reviewed in [62]).

1.2.1 Ubiquitin-Proteasome-System

The UPS degrades soluble proteins in a highly regulated and specific manner. This is achieved by covalent attachment of Ub, via its C-terminal glycine, onto lysine residues of proteins that are to be degraded (reviewed in [60]). To selectively target proteins to proteasomes a cascade of enzymes is employed. Ub is acitvated by an E1 enzyme in an ATP-dependent manner to form a high energy thioester. Subsequently, Ub is transferred to Ub-conjugating enzymes (E2) and finally to their target proteins by E3 enzymes. While there is a single E1 enzyme for Ub activation in yeast, eleven E2 enzymes and 60 - 100 putative E3 enzymes have been identified. The increasing number of enzymes culminates in E3-mediated ubiquitination of specific substrate proteins (reviewed in [60]). Ub is linked to lysine residues of target proteins and comprises seven lysine residues itself. By covalent linkage of Ub to a lysine of another Ub a diverse set of poly-Ub chains can be generated. The most important variant of these poly-Ub-chains for targeting proteins for proteasomal degradation are K48-linked ubiquitin-chains [63].
The proteasome is a multisubunit protease consisting of a 19S regulatory particle (RP) and a 20S core particle (CP). The CP adapts a cylindrical shape with a central pore and possesses proteolytic activity. The RP mediates cargo recognition, ATP-dependent

protein unfolding and translocation into the central pore of the CP (reviewed in [60, 64]). Deubiquitination enzymes recycle ubiquitin by cleaving it off the substrate protein, which serves as the major source of Ub-moieties for the UPS (reviewed in [60]).
As described above, proteasomal degradation is a specific process, suitable to remove misfolded, non-functional or currently undesired proteins that are still soluble and can be unfolded. Proteins within the PM are not targeted to the proteasome but are delivered to the vacuole. This process involves regulated endocytosis of such proteins and uptake into intraluminal vesicles (ILVs) which are delivered to and degraded in the vacuole.

1.2.2 Endosomal System and MVB-Biogenesis

The endosomal system is required for signal transduction as well as for degradation of PM proteins (reviewed in [65]). The importance and complexity of the endosomal system is underlined by the fact that three quarters of the human Rab GTPases are involved in this system (reviewed in [66]). The primary signal for degradation of PM proteins is mono-ubiquitination, which is catalyzed by E3 enzymes. These enzymes are targeted to such proteins by different sensors, including chaperones or arrestin (reviewed in [61]). Alternatively, specific sorting signals in the cytoplasmic tail of plasma-membrane receptors can bear internalization- and sorting-signals (reviewed in [67]). Internalization can be mediated by either clathrin-dependent, caveolin-dependent or clathrin- and caveolin-independent endocytosis (reviewed in [68]). Endocytic vesicles subsequently fuse with early endosomes (EEs). In EEs internalized cargo is sorted based on its ubiquitination (reviewed in [65]). Soluble cargo, which was bound to PM receptors, is released by a change in pH. Then cargo and transmembrane proteins are separated in EEs by formation of two domains, one for vacuolar sorting another tubular domain for recycling. Vesicle budding leads to the formation of recycling endosomes (RE), which transport proteins back to the PM. Cargo containing sorting endosomes (SE) mature to late endosomes and eventually fuse with the vacuole for degradation of their content (reviewed in [65]). As a consequence PM proteins need to be taken up into the lumen of SEs. This process is catalyzed by the ESCRT-machinery and involves cargo clustering by ESCRT-0, budding by ESCRT-I, -II and scission of ILVs by ESCRT-III resulting in MVBs [69]. Fusion of MVBs and lysosomes leads to lysosomal degradation of the cargo (reviewed in [65]), a process that is utilized by autophagy as well.

1.2.3 Autophagy

Autophagy is presumably the most versatile transport process regarding cargo-size and -shape. It delivers cytoplasmic material for vacuolar degradation and thereby facilitates recycling of building blocks for biosynthesis [62]. Autophagy (greek "self-eating") has

first been observed in hepatic cells in 1962 [70]. Three main forms of autophagy have been identified to date, including chaperone-mediated autophagy (CMA), microautophagy and macroautophagy (Figure 1.2).

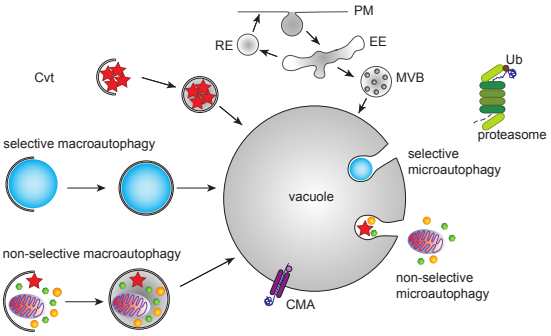

Figure 1.2: Degradation Mechanisms. Three major degradation mechanisms are used by cells. Ubiquitinated cytoplasmic proteins are proteolytically degraded by the proteasome (green). PM homeostasis, receptor recycling and degradation are mediated by the endocytic pathway. In addition, autophagy degrades cytoplasmic material either specifically or unspecifically by three different sub-pathways. CMA = chaperone mediated autophagy; Cvt = cytoplasm-to-vacuole targeting pathway; EE = early endosome; MVB = multivesicular body; PM = plasma membrane; RE = recycling endosome; Ub = ubiquitin; Adapted from [71]

1.2.3.1 Forms of Autophagy

CMA is a selective form of autophagy, translocating proteins into the lysosome (vacuole in yeast). The degradation process involves five steps (reviewed in [72]): First, Hsc70 recognizes the KFERQ-motif of substrate proteins to target them to lysosomal membranes [73, 74]. Second, Hsc70 binds to lysosome-associated membrane protein type 2A (LAMP2-A), thereby delivering its cargo to the lysosomal membrane [75]. This leads to multimerization of LAMP2-A forming a translocation channel [76]. The protein is unfolded in an ATP- and chaperone-dependent manner [77] and translocated into the lysosome with the help of a lysosomal Hsc70 [78]. Finally, the protein is proteolytically degraded. After substrate translocation the LAMP2-A channel is disassembled to enable a new round of substrate binding and translocation [76]. CMA has also important regulatory functions by degradation of key regulatory factors involved for example in cell cycle progression [79].

Not only CMA-substrates can access the vacuolar lumen directly. Other cytoplasmic components can be taken up by invaginations of the vacuolar membrane in a process that has been termed microautophagy. It is induced by starvation and is believed to mediate selective and non-selective cargo transport into the vacuole (reviewed in[80]). The selective microautophagy pathways have been shown to use specific subsets of Atg

proteins and other proteins [81, 82]. The mechanism of microautophagy is not well understood, but it has been proposed that protein-segregation and lipid-phase separation lead to spontaneous invaginations and membrane scission. Another potential mechanism involves vacuolar transporter chaperones (reviewed in[80]).

In macroautophagy (autophagy in the following) a double membrane is formed *de novo* in the cytoplasm at the PAS, engulfs cytoplasmic material and delivers it to the vacuole for degradation. Autophagy can be devided into five steps, including initiation, membrane expansion, autophagosome closure, fusion to the vacuole and degradation of cargo. These steps are catalyzed by a set of about 40 Atg-proteins in yeast. Eighteen of these proteins belong to the core family of Atg proteins being involved in all autophagy subtypes (reviewed in [83]). Two components of this core machinery, including the transmembrane protein Atg9 and the Atg1-kinase complex, are essential to initiate autophagy and are the first components to be recruited to the PAS [84, 85]. The Atg1-kinase complex recruits the class III PI3-kinase (PI3K) complex I [86]. PI3K complex I converts phosphatidylinositol (PI) to PI(3)P, which recruits downstream effectors [87, 88]. Expansion of the phagophore membrane has been shown to depend on Ub-like conjugation systems [89], which might, besides other factors, also play a role in autophagosome closure [3, 90–92]. Fusion of completed autophagosomes depends on the HOPS complex and SNARE proteins [46]. An overview of the major steps in autophagosome formation is given in Figure 1.3.

While non-specific autophagy is believed to randomly engulf cytoplasmic material a number of specific autophagy pathways have been identified for efficient degradation of protein aggregates (aggrephagy), ribosomes (ribophagy), ER (reticulophagy), mitochondria (mitophagy), peroxisomes (pexophagy) and invading microorganisms (xenophagy) (reviewed in [71]). For selective autophagy cargo receptor proteins and Atg8 are used to tightly link cargo to the growing membrane, excluding cytoplasmic material [22, 71], whereas non-selective autophagy is believed to randomly engulf cytoplasmic material (reviewed in [62]).

Autophagy runs at a basal level during vegetative growth and is induced by various stress conditions, such as nutrient starvation (reviewed in [62]). In yeast one specific, constitutive autophagy pathway exists, which has been termed cytoplasm-to-vacuole targeting (Cvt) pathway. This process delivers two hydrolases to the vacuole, aminopeptidase I (ApeI) and α-mannosidase (AmsI) in small vesicles (reviewed in [93]). Autophagy induction leads to the formation of larger autophagosomes, with diameters of 350 - 900 nm [94, 95]. Current evidence suggests that specific cargo is targeted to and thus transported by such large autophagosomes as well [62]. According to its crucial function in cellular homeostasis autophagy is a highly regulated process and has been linked to various diseases such as neurodegenerative diseases, cancer and immunity (reviewed in [96, 97]).

1.2.3.2 Membrane Sources for Autophagosome Biogenesis

The characteristic feature of autophagy is the *de novo* formation of a double membrane, which needs an initiation event and membrane expansion. In yeast, initiation occurs at the PAS, a poorly defined punctate structure in close vicinity to the vacuolar membrane and ER-exit sites [98, 99]. Different models have been proposed for autophagosome initation in yeast and mammals. In yeast, the Atg1-kinase complex is assembled and recruited to the PAS upon autophagy induction [84] and, in turn, recruits Atg9 containing vesicles [100]. Atg9 is the only integral membrane protein of the autophagic core machinery [101], forming cytoplasmic vesicle clusters in vegetative conditions and being relocalized to the PAS upon autophagy induction [100, 102]. A study based on fluorescene microscopy suggested that autophagosome biogenesis is initiated by the fusion of an average of three Atg9-vesicles [85]. This results in the formation of a small membrane sack, termed phagophore, which expands to sequester material from the cytoplasm. Lipids for phagophore expansion are thought to be provided by transport vesicles derived from various sources, including Golgi and Atg9-vesicles, ER-exit sites (ERES) and COPII-vesicles. Most evidence suggests that lipids are shuttled from ERES to the phagophore by COPII vesicles [43, 103]. The contribution of the Golgi to phagophore expansion was speculated to depend on Atg9-vesicle trafficking from Golgi to PAS [104]. For mammalian cells it has been proposed that the isolation membrane (IM, phagophore in yeast) is initiated at the ER at PI(3)P enriched patches [105]. This suggests that ER either serves as a platform for *de novo* formation of the IM, for example by providing donor vesicles, or directly donates a part of the ER membrane. The latter model was supported by an ultrastructural EM study, showing that the IM is inferred directly from the ER membrane, which encircles the expanding IM [106]. After initiation, lipids need to be transported to the IM for its expansion and different membrane sources have been proposed, including Golgi, ER-Golgi intermediate compartment (ERGIC), mitochondria and plasmamembrane [107, 108]. The most likely candidates are Golgi and ERGIC. It has been demonstrated recently, that a Golgi tethering factor is critical for starvation-induced recruitment of Atg9-containing membranes to the PAS. Deletion of this protein blocked autophagic flux [109]. Furthermore, the ERGIC has been reported to be the crucial membrane source to trigger LC3 (Atg8 in yeast)-lipidation, which is a key step in autophagosome formation [108]. These lipids seem to be transported from the ERGIC to the IM by COPII vesicles that form in a PI3K dependent manner upon starvation feed the growing IM [110].

Because of the complex cellular membrane trafficking network a clear cut assignment of membrane sources is difficult, but most likely a combination of membrane sources is used for autophagosome formation.

1.2.3.3 Autophagic Protein Machinery

Consistent with its complexity, autophagy requires a large set of proteins. So far about 40 Atg proteins have been identified eighteen of which belong to the core machinery, crucial for all kinds of autophagic processes [83, 111]. Proteins of the autophagic machinery are recruited to the PAS in a hierarchical manner [112]. The core machinery is grouped in five protein complexes that are described below (Figure 1.3). In addition, important non-core proteins are briefly introduced.

a) Atg1 Kinase Complex

Essential proteins of the autophagic machinery are recruited to the PAS in a hierarchical manner with the Atg1 kinase complex being the most upstream protein complex [112]. The Atg1 kinase complex is a pentamer comprising Atg1, Atg13, Atg17, Atg29 and Atg31. The latter three form a constitutive, inactive complex which dimerizes via Atg17. Full assembly of the Atg1 kinase complex with Atg1 and Atg13 depends on autophagy induction and results in its activation [84, 113]. Atg13 is hyperphosphorylated in vegetative conditions and its dephosphorylation upon starvation induces autophagy by full assembly of the Atg1-kinase complex [114]. It is still debated, whether Atg13 dephosphorylation promotes interaction with Atg1 or with Atg17 [115, 116]. In mammalian cells, two homologs of Atg1 (ULK1, ULK2) and one Atg13 homolog exist, but for Atg17, Atg29 and Atg31 no homologs have been identified. Instead two factors named FIP200 and Atg101 form a constiutive complex with Atg1-Atg13 (reviewed in [107]).
The Atg1 kinase complex has different kinase-dependent and kinase-independent functions. Atg17, a member of the active Atg1 kinase complex, has been reported to be the first protein to arrive at the PAS upon autophagy induction. It is thought to form a scaffold for recruitment of downstream Atg proteins [112]. Atg17 binds Atg9, suggesting that it initiates autophagy by recruitment of Atg9-vesicles to the PAS [100]. A potential function as scaffold for autophagosome biogenesis has been discussed based on the crystal structure of the trimeric Atg17-Atg29-Atg31 complex [117]. In addition to its proposed function in phagophore initiation, recruitment of the class III PI3K complex I is an early function not depending on Atg1 kinase activity. Recruitment is mediated by the Atg13 HORMA domain directly interacting with the PI3K subunit Atg14 [86]. PI3K activity at the PAS is essential to recruit downstream factors for phagophore expansion [112]. On the other hand, Atg1 kinase activity has been shown to be essential for recycling of Atg proteins from the PAS such as Atg8 and Atg17 [118]. Furthermore, Atg1 kinase activity is important for IM expansion [99]. Interestingly, a recent study identified Atg9 to be a direct target of Atg1 kinase activity and Atg9 phosphorylation is critical for Atg18 and Atg8 recruitment, leading to autophagosome formation[119].

b) Atg9

Atg9 is the only transmembrane protein of the core autophagy machinery [101]. The N- and C-terminal unstructured regions of Atg9 interact with Atg23 and Atg27, both of which are involved in regulating trafficking of Atg9 from the Golgi to its peripheral vesicle pool under vegetative conditions [120]. Atg9-vesicles are crucial for autophagosome biogenesis [85] and relocalize to the PAS upon autophagy induction in an Atg17-dependent manner [100, 102]. In selective autophagy, Atg11 has been shown to be the recruiting factor localizing Atg9 to the PAS [121]. Phagophore initiation has been suggested to involve fusion of about three Atg9-vesicles [85] and Atg9 expression levels control the number of autophagosomes. High levels of Atg9 correlate with a higher frequency of autophagosome formation and increased autophagic flux [122]. For Atg9-cycling through autophagosomes Atg1, Atg13 and the Atg18-Atg2 complex have been shown to be essential [123]. Whether this is a direct effect remains unclear since the same set of proteins is important for IM expansion [99] and it has been suggested that Atg9 is recycled from the vacuolar membrane after fusion of autophagosomes [85]. Furthermore, Atg9 is involved in recruitment of TRAPP-III and its Rab GTPase Ypt1 to the PAS by direct interaction with the TRAPP-III-specific subunit Trs85 [41]. Other studies revealed that TRAPP-III directly interacts with COPII components [124]. Consistently, COPII-vesicles, formed at the ERGIC, are important for autophagosome biogenesis [110]. In addtion, the interaction of human Atg9 with a RabGAP involved in endosomal trafficking, clathrin and AP2 has been proposed, connecting the endosomal system to Atg9 trafficking and consequently autophagosome formation [125].

c) PI3 Kinase Complex

The autophagy specific class III PI3K complex I consists of Vps34, Vps15, Vps30/Atg6, Atg14. A second complex which consists of the same subunits but Vps38 instead of Atg14 has been shown to be required for the endosomal vacuolar protein sorting pathway (reviewed in [126]). Additionally, Atg38 is a newly identified subunit stabilizing the PI3K complex I [111]. Recruitment of PI3K to the PAS is mediated by Atg13 probably by interaction with Atg14, since this is the only autophagy specific subunit of the PI3K complex I [127]. PI3K has been shown to be essential for autophagosome formation. It converts PI to PI(3)P which enables binding of PI(3)P effectors [88]. Even though the PI3K complex I localizes to the tips of the phagophore [99], PI3P is enriched in the inner autophagosomal membrane [87].

In mammalian cells the autophagy specific PI3K complex shares substantial homology with its yeast counterpart [128]. It has been shown that this complex is recruited to the ER via Atg14L, being crucial for omegasome formation and recruitment of downstream factors [129]. Additionally, a recent study revealed that the PI3K complex facilitates

COPII-vesicle formation from the ERGIC under starvation conditions being important for autophagosome biogenesis [110].

d) PROPPINs - Atg18 and Atg21

PROPPINs are β-propeller proteins binding phosphoinositides. In *S. cerevisiae*, a genetic study identified three proteins belonging to this family, Atg18, Atg21 and Hsv1 [130]. Atg18, Atg21 and Hsv1 were shown to bind phosphoinositides via a conserved motif of four consecutive amino acids, the FRRG-motif [131–134]. Mutation of this motif to FKKG (or FTTG) resulted in strong reduction of PIP binding [88, 132, 133]. Three independent structural studies used a PROPPIN family member (Hsv2) of thermotolerant yeast strains *Kluyveromyces lactis* or *Kluyveromyces marxianus* to structurally characterize this protein family. They revealed a seven-bladed β-propeller fold. More interestingly, they reported that the FRRG-motif forms two basic binding pockets for PI(3)P and PI(3,5)P_2 in blade 5 and blade 6 of the β-propeller [135–137]. Additionally, a loop region in blade 6 was important for membrane binding [135, 136].
All three PROPPINs have been reported to be involved in distinct autophagy pathways. Atg18 is a member of the autophagic core machinery being involved in all types of autophagosomal degradation [62, 90, 138]. Atg21 was reported to only act in the Cvt pathway but to be dispensable for ApeI degradation under starvation conditions [139]. Hsv1 was reported to only play a role in piecemeal nucleophagy [140].

Atg18

Atg18 has initially been shown to be essential for the Cvt pathway, pexophagy and autophagy [90, 138]. Furthermore, it was observed that *atg18*Δ cells do not sporulate, a characteristic feature of autophagy deficient cells. And finally, no autophagic bodies accumulated in starved cells chemically inhibited in vacuolar degradation when *ATG18* was deleted [138]. Today it is common sense that Atg18 belongs to the autophagic core machinery being essential for different forms of selective and non-selective autophagy [141, 142].
Fluorescence microscopy studies revealed that Atg18 localizes to the vacuolar membrane and punctate structures [90, 139, 143]. Its localization to endosomes and PAS has been shown to depend on PI(3)P binding [88, 133], while vacuolar rim localization depends on PI(3,5)P_2 formation at the vacuole [131]. Upon mutation of the FRRG-motif Atg18 becomes dispersed into the cytoplasm. Consequently, PI(3)P and PI(3,5)P_2 are critical for proper localization of Atg18. In addition to PIPs, PAS localization of Atg18 has been shown to be dependent on the Atg1 kinase complex, Atg9 and Atg2 in a hierarchical study of yeast Atg proteins [112, 123]. Consistently, Atg9 is phosphorylated by Atg1 which is required for PAS-recruitment of Atg18 [119]. Atg18 localizes not only to punctate structures but to the vacuola rim as well. Interestingly, a relocalization of Atg18 from the vacuolar rim to the PAS has been observed under starvation conditions

[95]. In *Pichia pastoris* Atg18 phosphorylation has been shown to regulate its vacuolar localization [144].

Atg18 has been reported to form a constitutive complex with Atg2 [88], a large 170 kDa protein. Consistently, deletion of *ATG2* shows similar phenotypes as deletion of *ATG18* [139, 145]. It was proposed by a number studies that Atg18 and Atg2 localize to the PAS interdependently [88, 90, 137] and the interaction site of Atg18 with Atg2 has been mapped to the propeller region oposite to the FRRG motif [137, 146]. This enables Atg18 to simultaneously bind Atg2 and PI(3)P containing membranes. In agreement with these results, a study using overexpressed ApeI to form giant cargo complexes showed that Atg18-Atg2 localize to the tip of the growing phagophore. Interestingly, PI(3)P has been proposed to be distributed along the phagophore membrane [87]. Therefore, simultaneous binding of PI(3)P and Atg2 determine the localization of Atg18.

Different functions have been suggested for Atg18, including phagophore expansion and closure as well as Atg9 cycling through the PAS, but no detailed mechanisms have been revealed [90, 99, 123]. Two studies show that recruitment of Atg2 is not the sole function of Atg18, since PAS-targeting of Atg2 fusion proteins did only partially recover the *ATG18*Δ phenotype [146, 147]. The involvement of Atg18 in phagophore completion was inferred from protease protection assays. Neither the specific cargo ApeI nor the bulk cargo Pho8 was protected from cleavage by an exogenously added protease. This implies that autophagic vesicles are not closed [90]. Interestingly, however, ApeI was associated with membranes as shown by floatation experiments [90]. Consistently, *ATG18* deletion results in accumulation of Atg8–PE and Atg8-puncta under starvation conditions and prevented GFP-Atg8 from being transported to the vacuole [132, 148]. In the hierarchical analysis on PAS recruitment of Atg proteins all Atg proteins examined accumulated at the PAS in *atg18*Δ cells, except for Atg5 and Atg16. These two proteins were even slightly impaired in PAS localization [112]. How this phenotype is elicited remains unclear. Another study showed that Atg18 and Atg2 are involved in membrane expansion around giant cargo. Consistently, they demonstrated that Atg18 and Atg2 localize to the tip of phagophore membranes. From these observations they speculated that the Atg18-Atg2 complex is involved in formation of a phagophore-ERES contact site [99]. A recent study reveald that mutating Atg9 to prevent its phosphorylation by Atg1 results in impaired phagophore expansion as well. This mutation also prevented Atg18 from being recruited to the PAS [119]. These data suggest that Atg18-Atg2 plays a role in membrane expansion. Whether the function of Atg18-Atg2 in phagophore expansion and closure lead to the proposed defect in Atg9 cycling through the PAS remains unclear [123]. But this seems likely, since Atg9 was suggested to be recycled from the vacuole after autophagosome fusion [85].

In addition to this late function in autophagy, in mammalian cells WIPI-2 (WD40-repeat

Protein Interacting with Phosphoinositides-2), the proposed Atg18 homolog [149], facilitates LC3-II (Atg8–PE) formation [150]. More specifically, WIPI-2B has recently been shown to directly bind ATG16L1 and WIPI-2B, when ectopically targeted to the PM, recruits Atg12–Atg5-Atg16 to the PM and mis-targets LC3-lipidation [151].
An additional role of Atg18 depends on its PI(3,5)P_2-dependent binding to the vacuole. In *Pichia pastoris* Atg18 phosphorylation has been implicated in its vacuolar localization and function [144]. No such phosphorylation has been detected in *S. cerevisae* Atg18 yet. Different functions have been reported, including regulation of PI(3,5)P_2 levels, vacuole fragmentation and vacuole-to-Golgi transport [131, 152, 153]. *ATG18* deletion has been shown to cause vacuole enlargement and an elevation of PI(3,5)P_2 levels [131]. Atg18 probably inhibits Fab1 via its upstream activators Vac7 and Vac14 [152] and has been suggested to be the inhibitory partner of a PI(3,5)P_2 regulatory complex [154]. Furthermore, Atg18 is involved in vacuolar fragmentation [152]. Consistently, it was proposed that Atg18 is involved in pinching-off vesicles from vacuole invaginations to control vacuole size [153]. Third, Atg18 plays an essential role in retrograde transport from the vacuole to the Golgi [131]. Consistently, Vac17, a myosin V adaptor, interacts with Atg18, therefore, it has been speculated that this interaction is important for retrograde transport mediated by Atg18 [152]. The function of Atg18 in vacuole-to-Golgi transport is in good agreement with its proposed function in Atg9-cycling [123], since Atg9 has been proposed to be recycled from the vacuolar membrane [85]. Consistent with this, an Atg18 fusion protein stably attached to the vacuole was blocked in Cvt pathway and impaired in ApeI processing under starvation conditions, indicating that Atg18 needs to detach from vacuoles to efficiently promote autophagy [152].

Atg21

In contrast to Atg18, Atg21 has been reported to be essential only for the Cvt pathway but not for starvation induced non-selective autophagy. This functional assignment was based on ApeI processing under vegetative and starvation conditions. Consistently, sporulation of *atg21*Δ cells was only reduced. Furthermore, in *atg21*Δ cells autophagic body accumulation was observed by transmission light microscopy [139]. In agreement with these findings, cells expressing $Atg21^{FKKG}$ have been shown to be deficient in Cvt pathway, but not in autophagy [132, 133, 148]. Interestingly, the same phenotype was observed in cells expressing $Atg18^{FKKG}$ in presence of wildtype Atg21 [148]. Cells expressing $Atg18^{FKKG}$ and $Atg21^{FKKG}$ or lacking Atg21, however, resulted in a complete block of non-selective autophagy [148]. This suggests a role for Atg21 in starvation-induced autophagy. Another study demonstrated strong autophagy impairment in *atg21*Δ cells even though autophagosomes were still being formed [143]. Despite these data, Atg21 is believed not to play a role in autophagy under starvation conditions.
Fluorescence microscopy studies revealed that Atg21 localizes to the vacuolar membrane

and punctate structures depending on its FRRG-motif, similar to Atg18 [139, 140, 143]. Consequently, PIP binding is the major localization factor for Atg21. As discussed for its functional implications, contradicting information about the PAS localization of Atg21 has been published. While one study did not observe PAS localization at all [132] another study found colocalization of Atg21 with ApeI in vegetative conditions [143].
Concerning the molecular function of Atg21, limited and partially contradictory data are available. Under vegetative conditions ApeI is not protected from protease cleavage in *atg21*Δ cells, but it is transported to the vacuole under starvation conditions. This implies a different mechanism in delivery of ApeI to the vacuole in vegetative and starvation conditions [132, 143]. Even though Atg21 is believed not to have a major impact on autophagy, Atg8–PE formation is impaired upon *ATG21* deletion under starvation conditions [132, 143]. In agreement with this a decrease in Atg8-puncta formation was observed in *atg21*Δ cells [132]. Surprisingly, another study reported the oposite effect, accumulation of Atg8-puncta in starved *atg21*Δ cells [148]. For vegetative conditions a very recent study showed that Atg21 recruits Atg12–Atg5-Atg16 to the PAS. This results in the Ub-conjugation machinery being targeted to the PAS. Additionally, they proposed a binding site for Atg21 in the coiled coil of Atg16 [155].
Another function of PROPPINs could be the stabilization of Atg proteins on forming autophagosomes, since depletion of a PI(3)P phosphatase resulted in accumulation of autophagosomes with Atg proteins, including Atg2, Atg9, Atg14, Atg16, Atg17 and Atg18, bound to it [156]. More specifically, Atg18 and Atg21 have been suggested to protect Atg8 from premature cleavage by Atg4. No clear distinction between Atg18- and Atg21-mediated function has been proposed in this study [148]. A clear-cut molecular function of Atg21 in starvation-induced autophagy is thus missing.

e) Ubiquitin-Like Conjugation Systems

An important function of PROPPINs apparently includes the recruitment of downstream factors that regulate phagophore expansion. Atg21 has been demonstrated to recruit Atg12–Atg5-Atg16 to the PAS during vegetative growth [155] and WIPI-2B, the human Atg18 homolog, recruits Atg12–Atg5-Atg16 to the PAS upon starvation [151]. The Ub-like proteins Atg8 and Atg12 are conjugated to the phagophore or Atg5, respectively (reviewed in [157]), and Atg12–Atg5 acts upstream of Atg8 [112].

Atg12 is expressed with an accesible C-terminal glycine. It is activated by covalent attachment to a cysteine in the active site of the E1-like enzyme Atg7 in an ATP-dependent manner [158]. Atg12 is transferred to Atg10 [159] which finally conjugates Atg12 to its target protein Atg5 forming an iso-peptide bond between the C-terminal glycine of Atg12 and Lys149 of Atg5 [158]. This Atg12–Atg5 conjugate forms a constitutive complex with Atg16 [160].
In the second autophagosomal ubiquitin-like system Atg8 is expressed as a precursor

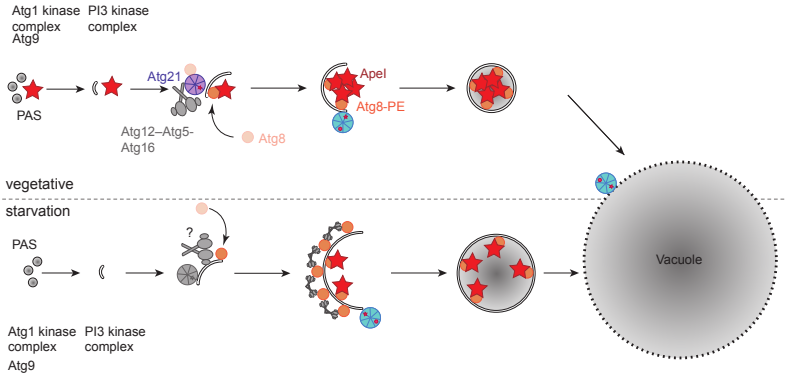

Figure 1.3: PROPPINs in autophagosome formation. Autophagosome formation starts with the *de novo* formation of a membrane. In vegetative conditions the yeast specific Cvt-pathway is constitutively delivering ApeI (asterisk) to the vacuole for its activation. Atg8 at the concave membrane links ApeI to the membrane forming a small double membraned vesicle of 140-160 nm in diameter. While Atg21 has a positive influence on Atg8-lipidation, Atg18 has been proposed to be involved in late steps of membrane formation. Under starvation conditions, more and larger autophagosomes are formed carying bulk cytoplasm to the vacuole for degradation. In addition they can also bind specific cargo by the concave Atg8 pool. The convex Atg8 pool forms a scaffold with Atg12–Atg5-Atg16. The influence of PROPPINs is not well defined, except that Atg18 is involved in late steps of autophagy.

carrying a C-terminal arginine, which is cleaved by the cysteine protease Atg4 [161]. Atg8 is activated by Atg7 and subsequently transferred to Atg3, before an iso-peptide bond with the membrane lipid phosphatidyl-ethanolamine (PE) is formed resulting in Atg8–PE [45]. Atg12–Atg5 functions as an E3-like enzyme catalyzing this conjugation of Atg8 to its target lipid [162]. Atg16 targets the complex to the PAS [112, 163] by interaction with its upstream factor Atg21 [155].

Atg8 localizes to the concave and the convex face of the phagophore [164]. These Atg8 pools serve different functions. The concave Atg8-pool funtions as cargo-adaptor and tethers specific cargo to the phagophore by recognizing the AIM motif in cargo receptors [22, 165]. Atg8 also controls autophagosome size [89]. In agreement with this finding, Atg8 has recently been identified to form a protein scaffold on supported lipid bilayers *in vitro*. Atg12–Atg5 binds Atg8–PE via a non-canonical Atg8-interaction motif (AIM). This interaction directly links the Atg12–Atg5-Atg16 complex to Atg8–PE. Dependent on Atg16 multimerization a protein scaffold of Atg12–Atg5-Atg16 and Atg8–PE is formed [21]. Consequently, higher Atg8 levels might lead to formation of larger protein scaffolds at the convex face of phagophores, resulting in larger autophagosomes. Interestingly, excess of Atg32, a cargo receptor for mitophagy, was able to compete with scaffold formation, leading to increased mobility of membrane bound Atg8. This raises the question whether cargo receptor proteins extract Atg8 from the protein scaffold *in vivo* to make it available for cargo binding at the convex face. This mechanism would involve shuttling

of Atg8–PE from the convex to the concave face. Passing through the highly bent edge of the phagophore is, however, energetically unfavourable suggesting that the concave Atg8-pool is generated independently. How this is done remaines, yet, elusive.
Atg8 has been found to tether membranes *in vitro* and to form multimers upon lipidation. This raised the possibility that Atg8 is involved in autophagosome closure [91]. Sealing of the phagophore generates the complete autophagosome from which Atg8 is recycled by Atg4. This is essential for autophagosome-vacuole fusion [161].

f) Cargo Receptor Proteins for Selective Autophagy

The selective degradation of cytoplasmic components by autophagy requires cargo to be tethered to the phagophore in a highly regulated manner. This is achieved by a set of cargo-receptors which bind cargo selectively. A tight contact of cargo with the phagophore is essential for their exclusive degradation which is achieved by binding to Atg8 in addition to cargo binding [22]. The yeast specific Cvt pathway uses Atg19 to efficiently target ApeI and Ams1 to Cvt vesicles [166, 167]. In autophagy induced conditions Atg34 is a specific receptor of Ams1 [165]. Atg32 is required for mitophagy. These three receptors share the feature that they bind cargo, Atg8 and Atg11 for efficient selective autophagy to occur. Atg11 is discussed to recruit the autophagic machinery to specific cargo [121]. Atg8-binding to cargo-receptors is mediated by their Atg8 interacting motif (AIM), which ensures tight binding of cargo to the phagophore [22]. Atg30 is involved in the recognition of peroxisomes by interaction with a peroxisomal membrane protein on the one hand [168] and Atg8 on the other hand. Interaction with Atg8 and Atg11 depends on phosphorylation ensuring regulated degradation [169]. A recent study identified two additional cargo receptors that bind Atg11 and Atg8 for efficient degradation of ER and nucleus. Atg39 and Atg40 are involved in degradation of distinct ER domains. Atg39 additionally mediates nucleophagy [170]. Furthermore, a new class of receptor proteins has been identified that binds polyQ-proteins as well as Atg8 for efficient autophagosomal degradation [171].

g) Non-Atg-proteins

Atg proteins have first been identified in autophagy and play major or essential roles in different steps of autophagosome formation. Additionally, proteins first identified in other cellular functions emerge to act in autophagy as well. Small GTPases are not only key regulators in membrane trafficking, but also regulate autophagy. More than 12 Rab GTPases have been identified so far, regulating all steps of autophagy (reviewed in [172]). For example Rab33 might play an important role in the targeting and recruitment of Atg16L to the IM (reviewed in [126]), therefore playing a role in early autophagosome formation. Fusion of autophagosomes with the lysosome is regulated by the GTPase Rab7, which is activated by the HOPS complex [173, 174]. Another important class of

proteins for vesicular trafficking are tethering factors and an autophagy-specific tethering complex of the TRAPP family has been identified and named TRAPP-III. Trs85 is the specific subunit of the complex targeting it to the PAS by interaction with Atg9 and/or Atg17 [41, 42]. The TRAPP-III complex, furthermore, is believed to connect vesicular trafficking with autophagy by direct interaction with COPII components. Therefore, it has been proposed that COPII vesciles might provide lipids for IM expansion [124].
Since IM expansion as well as delivery of autophagic cargo to the vacuole need membrane fusion events, it is not surprising that SNAREs have been reported to be involved in autophagy. An initial study by Nair et al. (2011) revealed that the exocytic t-SNAREs Sso1 and Sec9 are involved in autophagosome biogenesis. For this function they can interact with three endosomal SNAREs (Sec22, Ykt6 and Tlg2). All of these SNAREs have an influence on Atg9 cycling and Sso1 and Sec9 have been shown to facilitate Atg8 recruitment. Furthermore, SM family proteins (regulators of SNARE mediated fusion, Chapter 1.1.4) with an impact on autophagy have been identified in this study [3]. A later study identified additional SNAREs for autophagy. As mentioned above mammalian Atg14L is involved in membrane tethering and membrane fusion. Atg14L facilitates SNARE-mediated fusion by priming the t-SNAREs syntaxin17 and SNAP29 for fusion with their corresponding v-SNARE Vamp8 [175].

1.2.3.4 Autophagy Regulation

Autophagy is a tightly regulated process and consequently a multitude of different regulatory layers have been described, inculding transcriptional, post-transcriptional and post-translational mechanisms (reviewed in [96]). The target of rapamycin (TOR) is a kinase important in nutrient-sensing pathways and its complex TORC1 has been found to be a master regulator of autophagy phosphorylating Atg proteins[107]. Importantly, nutrient deprivation is a potent inducer of autophagy and different pathways are employed by amino acid and glucose starvation. It has been shown that TORC1 is activated via amino acid metabolites and tRNA-synthase activity [176, 177]. Active TORC1 localizes to the lysosome. Upon amino acid starvation TORC1 is detached from the lysosome and its activator Rheb. The deactivation of TORC1 results in autophagy induction (reviewed in [178]). An important regulator of TORC1 in glucose starvation is Akt. During high glucose levels Akt is active and inhibits TSC1/TSC2 which is a TORC1 inhibitor. In consequence autophagy is suppressed. This inhibition is released by Akt inactivation upon glucose deprivation (reviewed in [178]). Additionally, TORC1 has been shown to be regulated by AMPK, being a sensor for intracellular energy levels. In vegetative growth AMPK is inactive which in turn leads to an activation of TORC1. Upon glucose starvation AMPK activates autophagy via two routes. First, it inactivates TORC1, second, it directly activates ULK1 (human Atg1 homolog) by phosphorylation.

Atg13 is hyperphosphorylated by TORC1 in vegetative conditions and dephosphorylation upon TORC1 inhibition induces autophagy [114]. Furthermore, in vegetative conditions TORC1 inhibits autophagy by activation of an mRNA decapping enzyme. This results in destabilization of ATG mRNAs. Under starvation conditions decapping is inhibited causing an accumulation of ATG mRNAs [179]. On a transcriptional level, TORC1 has been shown to inhibit transcription factors important for lysosomal biogenesis under vegetative conditions and releases them upon starvation (reviewed in [180]). Transcriptional activation is a common theme of autophagy induction and upregulation had been reported for Atg8, Atg9 and other Atg proteins upon nitrogen starvation (reviewed in [96]). A recent study identified a new regulator for many Atg proteins. Rph1 suppresses *ATG* gene transcription in vegetative conditions. Under starvation conditions transcriptional repression of *ATG* genes is released by phosphorylation of Rph1 [181]. Another important transcriptional regulator is the tumor suppressor p53, which serves a dual role in autophagy regulation. First, p53 upregulates transcription of autophagic proteins promoting autophagy. Second, cytoplasmic p53 can inhibit autophagy (reviewed in [182]). In addition to these physiological regulatory mechanisms intracellular pathogens block autophagy to escape degradation by their host cell [183]. Taken together the detailed understanding of the regulatory network fine-tuning autophagy paves the way for therapeutic strategies against autophagy-related diseases.

1.2.3.5 Autophagy in Health and Disease

Autophagy is involved in various diseases, such as neurodegenerative diseases, cancer, pulmonary and cardiovascular disease. Furthermore, different roles in infectious diseases and autoimmunity have been reported (reviewed in [184–186]). In neurodegeneration protein aggregates accumulate within cells impairing cellular functions and ultimately leading to cell death. Autophagy can remove protein aggregates, thereby, preventing cell death. Impaired autophagy thus promotes the development of Alzheimer‘s, Parkinson‘s and Huntington‘s disease (reviewed in [187]). Interestingly, Huntingtin itself was recently discovered to initiate its own degradation by binding p62 and ULK1 [188]. Although autophagy plays a dual role in cancer by promoting or inhibiting tumorigenesis under specific circumstances, evidence accumulates that its promoting activity dominates (reviewed in [189]). Autophagy inhibition is, therefore, a current focus of drug-development. Combination therapies for cancer treatment are currently tested in pre-clinical trials showing that autophagy inhibition increases radiosensitivity of tumor cells [190]. First early phase clinical trials for combination of autophagy inhibtors and chemotherapeutics are underway to reveal potential benefits [191]. In contrast, in neurodegenerative diseases and infections upregualtion of autophagy would be beneficial, which might be achieved with approved drugs reported to induce autophagy (reviewed in [187]).

1.3 Aim of the Study

A key step in autophagosome formation involves the conjugation of the Ub-like protein Atg8 to the phagophore. Atg8–PE excerts two important functions. It promotes phagophore expansion by forming a protein scaffold [21, 89]. On the other hand, Atg8 tethers cargo to the phagophore as cargo adaptor [22]. How these two functions are coordinated is currently unknown.

Gaining insight into these functions is important since it forms the basis for selectivity in autopghagy. During vegetative growth autophagosomes capture cargo selectively and exclusively [22]. Thus, the cargo adaptor function of Atg8 dominates. Under starvation, however, bulk cytoplasm is degraded [62]. Consequently, the scaffolding function of Atg8 dominates under these conditions.

Potential candidates to regulate these activities by a yet unknown mechanism are the yeast PROPPINs, Atg18 and Atg21, both of which might act upstream of Atg8 to coordinate Atg8-function [151, 155]. The aim of this thesis was, therefore, the functional and molecular characterization of yeast PROPPIN function in autophagy using a combination of *in vitro* and *in vivo* assays. Starting from previously published data, the two PROPPINs and the Atg8 lipidation machinery had to be recombinantly expressed and purified. The PIP-binding specificity had to be determined on model membranes. Subsequently, the influence of PROPPINs on membrane recruitment of the Atg8-lipidation machinery and Atg8-lipidation had to be characterized *in vitro*, on different model membranes. Furthermore, an *in vitro* setup for single molecule examinations had to be established for more detailed characterization of the influence of PROPPINs on protein scaffold formation. It, then, had to be explored how the functions potentially revealed *in vitro* translate *in vivo*. Furthermore, possible compensation strategies of the two PROPPINs were to be examined. Therefore, the PAS localization of PROPPINs had to be determined by fluorescence microscopy. Subsequently, the influence of PROPPINs on Atg8-lipidation and autophagosome formation had to be analyzed by biochemical assays and fluorescence microscopy. To discriminate the exact function of PROPPINs an extensive set of genetically modified yeast had to be generated and analyzed in biochemical and fluorimetric autophagy assays. Another aim was to further characterize the role of Atg18 and especially Atg21 in starvation induced autophagy by electron microscopy. To identify potential reasons for functional differences of PROPPINs their exact localization of Atg18 and Atg21 on the autophagosomal membrane and their influence on membrane expansion around giant cargo had to be explored by fluorescence microscopy. For a more detailed characterization, the influence of PROPPINs on formation of distinct Atg8-pools had to be determined. Finally, the potential involvement of PROPPINs in alternative routes for delivery of cytoplasm to the vacuole had to be examined.

Materials and Methods

2.1 Chemicals

If not indicated otherwise, Chemicals were purchased from AppliChem (Darmstadt, Germany), Carl Roth (Karlsruhe, Germany), Merck (Darmstadt, Germany), Millipore (Darmstadt, Germany), Santa-Cruz (Heidelberg, Germany), Serva (Heidelberg, Germany) and Sigma-Aldrich (Seelze, Germany). Synthetic lipids 1-palmitoyl-2-oleoyl-sn-glycerol-3-phosphocholine (POPC), 1-palmitoyl-2-oleoyl-sn-glycerol-3-phosphoethanol-amine (POPE), 1-palmitoyl-2-oleoyl-sn-glycerol-3-phosphoserine (POPS), cholesterol, 1,2-dioleoyl-sn-glycero-3-phospho-(1'-myo-inositol-3'-phosphate) (PI(3)P) and 1,2-dioleoyl-sn-glycero-3-phosphoethanolamine-N-(lissamine-rhodamine B sulfonyl) were purchased from Avanti Polar Lipids (Alabaster, Alabama).

2.2 Enzymes and Antibodies

If not indicated otherwise, enzymes were purchased from New England Biolabs (Frankfurt am Main, Germany), Invitrogen (now Thermo Fisher Scientific, Waltham, MA), Clontech (Saint-Germain-en-Laye, France) or Agilent Technologies (Oberhaching, Germany). Antibodies were purchased from Roche Diagnostics and Invitrogen. Anti-Atg8 antiserum was raised in rabbits against the N-terminus of Atg8 as described in [164]. Anti-ApeI was a kind gift from Prof. Michael Thumm. Fusion proteins were proteolytically cleaved using PreScission Protease produced by the Core Facility of the Max Planck Institute of Biochemistry (Martinsried, Germany).

2.3 Buffers and Media

Incredients for buffers were purchased from vendors mentioned in Chapter 2.1 Chemicals, dissolved in MilliQ water and filtered with cellulose acetate filters, poresize 0.45 μm (Sartorius, Göttingen, Germany) or filter sterilized. Buffers used in this study are listed in Table 2.1.

Table 2.1: Buffers used in this study

Buffer	Composition
Lysis Buffer	100 mM Tris (pH 8.0), 300 mM NaCl, 10% (v/v) glycerol, 5 mM imidazole, add freshly: 5 mM β-mercaptoethanol, 5 μl benzonase, 1:100 Protease Inhibitor
Wash Buffer	50 mM Tris (pH 7.2), 300 mM NaCl, 10% (v/v) glycerol, 5 mM imidazole, add freshly: 5 mM β-mercaptoethanol
Elution buffer	50 mM Tris (pH 7.2), 300 mM NaCl, 10% (v/v) glycerol, 500 mM imidazole, add freshly: 5 mM β-mercaptoethanol
SEC buffer	25 mM Tris (pH 7.2), 275 mM NaCl
Reaction buffer	12.5 mM Tris (pH 7.2), 137.5 mM NaCl
5x SDS sample buffer	225 mM Tris (pH 6.8), 50% (v/v) glycerol, 5% (w/v) SDS, 0.05% (w/v) bromophenol blue, 250 mM DTT
1x PP	0.1 M Tris (pH 7.5), 2% SDS (w/v), 10% (v/v) glycerol (w/v), 20 mM DTT, trace amounts of bromophenol blue [192]
SDS buffer	25 mM Trizma-Base, 192 mM glycin, 0.1% (w/v) SDS
Coomassie Staining Solution	0.25% (w/v) Coomassie R-250, 30% (v/v) ethanol, 10% (v/v) acetic acid
Destaining Solution	40% (v/v) ethanol, 10% (v/v) acetic acid
Shrinking Solution	50% (v/v) methanol, 3% (v/v) glycerol
Blotting buffer	50 mM Trizma-Base, 40 mM glycin, 0.37% (w/v) SDS 20% (v/v) methanol
TBS-T	25 mM Tris (pH 7.5), 150 mM NaCl, 0.05% (v/v) tween-20
SORB	10 mM Tris (pH 8.0), 100 mM LiOAc, 1 mM EDTA (pH 8.0), 1 M sorbitol
PEG mix	10 mM Tris pH 8.0, 100 mM LiOAc 1 mM EDTA, 40% (v/v) PEG 3350
One-step buffer	240 mM LiOAc, 47% (w/v) PEG 3550, 100 mM DTT (added freshly)
Pho8-assay buffer	250 mM Tris (pH 9.0), 10 mM magnesium sulfate, 10 μM zinc sulfate
Stop buffer	2 M glycin, (NaOH pH 11.0)

Incredients for media were purchased from Becton Dickinson (Heidelberg, Germany), Carl Roth (Karlsruhe, Germany), Millipore (Darmstadt, Germany) and Sigma-Aldrich (Seelze, Germany), dissolved in MilliQ water and autoclaved for 25 min at 121°C and 1.5 bar. For solid medium 2% (w/v) agar was added. Media used in this study are listed in Table 2.2.

Table 2.2: Media for yeast and bacteria used in this study

Media	Composition
Luria-Bertani (LB) medium	5 g/l yeast extract, 10 g/l trypton, 7 g/l NaCl
Yeast extract peptone dextrose (YPD) medium	10 g/l yeast extract, 20 g/l peptone, 2% (w/v) glucose
Synthetic drop-out (SD) medium	0.67% (w/v) yeast nitrogen base, 0.5% (w/v) ammonium sulphate, 2% (w/v) glucose, auxotrophic amino acids or nucleosides as needed
Synthetic drop-out starvation (SD-N) medium	0.1675% (w/v) yeast nitrogen base, 0.125% (w/v) ammonium sulphate, 2% (w/v) glucose, auxotrophic amino acids or nucleosides as needed

2.4 Primers

Primers used for cloning of expression plasmids in *E. coli* and *S. cerevisiae* as well as genomic alterations of yeast are listed in Table 2.3.

Table 2.3: Primers

Numl	Sequence	Use
LP1	GGGCCCCTGGAACAGAACTTCCAG	FW primer for linearization of pCoofy1 for SLIC
LP2	CGCCATTAACCTGATGTTCTGGGG	RV primer for linearization of pCoofy1 for SLIC
V131	GAGAATCTAATAATTGTAAAGTTGAGAAAATCATAATAAAATAATTACTAGAGACATGCGTACGCTGCAGGTCGAC	S1 primer for deletion or N-terminal tagging of Atg8
V132	CTCTCCGACTCCGCCTTCCTTTTTTCAAATGGATATTCAGACTTAAATGTAGACTTCATCGATGAATTCTCTGTCG	S4 primer for N-terminal tagging of Atg8
V230	CATTTACATATCAGCATACGGGACATTATTTGAACGCGCATTAGCAGCCGTACGCTGCAGGTCGAC	S1 primer for deletion or N-terminal tagging of 60 amino acids of Pho8
V231	CCCATCCGTCACGAAGAATATGACATTCTTCTTCTTGTGTGATGCAGACATCGATGAATTCTCTGTCG	S4 primer for N-terminal deletion of 60 amino acids of Pho8 or for mtPho8Δ60 construction

V304	GTTCTGTTCCAGGGGCCCTGCATG-AAAGTATTACAATTCA	FW mutagenesis primer for N-terminal addition of Cys to Atg21
V305	TGAATTGTAATACTTTCATGC-AGGGCCCCTGGAACAGAAC	RV mutagenesis primer for N-terminal addition of Cys to Atg21
V306	CTATATGTCTTCAAGGTCACTGTT-TAAAGAATTTAAAAAGGGTACCAG-ATTGTGCAA	FW mutagenesis primer for Atg21^{wt} to ^{Atg21FKKG}
V307	TTGCACAATCTGGTACCCTTTTTA-AATTCTTTAAACAGTGACCTTGAA-GACATATAG	RV mutagenesis primer for Atg21^{wt} to Atg21^{FKKG}
B001	AAGTTCTGTTCCAGGGGCCCATGT-CTGATTCATCACCTACTATCAACT-TTATTAATTTCAATCAAACCG	FW primer for SLIC of Atg18 into pCoofy1
B002	CCCCAGAACATCAGGTTAATGGCG-TCAATCCATCAAGATGGAATACTG-TGACAATATTAAGCAATC	RV primer for SLIC of Atg18 into pCoofy1
B027	CAGGGGCCCTGTATGTCTGATTCA-TCACCTACTATCAACTTTATTAAT-TTCAATCAAACCG	FW mutagenesis primer for N-terminal addition of Cys to Atg18
B028	CGGTTTGATTGAAATTAATAAAGT-TGATAGTAGGTGATGAATCAGACA-TACAGGGCCCCTG	RV mutagenesis primer for N-terminal addition of Cys to Atg18
B055	GGTGATAAGATCTACCAATTCAAG-AAAGGGACGTACGCGACAAGAATT-TACTC	FW mutagenesis primer for Atg18^{wt} to Atg18^{FKKG}
B056	GAGTAAATTCTTGTCGCGTACGTC-CCTTTCTTGAATTGGTAGATCTTA-TCACC	RV mutagenesis primer for Atg18^{wt} to Atg18^{FKKG}
B109	GAGAGAGGCGGCGATTGCTTAATA-TTGTCACAGTATTCCATCTTGATG-GATCGTACGCTGCAGGTCGAC	S3 primer for C-terminal tagging of Atg18
B170	AATAGTGTTCCAGTTAACTCTGTA-TCCTTTTCTTCTTCGGCCTGACAA-TGCGTACGCTGCAGGTCGAC	S1 primer for deletion or N-terminal tagging of Atg18
B186	GGCGATCAACCTGCGCTTTCAGCA-GCGAGATTGCGTATAATCAACACA-AAAAAACATTCTATTATCTGTG	FW mutagenesis primer for Atg18^{wt} to Atg18^{PR72,73AA}
B187	CACAGATAATAGAATGTTTTTTTG-TGTTGATTATACGCAATCTCGCTG-CTGAAAGCGCAGGTTGATCGCC	RV mutagenesis primer for Atg18^{wt} to Atg18^{PR72,73AA}

B231	ATTGTGTATGCGTTGTGACGTACG-GAAGGCAGCGCGAGACACTTCCGT-GAATCGATGAATTCGAGCTCG	S2 primer for deletion or C-terminal tagging of Atg18
B253	ACCGCGGTGGAGCTC	FW primer for linearization of pC1 for exchange of GFP with Atg18 by SLIC
B254	GGATCCCGAATTCCTTTTAAG	RV primer for linearization of pC1 for exchange of GFP with Atg18 by SLIC
B255	CTACCTTAAAAGGAATTCGGGATC-CATGTCTGATTCATCACCTAC	FW primer for amplification of Atg18 for SLIC insertion into pC2
B256	GGGCGAATTGGAGCTCCACCGCGG-TTCAATCCATCAAGATGG	RV primer for amplification of Atg18 for SLIC insertion into pC2
B303	CAATCTGCAGATGTCTGATTCATC-ACCTACTATCAAC	FW primer for linerization of pC3 for SLIC deleting FUS1TM±4aa
B304	AATCAGACATCTGCAGATTGATAT-TGTTTGATAATTAAATC	RV primer for linerization of pC3 for SLIC deleting FUS1TM±4aa
B313	TAAGCGGCCGCCACCG	FW primer for linearization of pC1 for exchange of FUS1TM±4aa-mRFPruby with Atg21 by SLIC
B334	AGACAATTCCACTCCTTTGGATTT-GAAATAGACAGATAGAAAAGGATA-TGCGTACGCTGCAGGTCGAC	S1 primer for deletion or N-terminal tagging of Atg21
B335	ACGTGAATACGTACAATATCTATT-AAGATTATGAAAACTGCACATATG-CAATCGATGAATTCGAGCTCG	S2 primer for deletion or C-terminal tagging of Atg21
B341	AAGTTCTGTTCCAGGGGCCCATGA-AAGTATTACAATTCAATCAAGATG-CAACGTGCTG	FW primer for SLIC of Atg21 into pCoofy1
B342	CCCCAGAACATCAGGTTAATGGCG-TTATGTAAATTTATTATTTTTAGT-CAGCACACATTCACCAGGTTTTGA	RV primer for SLIC of Atg21 into pCoofy1
B347	ATTATCAAACAATATCAATCTGCA-GATGAAAGTATTACAATTCAATCA-AGATGC	FW primer for amplification of Atg21 and SLIC insertion into linearized pC1

B349	CTGCAGATTGATATTGTTTGATAA-TTAAATC	RV primer for linearization of pC1 for exchange of FUS1TM±4aa-mRFPruby with Atg21 by SLIC/to exchange Atg18^{wt} with mutants in pC4
B373	ACCGCGGTGGAGCTC	FW primer for linerization of pC4 to exchange Atg18^{wt} with mutants
B374	ATTATCAAACAATATCAATCTGCA-GATGTCTGATTCATCACCTACTAT-CAAC	FW primer for amplification of Atg18 mutants for SLIC into linearized pC4
B375	AATTGGAGCTCCACCGCGGTTCAA-TCCATCAAGATGGAATACTGTG	RV primer for amplification of Atg18 mutants for SLIC into linearized pC4
B378	ACCGCGGTGGCGGCCGCTTATGTA-AATTTATTATTTTTAGTCAGCACA-CATTC	RV primer for amplification of Atg21 and SLIC insertion into linearized pC1
B396	TATTATACTAGTGGTTCCATGGTG-AGCAAGGGC	FW primer for amplification of mCherry from #1035 [193] for consruction of pC8
B397	TATTATGGATCCACTTGTTCTAGA-CTTGTACAGCTCGTC	RV primer for amplification of mCherry from #1035 [193] for consruction of pC8
B398	TTCCGTCAAAACCTGGTGAATGTG-TGCTGACTAAAAATAATAAATTTA-CACGTACGCTGCAGGTCGAC	S3 primer for C-terminal tagging of Atg21
B409	CCCATCCGTCACGAAGAATATGAC-ATTCTTCTTCTTGTGTGATGCAGA-GGTACCCGGGGATCCG	S4 like primer for amplification of nat-GPD-mtSu9 cassette for mtPho8Δ60 construction
B463	GTGACCTAGTATTTAATCCAAATA-AAATTCAAACAAAAACCAAAACTA-ACATGCGTACGCTGCAGGTCGAC	S1 primer for deletion or N-terminal tagging of Pep4
B464	CTCTCTAGATGGCAGAAAAGGATA-GGGCGGAGAAGTAAGAAAAGTTTA-GCTCAATCGATGAATTCGAGCTCG	S2 primer for deletion or C-terminal tagging of Pep4
B472	AGACAAAAATAAAGCAGCATAGAG-TGCCTATAGTAGATGGGGTACAAA-TGCGTACGCTGCAGGTCGAC	S1 primer for deletion or N-terminal tagging of Vps4

B473	TTTTTTATTTTCATGTACACAAGA-AATCTACATTAGCACGTTAATCAA-TTGACTAATCGATGAATTCGAGCTCG	S2 primer for deletion or N-terminal tagging of Vps4

2.5 Vectors

Table 2.4: Vectors for expression and purification

Name	Description	Primers	Method	Origin
pE1	T7, His6-Atg18, KanMX	LP1; LP2; B001; B002	SLIC	This study
pE2	T7, His6-Cys-Atg18, KanMX	B027; B028	mutagenesis	This study
pE3	T7, His6-Atg18FKKG, KanMX	B055; B056	mutagenesis	This study
pE4	T7, His6-Atg18PR72,73AA, KanMX	B186; B187	mutagenesis	This study
pE5	T7, His6-Atg21, KanMX	LP1; LP2; B341; B342	SLIC	This study
pE6	T7, His6-Atg21FKKG, KanMX	V306; V307	mutagenesis	This study
pE7	T7, His6-Cys-Atg21, KanMX	V304; V305	mutagenesis	This study
pE8	T7, His6-Atg3, KanMX	-	-	[21]
pE9	T7, His6-Atg7, KanMX	-	-	[21]
pE10	T7, Atg10, Atg7, Atg12–His6-Cys-Atg5, Amp	-	-	[21]
pE11	T7, His6-MBP-Atg16K150C, KanMX	-	-	[21]
pE12	T7, His6-Atg8ΔR117, KanMX	-	-	[21]

Table 2.5: CEN-plasmids for expression in yeast

Name	Description	Primers	Method	Origin
pC1	pPmaI, FUS1TM+4aa-mRFPruby, LEU2	-	-	Max-Planck-Institute of Biochemistry, AG Wedlich-Söldner
pC2	pPmaI, FUS1TM+4aa-GFP, URA3	-	-	Max-Planck-Institute of Biochemistry, AG Wedlich-Söldner
pC3	pPma1, FUS1TM+4aa-Atg18, URA3	B253; B254; B255; B256	SLIC	This study
pC4	pPma1, Atg18, URA3	B303; B304	SLIC	This study
pC5	pPma1, Atg18PR72,73AA, URA3	B373; B349; B374; B375	SLIC	This study
pC6	pPma1, Atg18FKKG, URA3	B373; B349; B374; B375	SLIC	This study
pC7 Atg18PRAA-FKKG	pPma1, Atg18PR72,73AA/ FKKG, URA3	B186; B187	mutage-nesis	This study
pC8	pMet25, 2xmCherry-Atg8, URA3	B396; B397	SpeI; BamHI digest	This study, modified from pUG36 [193] provided by Prof. Thumm
pC9	pPma1, Atg21, LEU2	B347; B378; B313; B349	SLIC	This study
pC10	pPma1, Atg21FKKG, LEU2	B347; B378; B313; B349	SLIC	This study
pC11	pCup1, ApeI, LEU2	-	-	[119]

Table 2.6: Primers and vectors for genomic alteration of yeast cells

Name	Primer	Description	Origin
pYM-N15	V230;V231	deletion of Pho8 N-terminal 60 amino acids (pho8Δ::pho8Δ60::natNT2)	Max-Planck-Institute of Biochemistry, AG Wedlich-Söldner [194]
pYT-BH25	V230;B409	exchange of Pho8 N-terminal 60 amino acids with mitochondrial localization signal (pho8Δ::mtSu9pho8Δ60::natNT2)	This study, modified from [195]
pFA6a-KanMX6	B334; B335	deletion of *ATG21* (atg21Δ::kanMX)	Max-Planck-Institute of Biochemistry, AG Wedlich-Söldner [194]
pFA6a-KanMX6	B170; B231	deletion of *ATG18* (atg18Δ::kanMX)	Max-Planck-Institute of Biochemistry, AG Wedlich-Söldner [194]
pFA6a-hphNT1	B334; B335	deletion of *ATG21* (atg21Δ::hphNT1)	Max-Planck-Institute of Biochemistry, AG Wedlich-Söldner [194]
pFA6a-hphNT1	B170; B231	deletion of *ATG18* (atg18Δ::kanMX)	Max-Planck-Institute of Biochemistry, AG Wedlich-Söldner [194]
pYM44	B231; B109	C-terminal tagging of Atg18 with GFP (atg18-gfp::HIS3)	Max-Planck-Institute of Biochemistry, AG Wedlich-Söldner [194]
pYM44	B335; B398	C-terminal tagging of Atg21 with GFP (atg21-gfp::HIS3)	Max-Planck-Institute of Biochemistry, AG Wedlich-Söldner [194]
pYM33-2xmCherry	B335; B398	C-terminal tagging of Atg21 with 2xmCherry (atg21-2xmcherry::KanMX)	Max-Planck-Institute of Biochemistry, Yijian Rao, modified from [194]
pYM-N4-pAtg8	V131; V132	N-terminal tagging of Atg8 with GFP (natNT2::gfp-atg8)	Max-Planck-Institute of Biochemistry, Viola Beier, modified from [194]
pFA6a-natNT2	B463; B464	deletion of *PEP4* (pep4Δ::natNT2)	Max-Planck-Institute of Biochemistry, AG Wedlich-Söldner [194]

pFA6a-hphNT1	B472; B473	deletion of *VPS4* (vps4Δ::hphNT1)	Max-Planck-Institute of Biochemistry, AG Wedlich-Söldner [194]

2.6 Bacterial Strains

Table 2.7: Bacterial strains

Name	Genotype	Purpose	Origin
E. coli BL21 (DE3)	F– dcm ompT hsdS(rB– mB-) gal λ(DE3)	expression	Max-Planck-Institute of Biochemistry, Martinsried
E. coli OmniMax™ 2-T1^{R}	F' {proAB lacIq lacZΔM15 Tn10(TetR)Δ(ccdAB)} mcrA Δ(mrr-hsdRMS-mcrBC) φ80(lacZ)ΔM15 Δ(lacZYA-argF) U169 endA1 recA1 supE44 thi-1 gyrA96 relA1 tonA panD	SLIC	Max-Planck-Institute of Biochemistry, Martinsried
E. coli Rosetta (DE3) pLysS	F– ompT hsdSB(rB– mB–) gal dcm lacY1(DE3) pLysSRARE6 (CmR)	expression	Max-Planck-Institute of Biochemistry, Martinsried
E. coli XL-1 Blue	recA1 endA1 gyrA96 thi-1 hsdR17 supE44 relA1 lac [F' proAB lacIqZΔM15 Tn10 (Tetr)]	cloning	Max-Planck-Institute of Biochemistry, Martinsried
E. coli XL-10 Gold	Tetr Δ(mcrA)183 Δ(mcrCB-hsdSMR-mrr)173 endA1 supE44 thi-1 recA1 gyrA96 relA1 lac Hte [F' proAB lacIqZΔM15 Tn10 (Tetr) Amy Camr].	Mutagenesis	Max-Planck-Institute of Biochemistry, Martinsried

2.7 Cloning of Expression Vectors

To investigate PROPPIN functions *in vitro* a set of Atg proteins including PROPPINs (Atg18 and Atg21) and the Atg8-conjugation system (Atg3, Atg7, Atg12–Atg5, Atg16 and Atg8) had to be cloned into expression vectors and expressed in *E. coli*. Expression vectors for the Atg8 conjugation system were kindly provided by Viola Beier [21].
Atg18 and Atg21 were amplified from genomic DNA of *S. cerevisiae* SC288 and cloned into linearized pCoofy1 expression vector by seamless ligation independent cloning (SLIC) [196]. This cloning procedure is based on homologous recombination. The vector was linearized and the ORF of interest was amplified with primers adding homologous regions of 20 nucleotides to the 3'- and the 5'-end. For specific primer combinations see Table 2.4. Ligation was performed in 10 μl reaction volume containing 1x RecA buffer (NEB), 100 ng linearized vector and a three fold molar excess of insert DNA. RecA recombinase was added in a final dilution of 1:20,000 and the mixture was incubated for 30 min at 37°C. Plasmids were transformed into *E. Coli* Omnimax cells by incubation of competent cells with 10 μl recombination reaction for 1 h at 37°C, heatshock for 45 sec at 42°C and subsequent recovery at 37°C shaking. Cells were than grown on plates and cloning success was verified by sequencing. For introduction of N-terminal cysteins or point mutations the Quickchange lightning site directed mutagenesis kit (Agilent, Germany) was used. The template plasmid was amplified with primers designed according to manufacturer's instructions. Primers comprised mutations (insertion or nucleotide exchange) and ~20 bp flanking regions 5' and 3' of the mutations. Template plasmids were digested by DpnI addition and incubation for 1 h at 37°C. XL-10 Gold cells were immediately transformed with 2 μl of the PCR product according to manufacturer's instructions.

2.8 Yeast Strains

Table 2.8: Yeast strains

Name	Genotype	Background	Origin
YS1	Mat a; his3Δ1, leu2Δ0, met15Δ0, ura3Δ0	BY474x	Euroscarf
YS2	natNT2::gfp-atg8	BY474x	This study
YS3	pho8Δ::pho8Δ60::natNT2 atg18Δ::kanMX atg21Δ::hphNT1	BY474x	This study
YS4	pho8Δ::pho8Δ60::natNT2	BY474x	This study
YS5	pho8Δ::mtSu9pho8Δ60::natNT2	BY474x	This study
YS6	pho8Δ::mtSu9pho8Δ60::natNT2 atg18Δ::kanMX atg21Δ::hphNT1	BY474x	This study

YS7	atg21Δ::kanMX	BY474x	This study
YS8	atg18Δ::kanMX	BY474x	Euroscarf
YS9	pho8Δ::pho8Δ60::natNT2 atg18Δ::kanMX	BY474x	This study
YS10	atg18Δ::kanMX atg21Δ::hphNT1	BY474x	This study
YS11	atg18-gfp::HIS3	BY474x	This study
YS12	atg21-gfp::HIS3	BY474x	This study
YS13	atg18-gfp::HIS3 atg21-2xmCherry::kanMX	BY474x	This study
YS14	natNT2::gfp-atg8 atg18Δ::kanMX	BY474x	This study
YS15	natNT2::gfp-atg8 atg21Δ::kanMX	BY474x	This study
YS16	natNT2::gfp-atg8 atg18Δ::kanMX atg21Δ::hphNT1	BY474x	This study
YS17	atg18-gfp::HIS3 atg8Δ::kanMX	BY474x	This study
YS18	atg21-gfp::HIS3 atg8Δ::kanMX	BY474x	This study
YS19	atg18-gfp::HIS3 atg8Δ::kanMX atg21Δ::hphNT1	BY474x	This study
YS20	atg21-gfp::HIS3 atg8Δ::kanMX atg18Δ::hphNT1	BY474x	This study
YS21	pep4Δ::natNT2	BY474x	This study
YS22	pep4Δ::natNT2 atg18Δ::kanMX	BY474x	This study
YS23	pep4Δ::natNT2 atg21Δ::kanMX	BY474x	This study
YS24	pep4Δ::natNT2 atg18Δ::kanMX atg21Δ::hphNT1	BY474x	This study
YS25	pho8Δ::pho8Δ60::natNT2 atg21Δ::kanMX	BY474x	This study
YS26	pho8Δ::mtSu9pho8Δ60::natNT2 atg21Δ::kanMX	BY474x	This study
YS27	pho8Δ::mtSu9pho8Δ60::natNT2 atg18Δ::kanMX	BY474x	This study
YS28	pho8Δ::pho8Δ60::natNT2 vps4Δ::hphNT1	BY474x	This study
YS29	pho8Δ::pho8Δ60::natNT2 atg18Δ::kanMX vps4Δ::hphNT1	BY474x	This study
YS30	pho8Δ::pho8Δ60::natNT2 atg21Δ::hphNT1 vps4Δ::hphNT1	BY474x	This study

2.9 Cloning of CEN Plasmids

CEN plasmids are vectors containing a yeast centromer allowing distribution of one copy of each vector into both daughter cells during cell division [197]. In this thesis, CEN plasmids were used to ectopically express Atg8 proteins or ApeI.
For PROPPIN proteins ORFs were amplified from expression vectors and inserted into

the respective linearized CEN plasmids by SLIC as described in Chapter 2.7. For specific primer combinations see Table 2.9 and Table 2.3.
pC7 was cloned using the Quickchange lightning site directed mutagenesis kit (Agilent, Germany). To introduce RP72,73AA pC6 was amplified with primers B186 and B187 encoding the amino acid exchange (Table 2.3). The template plasmid was digested an transformed into XL-10 Gold cells as described in Chapter 2.7.
pC8 was constructed amplifying mCherry from pU36-mCherry-Atg8 (provided by Prof. Michael Thumm) with primers B396 and B397 introducing a 5' SpeI and 3' BamHI site. The PCR product and pUG36-mCherry-Atg8 were digested with SpeI/BamHI and ligation was performed in 20 μl reaction volume containing 1x ligation buffer (NEB), 100 ng linearized vector and a three fold molar excess of insert DNA. Samples were incubated for 30 min at room temperature after addition of 1 μl T4 DNA Ligase. *E. coli* XL-1 Blue cells were transformed with 2 μl of ligation reaction. Successful cloning was verified by sequencing.

2.10 Yeast Cloning

Saccharomyces cerevisiae is a well established model organism for eukaryotic processes. For Atg8–PE, ApeI processing, (mt)Pho8Δ60 assays and microscopic analysis, derivatives of the yeast strain BY4741 (Euroscarf) were used for *in vivo* experiments. Genomic deletions and tagging were performed as described before [194]. In brief, combinations of plasmids and primers listed in Table 2.6 were used for amplification of deletion or tagging cassettes. For deletions, PCR products carried a resistance marker flanked by 50 bp homology regions for replacement of the respective genomic locus. For 3'- or 5'-tagging of genomic loci, PCR products consisted of a tag-encoding sequence and a resistance marker. PCR products were gel purified. Yeast cells were made competent by growing them to OD_{600} = 0.6 and subsequently washing once with MilliQ water and once with SORB (Table 2.1), before resuspending cells in 360 μl SORB and freezing 50 μl aliquots at -80°C. For yeast cell transformation 5-10μl of gel purified PCR product, 50 μg activated carrier DNA (salmon sperm DNA, activated by incubation for 5 min at 95°C) and 300 μl PEG mix were added to cells. After 1 h incubation at 30°C, 35 μl DMSO were added and cells were heat shocked for 15 min at 42°C. Subsequently, cells were spinned down, resuspended in 300 μl YPD and incubated over night at 30°C shaking. Finally, cells were plated onto YPD plates with respective antibiotics. In case of amino acid auxotrophies as selection marker, cells were washed once with 300 μl PBS after heatshock and plated onto SD-media plates supplemented with respective amino acid dropout mix. For introduction of CEN-plasmids for ectopic expression of Atg protein variants and fusion proteins yeast cells were grown on respective media plates for two

days. A small amount of cells was resuspended in 85 μl one-step buffer (Table 2.1), supplemented with 50 μg carrier DNA and 1-2 μl plasmid DNA. Cells were transformed by incubation for 30 min at 45°C and subsequently plated onto SD-drop out plates, lacking respective amino acids for selection.

2.11 *In Vivo* Assays in *S. cerevisiae*

To assess PROPPIN functions *in vivo* different biochemical and microscopic assays have been performed with whole of yeast cells or their extracts.

2.11.1 Yeast Cell Growth

Yeast cells were grown to mid-log phase (OD_{600}=0.8) in YPD or SD media (Table 2.2), supplemented with antibiotics or lacking amino acids for selection, and starved for induction of autophagy. For starvation cells were harvested by centrifugation for 3 min at 1,500 g and washed twice in SD-N media prior resuspension in SD-N media and incubation at 30°C shaking for 2 - 24 h, as indicated. For Atg8–PE assays 10 mM PMSF were added to cells prior and during starvation. To examine Atg protein localization in more detail and gain information about PROPPIN fuction in phagophore expansion, cells overexpressing ApeI from a plasmid with a copper inducible Cup1 promoter were grown in presence of 100 μM $CuCl_2$. Autophagosome formation was induced in these cells by addition of 0.2 μg/ml rapamycin.

2.11.2 Yeast Cell Extract Preparation and Immunoblotting

Assays based on immunoblotting were the test of PROPPIN expression levels, ApeI-processing assay and Atg8–PE assay. For test of PROPPIN expression levels PROPPIN-GFP fusions were either expressed from their native locus or from a CEN-plasmid under control of a PmaI promoter under vegetative and starvation conditions. The ApeI-processing assay is a method to assess delivery of specific cargo to the vacuole under vegetative and starvation conditions [198]. ApeI is expressed as a precursor enzyme (prApeI) in the cytoplasm, assembles as dodecamers and subsequently forms larger aggregates. These are transported to the vacuole by autophagy in starvation or the Cvt-pathway under vegetative conditions. Upon vacuolar delivery prApeI is activated by proteolytic cleavage, resulting in mature (m)ApeI. The size difference can be visualized by SDS-PAGE and subsequent western blotting. The Atg8–PE assay is used to monitor amounts of Atg8 covalently bound to phosphatidylethanolamine (PE) [199]. Covalent attachment of PE to Atg8 causes faster migration on an SDS-Urea gel, compared to

soluble Atg8. Thereby Atg8 can be separated from Atg8–PE and both populations can be quantified. With this assay the influence of specific proteins on lipidation efficiency can be monitored.

For all immunoblot-based assays 1 OD_{600} of cells were taken at each time point. Cells were spinned down for 5 min at 1,500 g, resuspended in yeast lysis buffer (0.2 mM NaOH, 0.1 mM DTT) and incubated on ice for 15 min. Trichloracetic acid (TCA) was added to a final concentration of 10% (w/v), the mixture was vortexed for 10 seconds and incubated on ice for 15 min. Precipitated proteins were collected by 5 min centrifugation at 17,000 g. The supernatant was removed, protein pellets were resolved in 1 ml ice-cold acetone by sonification to remove residual TCA and stored at -20°C. Proteins were pelleted by centrifugation for 10 min at 17,000 g, 4°C, acetone was removed, pellets were dried and resuspended in 1xSDS-sample buffer. For Atg8–PE assays pellets were resuspended in 1x PP (Table 2.1) shaking at 65°C and subsequently denatured for 3 min at 95°C.

Proteins from samples corresponding to 0.25 OD_{600} were separated by SDS-PAGE using 10% SDS-PA gels for ApeI processing and 12% SDS-PA gels for expression level tests. For Atg8–PE assay samples corresponding to 0.25 OD_{600} (semi-dry blot) or 0.125 OD_{600} (wet blot) were loaded onto 13.5% SDS-PA gels with 6 M Urea. Gels were run in SDS buffer (Table 2.1) and subsequently blotted onto PVDF membranes by semi-dry blotting for 30 to 60 min depending on protein sizes. In case of Atg8–PE assay either semi-dry blotting or wet blotting (75 V, 90 min) in blotting buffer (Table 2.1) were used to transfer proteins onto the PVDF membrane. The membrane was blocked over night at 4°C with 3% (w/v) milk in TBS-T. Primary antibody was incubated in 1% (w/v) milk in TBS-T (1:3000 rabbit α-ApeI; 1:1000 mouse α-GFP; 1:5000 rabbit α-Atg8) for 1 h (ApeI, GFP) or 2.5 h (Atg8–PE) at room temperature. After washing four times with TBS-T, membranes were incubated for 1 h at room temperature with secondary antibody coupled to horseradish peroxidase diluted in TBS-T (1:4000 goat α-mouse; 1:5000 goat α-rabbit). Subsequent to another four washing steps with TBS-T, membranes were developed with Western BLoT Hyper HRP Substrate (Takara, Japan) using an LAS-3000 (Fujifilm) imaging system. After imaging, membranes were stripped and reprobed for Pgk1 as loading control (1:10000 mouse α-Pgk1) in TBS-T.

Protein bands were either quantified with Aida Image Analizer v.4.11. or with ImageJ [200]. For expression tests band intensities of PROPPIN-GFP fusions were divided by corresponding Pgk1 signals. Values obtained for endogenous expression under vegetative conditions were set to one and used for normalization. For ApeI processing band intensities of mApeI were divided by total ApeI (mApeI + prApeI). Values obtained for the wildtype after 4 h starvation were set to 100% and used for normalization. Atg8–PE formation was quantified by division of Atg8–PE signals through total Atg8 (Atg8 + Atg8–PE). To obtain PROPPIN specific Atg8–PE formation, values obtained for

*atg18*Δ*atg21*Δ cells were subtracted from values of all other strains. The resulting value for wildtype under vegetative conditions was set to 1 and used for normalization.

2.11.3 Pho8Δ60 Assay

To assess non-selective delivery of autophagic cargo to the vacuole a fluorimetric assay is frequently used. It is based on the alcalic phosphatase, Pho8, that is activated in the vacuole by proteolytic removal of a propeptide. Pho8 converts a specific substrate, 1-Naphthyl phosphate, to 1-Naphtol, which can be detected by its specific fluorescence properties [198]. In its native form Pho8 is membrane bound via an N-terminal peptide. To monitor non-selective delivery of bulk cytoplasm to the vacuole by autophagy a cytoplasmic version of Pho8 is engineered. The N-terminal 60 amino acids are deleted and a GPD promoter is introduced, resulting in high expression levels of cytoplasmic Pho8Δ60. Additionally, mitophagy was monitored. For this purpose the coding sequence of the native 60 N-terminal amino acids were exchanged with that of a mitochondrial localization sequence as described in [195]. Cells were grown and starved as described in Chapter 2.11.1.

Pho8Δ60 (autophagy) or mtPho8Δ60 (mitophagy) activity was assessed as described by Noda and Klionsky [201]. In brief, 4 OD_{600} of yeast cells during vegetative growth and after starvation were harvested by centrifugation (3 min, 17,000 g). Cells were resuspended in 200 μl ice-cold Pho8-assay buffer (Table 2.1). Acid washed glass beads were added and cells were lysed by six cycles of vortexing and cooling on ice in 30 sec intervals. 200 μl Pho8-assay buffer were added and cell debris were spinned down (5 min 17,000 g). The lysate was transfered to fresh tubes. For assessment of enzymatic activity, 50 μl lysate were added to 450 μl Pho8-assay buffer, pre-warmed to 30°C. After addition of 50 μl 1-Naphthyl phosphate (55 mM), samples were incubated for 20 min at 30°C. The enzymatic reaction was stopped by addition of 500 μl stop buffer (Table 2.1) and reaction tubes were kept on ice. Enzymatic activity was determined using a SynergyNeo microplate reader (BioTek) with an excitation wavelength of 345 nm and an emission wavelength of 472 nm. The Pierce®BCA Protein Assay Kit was used according to manufacturer's instructions to determine total protein content of samples. These values were used to correct fluorescence signals of the enzymatic activity assay. For normalization values obtained for wildtype samples after 4 h (autophagy) or 24 h (mitophagy) starvation were set to 100%.

2.11.4 Live Cell Imaging

Live cell imaging has been used extensively in autophagy research, since forming autophagosomes are visible as punctate structures of fluorescently labeled Atg proteins.

Investigation of the localization of Atg proteins therefore reveals important insights into possible functions. In this study, three types of fluorescence microscopy assays were used to unravel PROPPIN localization and functions. For all live cell imaging assays 15 μl of yeast cells in mid-log phase were diluted in 150 μl SD-medium with (vegetative) or without (starvation) amino acids. Cells were imaged in LabTek #1.0 Borosilicate chambers coated with 1 mg/ml concanavalin A.

2.11.4.1 Monitoring Autophagosomes by GFP-Atg8 Puncta

Atg8 is a key marker for autophagosome biogenesis [202]. During vegetative conditions only few cells accumulate Atg8 in punctate structures, whereas upon starvation Atg8-puncta formation is strongly induced according to enhanced autophagic flux. Atg8-puncta formation can therefore be used to monitor early and late events of autophagosome biogenesis. Disruption of early events prevents formation, while a block of late events most likely results in accumulation of Atg8-puncta.
In this study, yeast cells expressing GFP-Atg8 from their endogenous locus were imaged using a PerkinElmer (Waltham, Massachusetts, USA) UltraVIEW Vox Spinning Disk System. The system was equipped with a LEICA (Wetzlar, Germany) DMI6000 B inverted microscope and a LEICA HCX PL APO 100x/NA1.47 oil immersion objective. Z-stacks of yeast cells with a step size of 0.5 μm were acquired in DIC and fluorescence mode with a 488 nm laser line for GFP.
Stacks were converted into Z-projections of yeast cells with ImageJ using the Maximum Intensity Projection. Cells and GFP-Atg8 punctate structures were counted using the multi-point selection tool of ImageJ.

2.11.4.2 Colocalization of Atg Proteins

As mentioned above Atg8 serves as a PAS marker and was used here to monitor the localization of PROPPIN proteins, Atg18 and Atg21, to the PAS. Therefore, cells endogenously expressing PROPPIN-GFP fusions and expressing 2xmCherry-Atg8 from a CEN plasmid under control of a Met25 promoter were imaged during vegetative and starvation conditions. To examine colocalization of PROPPINs another cell line endogenously expressing Atg18-GFP and Atg21-2xmCherry was imaged under vegetative and starvation conditions. Cells were imaged using a ZEISS (Jena, Germany) LSM780 confocal laser scanning microscope equipped with a ZEISS Plan-APO 63x/NA1.46 oil immersion objective. Z-stacks of yeast cells were acquired in DIC and two fluorescence channels with 488 nm (GFP) and 562 nm (mCherry) excitation laser lines.

Cells and puncta of GFP and mCherry channels were counted in Z-stacks using the multi-point selection tool in ImageJ. To quantify colocalization selections of both fluorescence channels were overlayed and tested for colocalization.

2.11.4.3 Giant ApeI Assay

During autophagosome formation most Atg proteins localize to the PAS in a hierarchical manner [112]. Due to the size of autophagosomes and the resolution limit of conventional fluorescence microscopy Atg proteins are usually seen as punctate structures. To increase the size of autophagosomal membranes that enwrapp specific cargo, ApeI can be overexpressed to form giant ApeI aggregates. At these giant cargo complexes an autophagosomal membrane is formed and expanded resulting in a crescent shaped structure. This membrane crescent can be visualized by fluorescently labeled Atg8. Giant aggregates are only partially surrounded by the autophagosomal membrane [99].
In this thesis, cell endogenously expressing PROPPIN-GFP fusions and expressing tandem-mCherry-Atg8 (2xmCherry-Atg8) from a CEN plasmid under control of a Met25 promoter were used. To examine the influence of Atg18 expression levels on membrane expansion around giant cargo cells expressing GFP-Atg8 were supplemented with a plasmid encoding ApeI under control of a tunable CUP1 promoter. In addition, a strain lacking Atg18 and Atg21 was supplemented with a plasmid overexpressing Atg18. Cells were grown in presence of 100 μM $CuCl_2$ to induce ApeI overexpression from a CEN-plasmid. Autophagy was induced by addition of 0.2 μg/ml rapamycin for 3 h. Images were acquired with a LEICA (Wetzlar, Germany) TCS SP8 AOBS confocal laser scanning microscope equipped with a LEICA HCX PL APO 63x/NA1.4 oil immersion objective. Z-stacks of yeast cells were acquired in DIC and fluorescence channels with 488 nm (GFP) and 561 nm (mCherry) laser lines.
Cells, Atg8-structures (puncta, crescents and full circles) and PROPPIN-puncta were quantified using ImageJ. Colocalization of PROPPINs with Atg8 puncta and Atg8-crescents was quantified in Z-stacks with overlayed GFP and mCherry channel. Positions of PROPPINs colocalizing with Atg8-crescents were divided in two groups (mid and tip). The length of Atg8-crescents forming around giant ApeI was determined using ImageJ.

2.11.5 Transmission Electron Microscopy

Electron microscopy is a powerful method to investigate the ultrastructural properties of cells. Different staining procedures allow for highlighting specific features. To monitor autophagic body formation, in this study a previously described membrane staining protocol was applied [203]. Therefore, yeast strains with *pep4*Δ background were used. Cells were grown to mid-log phase and starved for 4 h as described above (Chapter

2.11.1). Samples were fixed embedded, stained and imaged by Anna Kaufmann. In brief, cells were mixed 1:1 with pre-fixative solution (0.2 M PIPES pH 6.8, 0.2 M sorbitol, 2 mM MgCl2, 2 mM CaCl2, 4% glutaraldehyde) and incubated for 5 min. Cells were centrifuged and incubated in pre-fixative at 4°C over night. Samples were washed with autoclaved water thrice and postfixated with 2% potassium permanganate (Sigma-Aldrich) for 45 min. After another washing step cells were stained with 1% uranyl acetate (Serva) for 1 h and subsequently dehydrated with ethanol solutions of increasing percentage up to 100%. After dehydration cells were resuspended in 2:1 ethanol:resin (Spurr's standard medium frim', Spurr Low Viscosity Embedding Kit, Sigma-Aldrich) and incubated for 2 h. Ethanol was evaporated over night and cells were repeatedly incubated in 100% resin and dried in vacuum. Cells were transfered to beem embedding capsules (Electron Microscopy Sciences) dried in vacuum, spinned to the capsule bottom and dried in vacuum again. To harden samples they were subjected to 70°C for 24 h. Ultrathin sections (60-100 nm) were cut using an UltracutE ultramicrotome (Reichert-Jung). Sections were mounted on Formvar carbon film coated grids (FCF-100-Cu, Electron Microscopy Sciences) and post stained with Reynold's lead citrate (kindly provided by R. Kutlesa). Stain was washed off with water. Transmission electron microscopy images were acquired using a JEM-1230 (JEOL) transmission electron microscope with avoltage of 80 kV and an Orius SC1000 camera (Gatan). Measurements were performed with the DigitalMicrograph software.
Quantification of size and number of autophagic vesicles and cells was done in ImageJ using the line tool and measurement function or the multi-point-selection tool, respectively.

2.12 Protein Expression and Purification

To investigate specific molecular functions of PROPPINs and their influence on Atg8-lipidation the respective proteins had to be expressed and purified. These include the two PROPPINs, Atg18 and Atg21, as well as the Atg8 conjugation system, Atg7, Atg3, Atg12–Atg5, Atg16 and Atg8.

2.12.1 PROPPINs

Atg18 and Atg21 variants were expressed in *E. coli* Rosetta cells as N-terminally His_6-tagged proteins. Pre-cultures were grown in LB-medium supplemented with ampicillin and chloramphenicol over night at 30°C. Main cultures were inoculated by a 1:100 dilution of pre-cultures in 500 ml LB-medium per flask (3 l in total) supplemented with ampicillin and chloramphenicol. Cells were grown to an OD_{600} of 0.6 at 37°C, 180 rpm.

Subsequently, cultures were shifted to 18°C and expression was induced by addition of 0.3 mM IPTG for 16 h. Cells were harvested by centrifugation at 4,500 g for 10 min at 4°C. Pellets were resuspended in lysis buffer (Table 2.1) and lysed on ice by two times 10 min sonification with 80% intensity using a Bandelin Sonopuls Ultrasound homogenizer. Cell debris and unlysed cells were removed by centrifugation at 45,000 g for 1 h at 4°C. Supernatants were incubated with Ni-NTA agarose beads (Quiagen), pre-equilibrated in lysis buffer, for 1 h at (Table 2.1) to bind His_6-tagged proteins. Beads were washed with 500 ml ice cold washing buffer and proteins of interest were eluted with 3.5 ml elution buffer for 10 min at roomtemperature (Table 2.1). To prevent cleavage of purified protein by residual proteases 1 mM EDTA was added. To cleave of the N-terminal His_6-tag the eluate was supplemented with 5 mM DTT and incubated for 30 min at roomtemperature with His-Precission protease (Core Facility, Max-Planck-Institute of Biochemistry). After cleavage proteins were subjected to size exclusion chromatography (SEC) for further purification and removal of His-Prescission protease. SEC was run on a HiLoad 16/60 Superdex 200 column (GE Healthcare) in SEC buffer (Table 2.1). SEC aliquots containing purified protein were pooled and concentrated in Amicon® Ultra concentrators with regenerated cellulose membrane and a molecular weight cut-off of 10 kDa. Samples at different steps of the purification procedure were mixed with 5x SDS sample buffer and run on an SDS-PAGE gel to monitor purification. Finally, the mass of purified proteins was verified by mass spectrometry in the Core Facility of the Max-Planck-Institute of Biochemistry using a BRUKER microTOF mass spectrometer in LC-MS (liquid chromatography-mass spectrometry) mode. Protein concentrations were determined using a NanoDrop 2000c (Thermo Scientific) at an absorbtion wavelength of 280 nm. Aliquots of purified protein, supplemented with 10 mM DTT to prevent disulfide bond fromation, were flash frozen in liquid nitrogen and stored at -80°C until use.

2.12.2 Atg8 Conjugation System

Proteins of the Atg8 conjugation system were expressed and purified as described before [21]. Proteins were expressed as N-terminally His_6-tagged proteins (Atg3, Atg7, Atg8ΔR) or as fusion protein with N-terminal His_6-MBP-tag (Atg16K150C). *In vivo* Atg8 first needs to be activated by cleavage of its C-terminal arginine to make the C-terminal glycine available for covalent bond formation. In this thesis, Atg8 was expressed as its active variant lacking its C-terminal arginine. Atg12–Atg5 was coexpressed with Atg7 and Atg10 from pST39, a polycistronic vector [204]. Atg5 was fused to an N-terminal His_6-tag. Atg7 was coexpressed with chaperones encoded on pG-KJE8 (Takara, Japan) in BL21 cells. All other proteins were expressed in *E. coli* Rosetta. Pre-cultures were grown at 30°C and used to inoculate main cultures (6 flasks à 500 ml LB-medium).

Cultures were grown at 37°C, 180 rpm to an OD_{600} of 0.6, shifted to 18°C and protein expression was induced by addition of 0.3 mM IPTG. For chaperone induction 2 mg/ml arabinose and 5 ng/ml tetracyclin were added to main cultures immediately after inoculation.
Cell harvesting and purification were performed as described for PROPPINs (Chapter 2.12.1). Cells were harvested by centrifugation, resuspended in lysis buffer and lysed by sonification on ice. Cell debris were removed by a 1 h centrifugation step and lysates incubated with Ni-NTA beads (Qiagen). Beads were washed with washing buffer and proteins of interest were eluted with elution buffer (Table 2.1). The N-terminal tags were cleaved by Prescission protease (except for Atg12–Atg5). Subsequently, proteins were subjected to size exclusion chromatography on a Hiload 16/60 Superdex 75 column (Atg8ΔR, Atg16K150C) or a Hiload 16/60 Superdex 200 column (Atg3, Atg7, Atg12–Atg5) using SEC buffer (Table 2.1). Target protein fractions were pooled and concentrated in VivaSpin concentrators (Sartorius) with molecular weight cut-offs depending on target protein size. Protein concentrations were determined using a NanoDrop 2000c (Thermo Scientific) at an absorbtion wavelength of 280 nm. The identiy of purified proteins was verified by mass spectrometry. Concentrated proteins were flash frozen in liquid nitrogen and stored at -80°C.

2.12.3 Fluorescent Labeling

For fluorescence microscopy of purified proteins incubated with synthetic membranes proteins were labeled with fluorescent dyes AlexaFluor488, AlexaFluor633 or PacificBlue (all Invitrogen) via a C_6-linker. Coupling was performed as described previously by [21]. Briefly, the coupling reaction depends on formation of a covalent bond between the maleimide group at the terminus of the C_6-linker and a cysteine side chain of the target protein. To minimize interference with protein function a cystein was attached to the N-terminus of proteins by genetic engineering described in Chapter 2.7 prior to expression. Purified proteins were incubated for 30 min at roomtemperature in a 1:1 molar ratio with the respective dye under exclusion of light. Free dye was removed from labeled protein using a desalting column and SEC buffer. Fractions of labeled protein were pooled and concentrated in Amicon® Ultra (Atg18, Atg21) or VivaSpin (Atg8, Atg12–Atg5, Atg16K150C) concentrators. Protein concentrations and labeling efficiencies were determined according to manufacturer's instructions of fluorescent dyes used. Aliquots of labeled protein were flash frozen and stored at -80°C.

2.13 Dynamic Light Scattering

Dynamic light scattering (DLS) was applied to estimate the hydrodynamic radius of a protein in solution and test for protein aggregation. DLS was performed using a PDDL-S/cool Batch 90T with PD 2000 DLS Plus detector system (Precision Detectors). Atg18 was prepared in SEC buffer with a final concentration of 10 μM in a volume of 200 μl. Acquisition time was 10 sec and 10 measurements were averaged. Hydrodynamic radii and polydispersity were determined using the Precision Dconvolve32 software (Precision Detectors).

2.14 Preparation of Synthetic Membranes

To investigate the function of PROPPINs different synthetic membrane systems were used. Large unilamellar vesicles (LUVs) with a diameter of 100 nm were used for Biacore measurements to determine lipid binding specificity of PROPPINs. Giant unilamellar vesicles (GUVs) with a diameter of 1 to 100 μm served as model membranes for fluorescence microscopy analysis of PROPPIN-membrane binding and analysis of effects on downstream factors. Supported lipid bilayers (SLBs) are model membranes formed on top of a solid surface. In this thesis they were used for fluorescence microscopy analysis of the influence of PROPPINs on Atg8-lipidation and for total internal reflection fluorescence (TIRF) microscopy as well as atomic force microscopy (AFM).

2.14.1 PI(3)P Protonation

For efficient incorporation into GUVs PI(3)P had to be protonated prior to preparation of the lipid mix. PI(3)P was purchased as a powder in aliquots of 100 μg. The powder was dissolved in 1 ml chloroform, dried under a stream of nitrogen and dessicated in vacuum for 1 h. Protonation was achieved by dissolving PI(3)P in 200 μl of a 2:1:0.01 (v/v/v) chloroform:methanol:1M HCl mixture and incubation for 15 min at roomtemperature. Chlorofrom:methanol:1M HCl was evaporated under a nitrogen stream and dessicated in vacuum for 1 h . The lipid was washed once with 200 μl of a 3:1 (v/v) chloroform:methanol and once with pure chloroform. Solvents were evaporated under a nitrogen stream and finally dissolved in 200 μl chloroform resulting in a 0.5 mg/ml PI(3)P solution.

2.14.2 Preparation of Large Unilamelar Vesicles

For LUVs lipids were mixed in chlorofrom as follows: 20 mol% Cholesterol, 47 mol% POPC, 10 mol% POPS, 20 mol% POPE and 3 mol% PIPs (PI(3)P, PI(3,5)P_2 or PI(4,5)P_2) with a total lipid amount of 1 mg. For LUVs lacking PIPs 50 mol% of POPC was used instead. Lipids were transfered to a glass vial (Duran, 8 x 70 mm), dried rotating under a nitrogen stream and dessicated in vacuum over night. Lipids were rehydrated in 1 ml reaction buffer (Table 2.1) for 30 min at roomtemperature and repeated vortexing for 1 min. The resulting opaque solution contained multi lamellar vesicles (MLVs). To obtain LUVs of defined size the MLV solution was extruded 20 times using a Mini-Extruder (Avanti) equipped with Nuclepore Track-Etch membranes with a pore size of 100 nm in diameter (Whatman).

2.14.3 Preparation Giant Unilamelar Vesicles

For GUVs lipids were mixed in chlorofrom as follows: 20 mol% Cholesterol, 44.9 mol% POPC, 10 mol% POPS, 20 mol% POPE, 0.1 mol% Lissamine-RhodamineB-PE and 5 mol% PI(3)P with a total lipid concentration of 5 μg/μl. For GUVs lacking PIPs 49.9 mol% of POPC was used instead. To obtained thin lipid films 7 μl lipid mix were applied to platinum electrodes and dried in vacuum for 1 h. Lipids were rehydrated in 350 μl 600 mOsm sucrose in self-made teflon chambers. Electroswelling of GUVs was performed as previously described by applying an AC field of 2 V and 10 Hz for 1.5 h at roomtemperature [205]. Detachment of GUVs was obtained by an AC field of 2 V and 2 Hz for 30 min at roomtemperature. GUVs were incubated with proteins for fluorescence microscopy as described below (Chapter 2.16).

2.14.4 Preparation of Supported Lipid Bilayers

For SLBs lipids were mixed in chlorofrom as follows: 20 mol% Cholesterol, 46.9 mol% POPC, 10 mol% POPS, 20 mol% POPE, 0.1 mol% Lissamine-RhodamineB-PE and 3 mol% PI(3)P with a total lipid concentration of 5 μg/μl. For SLBs containing lower concentrations or no PI(3)P POPC was adjusted to accordingly. First, MLVs were prepared by drying 100 μl of the lipid mix in a glass vial rotating under nitrogen stream and dessication in vacuum for 1 h. Lipids were rehydrated in reaction buffer (Table 2.1) and vortexed to obtain an opaque MLV solution. Aliquots of 20 μl were frozen at -20°C until use. For small unilamellar vesicle formation MLV stocks were diluted 10-fold and sonicated in a Sonorex Digitec (Bandelin) for 10 min at 30°C resulting in a clear solution. Reaction chambers were prepared as follows. As membrane support coverslips (#1.0 Menzel) were plasma-cleaned for 5 min. An eppendorf tube with cut-off

tip was glued on top of the coverslip using Norland Optical Adhesive 63 polymerized for 15 min under UV light. 180 μl SUV solution were deposited onto coverslips and fusion of SUVs was induced by addition of $CaCl_2$ in a final concentration of 2 mM. After 20 min incubation at roomtemperature unbound SUVs were removed by repeated washing with reaction buffer.

2.15 Biacore Measurements

To determine lipid binding specificity of Atg18 surface plasmon resonance (SPR) measurements were employed with LUVs containing different PIPs or no PIPs, prepared as described above (Chapter 2.14.2). Measurements were carried out on a Biacore 2000 instrument using an L1-chip and BIACORE 2000 control software (Version 3.2, GE Healthcare). The L1 chip consists of a dextran surface functionalized with alkyl groups that capture membrane vesicles [206].
Each flow cell of an L1 chip was loaded with one specific type of LUVs (no PIP, PI(3)P, PI(3,5)P_2 or PI(4,5)P_2) to obtain a change in signal of ΔRU = ~5000. Atg18 solutions of 39 nM to 5 μM were prepared in reaction buffer (Table 2.1). Binding of $Atg18^{wt}$ or $Atg18^{FKKG}$ to immobilized LUVs was examined by consecutively passing increasing concentrations of protein over LUVs at a flow rate of 10 μl/min for a contact time of 10 min. Dissociation was monitored by passing reaction buffer over LUVs at a flow rate of 10 μl/min for 10 min. After each round of protein binding and unbinding remaining proteins were removed by washing with 50 mM NaOH, 137.5 mM NaCl with a flow rate of 30 μl/min for 1 min followed by a second washing step with 50 mM HCl, 137.5 mM NaCl with a flow rate of 30 μl/min for 1 min. Binding and unbinding were monitored as change in resonance units.
For evaluation raw data of three measurments were exported and separately evaluated with Excel and Origin 9.1 (OriginLab). To correct for PIP-independent membrane or chip binding of proteins values obtained for LUVs without PIPs were subtracted from values for LUVs with PIPs using equation 2.1. The mean of the last five resonance units values during protein association phase of each corrected binding curve (RU_{corr}) were plotted against the respective protein concentrations. For an initial estimation of the binding affinity experimental data of three replicates were fitted using an equilibrium 1:1 Langmuir binding model (equation 2.2). The mean and standard deviation of values obtained by each fit were calculated.

$$RU_{\mathrm{corr}}(t) = RU_{\mathrm{PIP}}(t) - RU_{\mathrm{noPIP}} \tag{2.1}$$

With $RU_{corr}(t)$ being the corrected resoncance unit signal for specific PIP-containing LUVs, $RU_{PIP}(t)$ being the raw signal intensities obtained by passing protein over LUVs with certain PIPs and RU_{noPIP} being the raw signal intensities obtained by passing protein over LUVs without PIPs.

$$RU_{corr} = \frac{\frac{1}{K_D} \cdot C \cdot R_{max}}{\frac{1}{K_D} \cdot C + 1} \tag{2.2}$$

With RU_{corr} being the corrected binding signal of proteins passing over LUVs with sepcific PIPs, K_D being the equilibrium dissociation constant, C being the protein concentration and R_{max} being the maximal resonance units signal reflecting the maximum binding capacity.

2.16 Fluorescence Microscopy of *In Vitro* Systems

2.16.1 Membrane Binding of PROPPINs and Recruitment of Downstream Factors

To visualize PROPPIN membrane binding and membrane recruitment fluorescently labeled proteins were incubated with GUVs prepared as described above (Chapter 2.14.3) in a total reaction volume of 200 μl reaction buffer (Table 2.1) and imaged by confocal microscopy. In order to obtain comparable results for different reaction mixtures all labeled proteins were adjusted to a labeling efficiency of 25%. For membrane binding experiments of PROPPINs Atg18^{PacificBlue} or Atg21^{PacificBlue} in SEC buffer were deposited onto LabTek #1.0 Borosilicate chambers coated with 5 mg/ml BSA to prevent proteins from sticking to chamber surfaces. GUVs in 600 mOsm sucrose were added gently stirring in a 1:1 (v/v) ratio resulting in a final PROPPIN concentration of 0.5 μM and a buffer composition of 12.5 mM Tris (pH 7.2), 137.5 mM NaCl, 300 mOsm sucrose. To examine potential membrane recruitment functions of PROPPINs, Atg12–Atg5^{Alexa488}-Atg16 were incubated with GUVs either in absence or in presence of PROPPINs. Protein mixtures (Atg12–Atg5^{Alexa488}-Atg16, Atg12–Atg5^{Alexa488}-Atg16 + Atg18^{PacificBlue} , Atg12–Atg5^{Alexa488}-Atg16 + Atg21^{PacificBlue}) were prepared in 100 μl SEC buffer. Proteins were deposited onto LabTek chambers and mixed with GUVs as described above, resulting in a concentration of 0.5 μM for each protein.

After incubation for 15 min at roomtemperature membrane binding of proteins was examined with a ZEISS (Jena, Germany) LSM780 confocal laser scanning microscope equipped with a ZEISS Plan-APO 63x/NA1.46 oil immersion objective. Images of GUVs were acquired using the ZEN2011 software with 405 nm (PacificBlue, PROPPINs),

488 nm (AlexaFluor488, Atg12–Atg5) and 561 nm (Lissamine-RhodamineB, membrane) laser line.

2.16.2 Atg8-Lipidation on GUVs

To assess the influence of PROPPINs on Atg8–PE formation GUVs were incubated with the complete purified Atg8-lipidation machinery in absence or presence of Atg18 or Atg21. First, Atg7, Atg3 and Atg8ΔR$^{\text{Alexa488}}$ were mixed in 25 μl per reaction in SEC buffer supplemented with DTT and ATP and incubated for 30 min at 30°C for formation of thioester intermediates. Atg12–Atg5 and Atg16 were mixed in 25 μl per reaction SEC buffer and incubated for 30 min on ice for Atg12–Atg5-Atg16 complex formation. Protein pre-mixes were combined in SEC buffer in absence or presence of Atg18$^{\text{PacificBlue}}$ or Atg21$^{\text{PacificBlue}}$ in a final volume of 100 μl. These protein solutions were mixed in a 1:1 ratio with GUVs in 600 mOsm sucrose. The final concentrations were 0.5 μM PROPPIN$^{\text{PacificBlue}}$ (if present), 0.5 μM Atg12–Atg5, 0.5 μM Atg16, 1 μM Atg3, 1 μM Atg7, 3 μM Atg8ΔR$^{\text{Alexa488}}$, 12.5 mM Tris (pH 7.2), 137.5 mM NaCl, 0.1 mM DTT, 0.5 mM ATP. Lipidation was carried out for 15 min at 30°C and was stopped by addition of DTT in a final concentration of 25 mM. GUVs, membrane bound protein and lipidation efficiency were monitore by confocal microscopy using a ZEISS Plan-APO 63x/NA1.46 oil immersion objective. Images of GUVs were acquired using the ZEN2011 software with 405 nm (PacificBlue, PROPPINs), 488 nm (AlexaFluor488, Atg8) and 561 nm (Lissamine-RhodamineB, membrane) laser line.

2.16.3 Mobility of Lipidated Atg8 and Membrane on GUVs

To investigate whether PROPPINs have an influence on the mobility of Atg8–PE lipidation, reactions were performed as described in Chapter 2.16.2. Mobility was assessed by fluorescence recovery after photobleaching (FRAP). Therefore, ~10% of the GUV surface was bleached using 405 nm, 488 nm and 561 nm laser lines at 100% in one to three iterations. Fluorescence recovery was monitored in all channels (blue = PROPPIN, green = Atg8, red = membrane) for 90 s in 2 s intervals. Kymographs were obtained using the MultipleKymograph plugin for ImageJ (written by J. Rietdorf and A. Seitz, EMBL). To analyse the mobility of Atg8 and the membrane double normalization of FRAP data was performed as described by Phair et al. [207]. Fluorescence intensities were measured as demonstrated in Figure 2.1 for the bleached area (I_{frap}, orange), for the complete GUV rim (I_{whole}, blue) and at a position next to the GUV observing the background fluorescence (I_{bkg}, pink). Fluorescence values were corrected for background levels and fluorescence loss during the bleach pulse and following acquisition as described

in equation 2.3 [207].

$$I_{\text{frap-norm}}(t) = \frac{I_{\text{frap}}(t) - I_{\text{bkg}}(t)}{I_{\text{frap}}(prebl) - I_{\text{bkg}}(prebl)} \cdot \frac{I_{\text{whole}}(prebl) - I_{\text{bkg}}(prebl)}{I_{\text{whole}}(t) - I_{\text{bkg}}(t)} \tag{2.3}$$

With I(t) being the fluorescence intensity at a certain time t and I(prebl) being the fluorescence intensity before bleaching.

Normalized data were fitted with a single exponential function using Origin 9.1 (equation 2.4).

$$f(t) = y_0 + A \cdot e^{\frac{-t}{\tau}} \tag{2.4}$$

With f(t) being the fitted intensity value at a time t, y_0 being the fitted intensity at time t_0, A being the amplitude of the exponential function and τ altering the bending of the exponential function.

The mobile fraction was calculated as described in equation 2.5:

$$M = \frac{-A}{1 - (y_0 + A)} \tag{2.5}$$

With M being the mobile fraction and y_0 being the fitted intensity at time t_0, A being the amplitude of the exponential function as described in equation 2.4.

Finally the time ($t_{1/2}$) needed for membrane or Atg8 to recover to its half maximal value was calculated by equation 2.6:

$$t_{1/2} = -\tau \cdot ln(0.5) \tag{2.6}$$

With τ obtained by the fit with equation 2.4.

2.16.4 Atg8-lipidation on SLBs

To assess the influence of PROPPINs on Atg8-PE formation in a second membrane system SLBs were incubated with the complete purified Atg8-lipidation machinery in absence or presence of Atg18 or Atg21. First, Atg7, Atg3 and Atg8ΔR$^{\text{Alexa488}}$ were mixed in reaction buffer (25 μl per reaction) supplemented with DTT and ATP and incubated for 30 min at 30°C for formation of thioester intermediates. Atg12–Atg5 and Atg16 were mixed in reaction buffer (25 μl per reaction) and incubated for 30 min

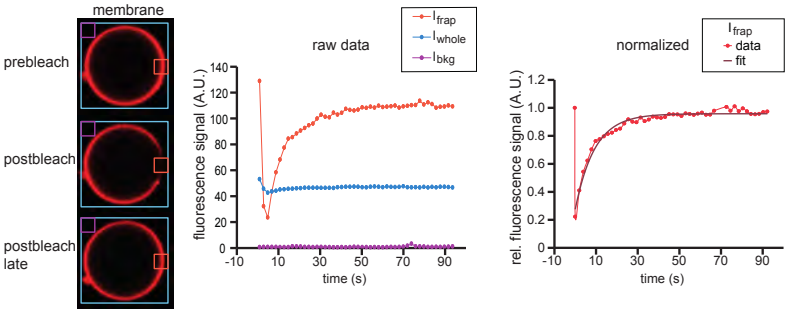

Figure 2.1: Double normalization of FRAP data. Three different ROIs are defined for each experiment. One in the bleached region (orange), one covering the complete GUV rim (blue) and one besides the GUV to monitor background fluorescence. Fluorescence intensities of these three ROIs are monitored over time, I_{frap}, I_{whole}, I_{bkg}. I_{bkg} is used to correct for background fluorescence and I_{whole} to correct for the loss of total fluorescence signal during bleaching and subsequent image acquisition. Double normalization results in $I_{frap\text{-}norm}$ values with a maximum of 1 for fitting.

on ice for Atg12–Atg5-Atg16 complex formation. Protein pre-mixes were combined in reaction buffer in absence or presence of Atg18^{PacificBlue} or Atg21^{PacificBlue} and added on top of SLBs in a final volume of 200 μl. The final concentrations were 0.5 μM PROPPIN^{PacificBlue} (if present), 0.5 μM Atg12–Atg5, 0.5 μM Atg16, 1 μM Atg3, 1 μM Atg7, 3 μM Atg8ΔR^{Alexa488}, 12.5 mM Tris (pH 7.2), 137.5 mM NaCl, 0.1 mM DTT, 0.5 mM ATP. Lipidation was carried out for 30 min at roomtemperature and was stopped by addition of DTT in a final concentration of 25 mM. Atg8 not covalently attached with the membrane was removed by washing three times with 500 μl lipidation buffer. Lipidation efficiency was monitore by confocal microscopy using a ZEISS Plan-APO 63x/NA1.46 oil immersion objective. Images of GUVs were acquired using the ZEN2011 software with 405 nm (PacificBlue, PROPPINs), 488 nm (AlexaFluor488, Atg8) and 561 nm (Lissamine-RhodamineB, membrane) laser line. Alternatively, a ZEISS (Jena, Germany) LSM510 equipped with a 40x/NA1.2 UV-VIS-IR C Apochromat water-immersion objective was used with laser lines 405 nm (PacificBlue, PROPPINs), 488 nm (AlexaFluor488, Atg8) and 561 nm (Lissamine-RhodamineB, membrane).

2.17 Total Internal Reflection Fluorescence Microscopy

For single-molecule detection by fluorescence microscopy it is critical to optimize signal-to-noise ratio. This can be technically achieved in two ways. Confocal microscopy uses a pinhole in the emission lightpath to exclude photons emitted from molecules that are not in the focal point. On the other hand TIRF microscopy restricts the illuminated volume and thereby reduces background fluorescence from out of focus molecules.

When light travels from a medium of higher (glass) to one of lower (water) refractive index the angle of the beam is changed according to Snell's law. If the laser beam hits the media interface at a specific critical angle the light travels parallel to the glass-to-water interface. In case of an incident angle larger than the critical angle the incident light is totally reflected at the glass-to-water interface. Thereby an evanescent field is generated that exponentially declines in intensity with increasing distance to the reflection surface. Consequently, fluorescent molecules in close proximity (about 200 nm) to the coverslide can be excited. Due to the limited thickness of illuminated sample a good resolution in z-direction is achieved and signal-to-noise ratio is improved. However, observations are limited to the proximity of the coverslide. Therefore, TIRF microscopy is often used for single-molecule measurements of surface bound molecules such as membrane associated proteins [208].
For TIRF microscopy experiments SLBs were prepared as described above (Chapter 2.14.4) with varying concentrations of PI(3)P. Different concentrations (1.5 nM to 500 nM) $Atg18^{Alexa633}$ were incubated with SLBs in reaction buffer for 15 min. TIRF imaging was performed on a ZEISS Axio Observer.D1 equipped with 100X Alpha Pln-Apo/NA1.46 Oil objective, a ZEISS TIRF-slider and a custom made laser box (Acal BFi). $Atg18^{Alexa633}$ was excited with a 640 nm laser line and fluorescence images were acquired with an Andor iXon Ultra 897 EM-CCD camera with a gain of 300 and an acquisition time of 10 ms.

2.18 Atomic Force Microscopy

Atomic Force Microscopy (AFM) is based on interactions of a pointed tip with a surface. The tip is mounted onto a cantilever with defined spring constant. The sample surface is scanned with the tip with specific speed and force. A laser is focused on the back of the tip and is reflected to a quadrant detector. In ground position the reflected laser beam hits the detector in the middle. When the tip encounters an obstacle on the sample surface the cantilever is bent and the reflected laser light is detected at a different position of the quadrant detector. Considering the spring contant of the cantilever a height profile is calculated. Consequently, the resolution of AFM does not depend on the laser wavelegth, but on the tip which allows for very high resolution images [209].
For AFM measurements performed in this thesis, SLBs were prepared on plasma-cleaned glass as described in Chapter 2.14.4 containing 0.5 mol% PI(3)P. Atg18 was incubated with membranes in indicated concentrations for 15 min at roomtemperature. Images were acquired using a Nanowizard III BioAFM (JPK Instruments) equipped with a BioLever BL-AC40TS-C2 (Olympus). The samples were scanned in tapping mode with an oscillation frequency of 20 to 25 kHz, a scan rate of 0.9 Hz and a setpoint of ~0.6 V

(constantly readjusted during the measurement). Images were processed using the polynomial line fit algorithms of JPKSPM Data Processing Software v4.2.47 (JPK Instruments). The particle size was estimated using Gwyddion v2.30 (Czech Metrology Institute). Lines were drawn accross particles to obtain height profiles. The diameter obtained by these profiles was roughly corrected for the tip size, subtracting 20 nm from raw data.

Results

3.1 Purification of PROPPINs

Autophagy is a well conserved pathway that delivers cytoplasmic cargo to the vacuole for degradation [62]. During autophagy a cup shaped membrane is formed *de novo* sequestring cargo An essential step is the covalent attachment of Atg8 to the growing membrane resulting in Atg8–PE. Two pools of Atg8–PE exist at the phagophore and serve different functions. The concave Atg8–PE pool tethers phagophore and cargo by interaction with cargo-adaptors for specific uptake by the autophagosome [22]. Atg8 has also been suggested to form a membrane scaffold on the convex face of autophagosomes [21], thereby, regulating the size of autophagosomes [89]. How these different Atg8–PE pools are generated is, however, not yet understood. Interestingly, recruitment of Atg8 to the PAS critically depends on PI(3)P within the phagophore membrane. The two PI(3)P effectors, Atg18 and Atg21, are subsequently recruited to the PAS by binding PI(3)P and potentially other Atg proteins [88]. Yeast PROPPINs have been reported to play roles in different autophagy pathways. While Atg21 is believed to be essential for the Cvt pathway [132, 139] but dispensable for autophagy, Atg18 is crucial for both selective and non-selective autophagy [138]. Atg18 has been proposed to play an essential role in late steps of autophagosome formation [90], including Atg9 cycling, phagophore expansion and closure [90, 99, 123]. In mammalian cells, WIPI-2B (an Atg18 homolog)

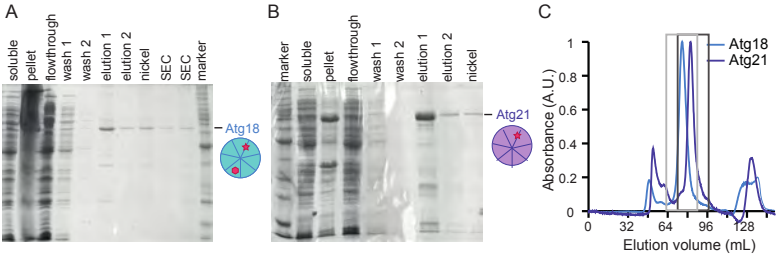

Figure 3.1: Purification of PROPPINs. PROPPINs were expressed in *E. coli* as N-terminal His_6 conjugates. Samples were taken at different steps of Ni^{2+}-affinity purification and size exclusion chromatography (SEC) and analyzed on an SDS-PAGE(A,B). Cartoons show β-propellers of Atg18 (cyan) and Atg21 (purple) with PI(3)P- (star) and Atg2-(hexagon) binding sites. (C) SEC elution profiles of PROPPINs suggest monomeric soluble proteins and pooled fractions are indicated by grey boxes (light = Atg18, dark = Atg21).

has recently been shown to promote and direct lipidation of the mammalian Atg8 homolog (LC3) to the growing phagophore. In *S. cerevisiae*, however, no such function for Atg18 has been described. In contrast, a recent study revealed that Atg21 recruits

Atg12–Atg5-Atg16 to the PAS under vegetative conditions, resulting in efficient recruitment of the Ub-like conjuagtion machinery to the PAS [155]. Therefore, PROPPINs are, due to their previously reported activity in recruiting the Ub-like conjugation machinery to the PAS, good candidates to regulate Atg8-distribution and thus Atg8-function at the phagophore. To determine whether both PROPPINs are in principle able to promote Atg8-lipidation, a minimal system was used to analyse their function. This system consisted of the two autophagic Ub-conjugation systems and the two PROPPINs omitting any additional factors. Therefore, PROPPINs as well as the Atg8 lipidation machinery were expressed and purified for further investigations.

PROPPINs were expressed in *E. coli* with an N-terminal His_6-tag. After Ni^{2+}-affinity purification and size exculsion chromatography (SEC) proteins of high purity were obtained. In case of Atg18 two stable degradation products were detected on SDS-PAGE gels (Figure 3.1 A). Liquid chromatography and mass spectrometry (LC-MS) analysis was used to determine the mass of degradation products and compared to the masses of possible Atg18 fragments. Thereby, the fragments were found to result from a cleavage between residues T204 and K205. The amount of these cleavage products was reduced by a small culture volume per flask and fast sample processing. Atg21 was not degraded and highly pure and stable recombinant protein was produced (Figure 3.1 B). To exclude that PROPPINs were aggregating, as it has been suggested by previous studies [135, 136], dynamic light scattering measurements (DLS) were performed (Appendix Figure A.1). The results showed that Atg18 was monomeric and monodispers, which is in agreement with SEC-profiles observed (Figure 3.1 C). These proteins were used for further experiments to characterize their membrane binding behavior and functions on assumed downstream proteins. For microscopy experiments proteins with and additional N-terminal cysteine were expressed. Fluorescence dyes were coupled to cysteins via a maleimide group attached to the dye and free dye was removed using a desalting column.

3.2 PROPPIN Membrane Binding Specificity

With these proteins in hand, their functional characterization *in vitro* was possible. As can be inferred from their name, PROPPINs have been shown to bind phosphoinositides (PIPs) and their subcellular localization depends on PI(3)P and $PI(3,5)P_2$ [88, 131–134]. The phosphoinositide binding motif was identified to be a conserved FRRG-motif in the loop between blade 5 and blade 6 of the β-propeller forming two basic binding pockets [135, 136]. To establish an *in vitro* assay and to confirm PIP-binding activity of purified PROPPINs, two model membrane systems were used.

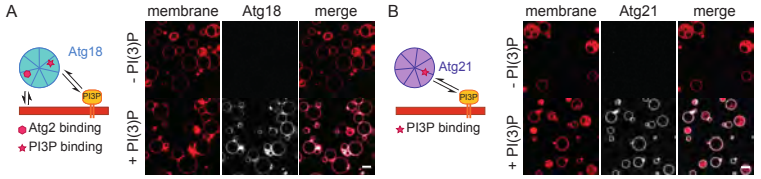

Figure 3.2: PROPPINs bind GUVs by interaction with PI(3)P. Cartoons show the experimental setup. PROPPINs were incubated with GUVs containing no or 5 mol% P(3)P and imaged by confocal fluorescence microscopy. Both PROPPINs bind membranes dependent on PI(3)P (A,B). Atg18 does not need additional Atg2-binding for membrane recruitment (A). Scale bars = 10 μm

Giant unilamellar vesicles (GUVs) have a diameter of 1 - 100 μm and can be visualized by adding small amounts of fluorescence-labeled lipids. Therefore, GUVs are an extensively used system for microscopy-based studies on protein-membrane-interactions and functions [69, 210]. Another advantage of these model membranes is the possibility to use defined lipid compositions. Thereby, it is possible to identify specific lipids as binding partners for proteins in their native environment. In this thesis, a lipid mix resembling endosomal membrane composition was used. Electroformation of GUVs was performed in a sucrose solution as described in Chapter 2.14.3. GUVs containing no or 5 mol% PI(3)P were incubated with 0.5 μM Atg18$^{\text{PacificBlue}}$ or Atg21$^{\text{PacificBlue}}$ and imaged by confocal fluorescence microscopy. Both PROPPINs were homogeneously distributed on GUVs binding in a PI(3)P-dependent manner (Figure 3.2). Of note, homogeneous distribution of PROPPINs was dependent on homogeneous PI(3)P incorporation. This was achieved only if PI(3)P was protonated prior to preparation of the lipid mix as described in Chapter 2.14.1.

To further investigate Atg18-membrane-binding, large unilamellar vesicles (LUVs) with a diameter of 100 nm were used. LUVs contained either no PIPs or 3 mol% PI(3)P, PI(3,5)P_2 or PI(4,5)P_2, respectively. For Biacore measurements each flowcell of an L1 chip (GE Healthcare, Germany) was loaded with comparable amounts of one specific type of LUVs. Subsequently, a series of concentrations ranging from 39 nM to 5 μM of Atg18$^{\text{wt}}$ or Atg18$^{\text{FKKG}}$ was injected. Binding of Atg18$^{\text{wt}}$ and Atg18$^{\text{FKKG}}$ was observed in all flow cells with different overall binding capacity. In general two trends were observed. First, binding signals on LUVs with PIPs were always higher than for LUVs without PIPs (Appendix Figure A.1). This indicates that Atg18, in addition to PIP binding, interacts with either LUVs independent of PIPs or with the chip surface. Second, for LUVs containing PI(3)P and PI(3,5)P_2 binding signals obtained for Atg18$^{\text{wt}}$ were higher compared to signals obtained for Atg18$^{\text{FKKG}}$ on LUVs with the same composition (Appendix Figure A.1). In contrast, similar binding signals were obtained for Atg18 variants on LUVs without PIPs or with PI(4,5)P_2. To correct for PIP-independent Atg18-LUV binding, signals obtained for LUVs without PIPs were subtracted from signals obtained

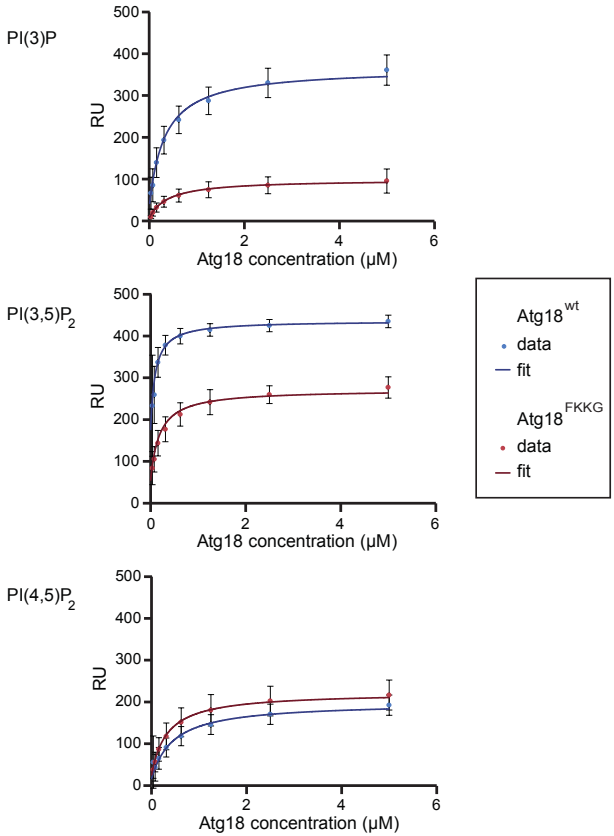

Figure 3.3: Atg18 binds to PI(3)P and PI(3,5)P_2 in LUVs. Atg18 wildtype (blue) and Atg18^{FKKG} (red) were probed for PIP-dependent membrane binding using Biacore. Each flow cell of an L1 chip was loaded with comparable amounts of distinct LUVs each containing 3 mol% of a specific PIP or no PIPs. A series of concentrations ranging from 39 nM to 5 μM of Atg18^{wt} or Atg18^{FKKG} were passed over immobilized LUVs. Binding isotherms were estimated for LUVs with PIPs and fitted with a 1:1 Langmuir function. Here, mean ± SD of binding signals of three experiments are shown (puncta). Additionally, fits using a 1:1 Langmuir binding model are shown (lines). Binding of Atg18 to PI(3)P and PI(3,5)P_2 containing LUVs was partially dependent on its FRRG-motif. No FRRG-dependent interaction with PI(4,5)P_2 was observed.

for LUVs with PIPs. Saturation of binding places was observed for concentrations of ~2 μM (Appendix Figure A.2). The tendencies described for raw data were preserved. Although the number of available binding sites on the sensor-chip surface was kept constant, binding signals of $Atg18^{wt}$ were higher than that of $Atg18^{FKKG}$. This suggests that two different modes of binding are detected for $Atg18^{wt}$. To evaluate this possibility, binding isotherms were calculated from corrected binding data. Of note, in case of PI(3,5)P_2 containing LUVs binding did not reach the equilibrium. Therefore, the corresponding isotherm serves only as an estimate. Data were fitted with Origin (OriginLab, version 9.1) with a either one or two exponentials. For all data sets no significant improvement of the fit quality, estimated from adjusted R^2 values, was observed for equations with two exponentials compared to equations with one exponential. Consequently, all data were fitted with a 1:1 Langmuir fit and binding parameters obtained are listed in Table A.3 and Table A.2. Dissociation constants (K_D) obtained by fitting did not reveal a significant difference in binding affinities between $Atg18^{wt}$ and $Atg18^{FKKG}$ for LUVs with PIPs. Still, while for LUVs with PI(3)P ($K_{D\text{-}wt}$ = 300 ± 100 nM, $K_{D\text{-}FKKG}$ = 370 ± 60 nM) or PI(3,5)P_2 ($K_{D\text{-}wt}$ = 60 ± 30 nM, $K_{D\text{-}FKKG}$ = 150 ± 60 nM) K_D values were increased for $Atg18^{FKKG}$ compared to $Atg18^{wt}$, the opposite trend was observed for LUVs with PI(4,5)P_2 ($K_{D\text{-}wt}$ = 400 ± 200 nM, $K_{D\text{-}FKKG}$ = 300 ± 100 nM). Since K_D values obtained for sequential measurement series show the tendency towards higher values for later series a systematic error cannot be excluded (Table A.3). Possible explanations are that either the protein loses activity over time or PIPs in LUVs are unstable.

As expected from raw binding data the values obtained for maximum binding (R_{max}) show that LUVs containing PI(3)P ($R_{max\text{-}wt}$ = 370 ± 20 RU, $R_{max\text{-}FKKG}$ = 100 ± 30 RU) or PI(3,5)P_2 ($R_{max\text{-}wt}$ = 436 ± 6 RU, $R_{max\text{-}FKKG}$ = 270 ± 20 RU), but not LUVs containing PI(4,5)P_2 ($R_{max\text{-}wt}$ = 200 ± 10 RU, $R_{max\text{-}FKKG}$ = 220 ± 30 RU) provide more binding places for $Atg18^{wt}$ than for $Atg18^{FKKG}$. For R_{max}, values of sequential experiments showed only little decrease from the first to the third run. Therefore, instability of Atg18 proteins seems to be the cause for the decrease of K_D values. Thus, biacore data confirm that Atg18 binds to PI(3)P and PI(3,5)P_2 with its FRRG motif [88, 131–134]. A reliable determination of K_D values was, however, not possible.

3.3 PROPPINs Recruit the Atg12–Atg5-Atg16 Complex to Membranes *In Vitro*

Recent studies in human and yeast revealed that PROPPINs are involved in determining the localization of Atg8-lipidation. Atg8-lipidation had previously been demonstrated to be catalyzed by two interconnected Ub-like conjugation systems with Atg12–Atg5 being

the E3-like ligase for Atg8-PE formation [45, 162]. In addition, Atg12–Atg5-Atg16 form a complex [160] and targeting of Atg8-lipidation to the PAS is mediated by Atg16 [112, 163]. The potential of yeast PROPPINs to recruit the Ub-like conjugation system to membranes was investigated using purified Atg12–Atg5 and Atg16 with GUVs as model membranes. For visualization Atg12–Atg5 was fluorescence labeled with AlexaFluor488. GUVs containing 5 mol% PI(3)P were prepared as described above and incubated with 0.5 μM Atg12–Atg5$^{\text{Alexa488}}$-Atg16 in presence or absence of 0.5 μM PROPPINs. To monitor membrane localization PROPPINs were labeled with PacificBlue. Atg12–Atg5-Atg16 localized to GUV membranes very inefficiently in distinct patches. Upon addition of Atg21, however, Atg12–Atg5-Atg16 was efficiently recruited to GUVs (Figure 3.4 B). This is in good agreement with data published recently during this study revealing that Atg21 targets Atg12–Atg5-Atg16 to the PAS in vegetative growth [155]. Surprisingly, the same effect was observed for Atg18 (Figure 3.4 A), leading to homogeneous distribution of Atg12–Atg5-At16 at the GUV membrane. Therefore, both PROPPINs recruit Atg12–Atg5-Atg16 to membranes *in vitro*.

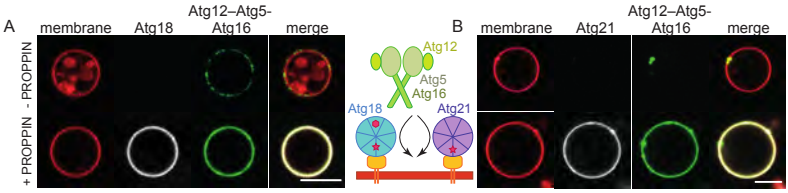

Figure 3.4: PROPPINs recruit Atg12–Atg5-Atg16 to membranes *in vitro*. The experimental setup is shown schematically. Atg12–Atg5$^{\text{Alexa488}}$-Atg16 was incubated with GUVs containing 5 mol% PI(3)P in absence or presence of PROPPINs$^{\text{PacificBlue}}$. Weak, inhomogeneous membrane binding of Atg12–Atg5-Atg16 is observed in absence of PROPPINs. Atg18 and Atg21 recruit Atg12–Atg5-Atg16 to membranes efficiently and lead to homogeneous distribution. Scale bars = 10 μm

To investigate whether PROPPIN-Atg12–Atg5-Atg16 complexes form a scaffold-like structure as observed for Atg8-Atg12–Atg5-Atg16 [21], FRAP experiments were performed on GUVs incubated with Atg12–Atg5-Atg16 and PROPPINs. As shown in Figure 3.5 A, B the membrane as well as all protein components are mobile. Therefore, no protein scaffold is formed by PROPPINs and the Atg12–Atg5-Atg16 complex. Mobile fractions and recovery half-life ($\tau_{1/2}$) were determined by fits with a single exponential. Recovery half-life of Atg12–Atg5-Atg16 was $\tau_{1/2} = 16 \pm 4$ s in samples containing Atg18. In these samples, recovery of Atg18 could not be determined because of extensive bleaching of PacificBlue. Interestingly, Atg21 recovered considerably faster ($\tau_{1/2} = 6.2 \pm 0.6$ s), but Atg12–Atg5-Atg16 recovered with the same speed as Atg21 ($\tau_{1/2} = 6.6 \pm 0.6$ s). This suggests that at least Atg21 forms a complex with Atg12–Atg5-Atg16 in solution and together they bind membranes by interaction with PI(3)P.

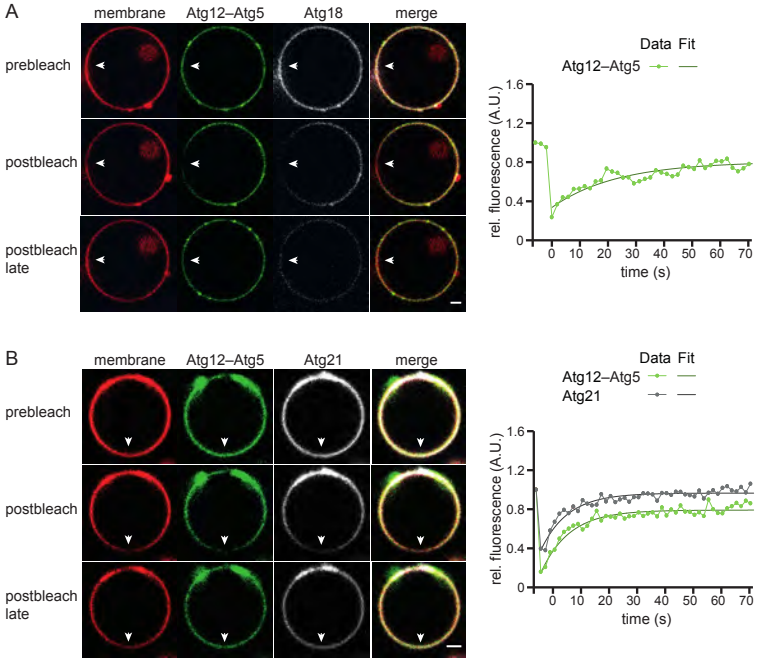

Figure 3.5: Mobility PROPPINs and Atg12–Atg5-Atg16 to membranes *in vitro*. Membrane recruitment of Atg12–Atg5-Atg16 by Atg18 (A) or Atg21 (B) was tested on GUVs containing 5 mol% PI(3)P. Mobility of proteins was analyzed by FRAP (left panel). Fluorescence recovery was monitored for 70 sec and normalized data were fitted using a single exponential function (right panel). (A) Atg18 seems to fully recover, but analysis is hampered by strong bleaching. A large fraction of Atg12–Atg5-Atg16 recovers as well. (B) Atg21 fully recovers and a large fraction of Atg12–Atg5-Atg16 recovers as well. scale bar = 2 μm

Analysis of mobile fractions (MF) showed that Atg21 fully recovers ($MF_{Atg21} = 94 \pm 1\%$) and Atg12–Atg5-Atg16 is largely mobile ($75 \pm 1\%$). Taken together these data strongly suggest that PROPPINs form a complex with Atg12–Atg5-Atg16 in solution and this complex is targeted to membranes by interaction of PROPPINs with PI(3)P. Differences in mobile fractions suggest that about 75% of PROPPINs are bound to an Atg12–Atg5-Atg16 complex in the setup tested. These data raised the question whether recruitment of Atg12–Atg5-Atg16 facilitates Atg8-lipidation.

3.4 Influence of PROPPINs on Atg8-Lipidation *In Vitro*

Membrane recruitment of Atg12–Atg5-Atg16 by Atg18 and Atg21 suggests that both PROPPINs can facilitate Atg8-lipidation. In contrast, previous studies in yeast suggested that only Atg21 facilitates Atg8-lipidation [132]. In mammalian cells, however, WIPI-2B (an Atg18 homolog) enhances LC3-lipidation (mammalian Atg8 homolog) [150]. To further characterize the molecular function of yeast PROPPINs, Atg8-lipidation was analyzed using supported lipid bilayers (SLBs) as model membranes. SLBs containing 3 mol% PI(3)P were incubated with the complete Atg8-lipidation machinery in absence or presence of PROPPINs labeled with PacificBlue. Atg8^{Alexa488} was used to monitor lipidation. To prevent the reaction from reaching saturation, lipidation was terminated by adding DTT. Free Atg8 was removed and lipidation efficiency was assessed by fluorescence microscopy. Consistent with a previous study [21], Atg8-lipidation could be observed in absence of PROPPINs (Figure 3.6 A,B upper panel). Interestingly, both PROPPINs enhanced Atg8-lipidation, as can be seen by the increased Atg8^{Alexa488} signals in presence of PROPPINs compared to reactions without PROPPINs (Figure3.6 A,B lower panel).

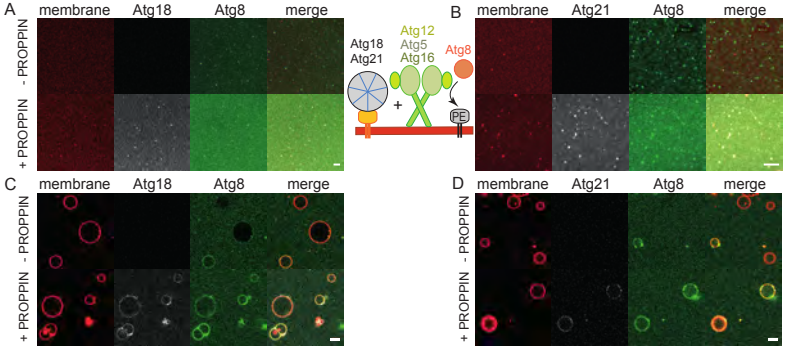

Figure 3.6: PROPPINs promote Atg8-lipidation *in vitro*. Two synthetic membrane systems were used to investigate the influence of PROPPINs on Atg8-lipidation as indicated in the cartoon. SLBs were incubated with proteins of the lipidation machinery in absence or presence of PROPPINs. Atg8-lipidation was monitored using Atg8^{Alexa488} and PROPPIN-membrane binding was examined by PROPPIN^{PacificBlue}. Atg8-lipidation efficiencies were determined by confocal fluorescence microscopy. Atg8 is lipidated on SLBs in absence of PROPPINs, but lipidation is strongly enhanced in presence of Atg18 (A) and Atg21 (B). Second, lipidation was performed on GUVs and stopped after 15 min. In presence of Atg18 (C) or Atg21 (D) more Atg8-decorated GUVS and higher Atg8-intensity on GUVs was observed. Scale bars = 10 μm

To confirm these results, GUVs were used as an alternative membrane system. GUVs were prepared as described in Chapter 2.14.3 containing 3 mol% PI(3)P. Lipidation

reactions were performed as described for SLBs in absence or presence of PROPPINs. However, reactions were stopped after 15 minutes incubation at 30 °C by addition of DTT. Imaging of GUVs by confocal fluorescence microscopy confirmed results obtained for Atg8-lipidation on SLBs. In presence of either Atg18 or Atg21, an increased number of GUVs positive for Atg8 was observed. Furthermore, the Atg8-intensity on GUV membranes was enhanced in presence of either PROPPIN (Figure 3.6 C,D). These data thus demonstrate that both PROPPINs have similar functions *in vitro*. They promote lipidation of Atg8 by recruiting the E3-like enzyme Atg12–Atg5-Atg16 to PI(3)P-positive membranes. This is consistent with the fact that PI(3)P acts upstream of the Atg8-lipidation machinery in yeast [112].

3.5 Does Atg18 alter Atg8-Atg12–Atg5-Atg16 scaffold formation?

Since PROPPINs influence lipidation efficiency the next question to address was whether they alter the autophagic protein scaffold recently proposed [21]. For this purpose mobility of lipidated Atg8 on GUV membranes was analyzed using fluorescence recovery after photobleaching (FRAP). Atg8-lipidation on GUVs was performed as described above (Chapter 3.4). To obtain saturated lipidation the reaction was terminated by DTT addition after 1 h. Mobility of lipidated Atg8 on GUV membranes was determined by bleaching a small region of the GUV and the proteins attached to it. Fluorescence recovery of the membrane, Atg18 and Atg8 was monitored for 90 sec and mobile fractions as well as the recovery half-life were determined as described by Phair et al. [207].
As shown in Figure 3.7 and Figure 3.8 A the membrane fluorescence recovered almost completely, irrespective of the presence or absence of Atg18. MFs were 98 ± 4% without and 89 ± 6% with Atg18. In contrast, Atg8 recovery was strongly impaired (MF = 16 ± 6%) in samples without Atg18. This immobility was suggested to be caused by the formation of a protein scaffold consisting of Atg8 and Atg12–Atg5-Atg16 [21]. On GUVs with Atg18 the average mobility of Atg8 was not changed (MF = 26 ± 16%) compared to samples lacking Atg18, however, two situations were observed. Atg8 either recovered only to a small extent (MF = 5 ± 2%) or a larger fraction of Atg8 recovered (MF = 37 ± 8%, Figure 3.7 B,C and Figure 3.8 C, D). Two differences between GUVs with immobile Atg8 and GUVs with mobile Atg8 could be observed. First, the fluorescence intensity of Atg18 was weaker on GUVs with immobile Atg8. Second, Atg8 levels were weaker on GUVs with mobile Atg8. Therefore, the reason for the two different observations cannot be assigned unambiguously. Either Atg18 needs to be present at a certain treshold level to prevent scaffold formation, thereby mobilizing Atg8, or a critical amount of Atg8–PE

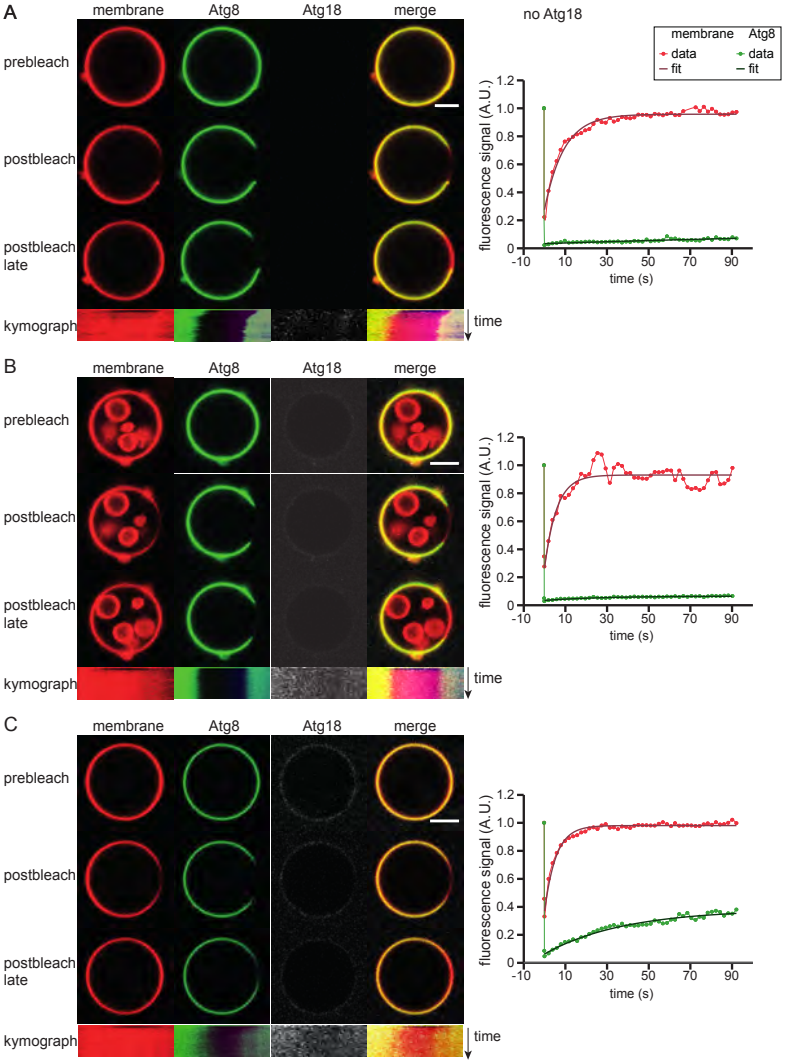

Figure 3.7: Atg8–PE mobility on GUVs in absence or presence of Atg18. Atg8-lipidation was performed in the absence (A) or presence (B,C) of Atg18 on GUVs containing 3 mol% PI(3)P. Mobility of membrane and Atg8 was analyzed by FRAP (left panel). Fluorescence recovery was monitored for 90 sec and normalized data were fitted using a single exponential function (right panel). (A) On GUVs without Atg18 the membrane recovers almost completely while the mobile fraction of Atg8 is small. (B, C) In presence of Atg18 membrane mobility is not altered significantly. Atg8 mobility is either comparable to reactions without Atg18 (B) or the mobile fraction is increased (C). scale bar = 5 μm

needs to be formed in order to promote scaffold assembly. The mobility of Atg18 could not be monitored in these experiments due to low signal-to-noise ratio.

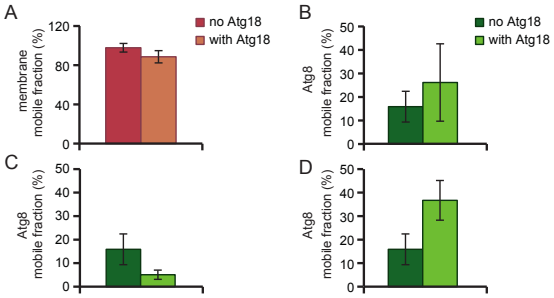

Figure 3.8: Quantification of membrane and Atg8 mobile fractions on GUVs. Mobile fractions of membrane and Atg8 were determined in absence or presence of Atg18 by fitting normalized fluorescence signals with a single exponential. (A) The membrane mobility is not significantly altered by Atg18. (B) The average mobility of Atg8 is not significantly altered by Atg18. (C) On GUVs with low Atg18 abundance Atg8 mobility is not significantly altered. (D) On GUVs with higher Atg18 abundance and lower Atg8 signal Atg8 mobility is increased. Bar graphs show mean ± SD, or mean ± SEM for N = 4 without Atg18, N = 6 with Atg18, N = 2 immobile Atg8 with Atg18, N = 4 mobile Atg8 with Atg18

3.6 Establishing Atomic Force Microscopy for Membrane Bound Atg18 *In Vitro*

Previous experiments provide evidence that PROPPINs facilitate Atg8-lipidation by recruitment of the E3-like ligase Atg12–Atg5-Atg16. AFM experiments demonstrated that Atg8 covalently attached to membranes forms an autophagic protein scaffold with Atg12–Atg5-Atg16 [21]. FRAP experiments did not reveal whether PROPPINs are incorporated into protein scaffolds. Consequently, the exact influence of PROPPINs on scaffold formation remains elusive. One hypothesis is that PROPPINs coordinate scaffold formation by defining the initiation site. Another possibility is that PROPPINs are incorporated into the scaffold. To test these hypotheses AFM-experiments were established.

If PROPPINs would only initiate scaffold formation, protein scaffold patches spreading radially from a PROPPIN should be observed. In contrast, if PROPPINs would be incorporated into the protein scaffold the topology would differ from the scaffold observed previously [21]. First, Atg18 concentrations suitable to detect single membrane bound proteins had to be established, since this is the basis to observe radial growth of the protein scaffold.

SLBs containing 0.5 mol% PI(3)P were prepared as described before on plasma cleaned-glass to obtain a flat surface. The membrane was incubated with 100 nM $Atg18^{Alexa488}$ for 15 min. Atg18-binding was monitored by confocal microscopy. Subsequently, excess protein was removed by washing with reaction buffer and the membrane was imaged with AFM in tapping mode to minimize dragging of membrane-bound particles by the cantilever tip. Interestingly, well separated particles on a largely intact membrane were observed (Figure 3.9 left panel). Using 400 nM Atg18 in the same experimental procedure, as expected, more particles were detected on the membrane. Two remarkable difference were observed compared to reactions with 100 nM Atg18. First, the membrane displayed a higher roughness after incubation with 400 nM Atg18 than after incubation with 100 nM Atg18. Second, protein particles preferentially localized to rough membrane areas. Furthermore, particles of different sizes were observed for both Atg18 concentrations (Figure 3.9 right panel). The size distribution of particle diameters corrected for the tip size was determined as described in Chapter 2.18 and depicted in a histogram (Figure 3.9 B). According to the size distribution two populations (P1 and P2) were defined. The average diameter of these populations was 5 ± 2 nm (P1) and 13 ± 3 nm (P2). In addition, some bigger structures were observed. Whether these large structures correspond to functional multimers or aggregates is not clear. To answer the question whether the two size populations correspond to different multimers of Atg18 the symmetry related molecules in the crystal structure of Hsv2, a PROPPIN homolog of Atg18 and Atg21, were analyzed [135, 136]. From these data it seems likely that Atg18 forms trimers (Figure 3.9 C). The diameter of monomeric (5.8 nm) and the edge length of trimeric (10.6 nm) Hsv2 were obtained from its crystal structure [136] and were found to be in good agreement with experimental data. Since PROPPINs are β-propeller proteins it is worth noticing that the β-propellers of β'-COP subunits mediate trimerization of corresponding coat proteins [211]. Therefore, it seems likely that particles of P2 represent Atg18-trimers. The frequency of small particles at membranes was increased from 12.5% (100 nM) to 41% (400 nM) for higher concentrations of Atg18. One possible explanation might be a lower membrane binding affinity of single Atg18 proteins compared to multimers. Consequently, the ratio of small spots to large spots would increase in higher concentrations if binding of multimers but not monomers is already reaching saturation.

Independent of the exact nature of larger spots a concentration of 100 nM Atg18 seems to be a suitable starting point to explore the influence of PROPPINs on scaffold formation. These results, therefore, provide the basis for further investigations on the influence of PROPPINs on autophagic scaffold formation. Furthermore, AFM seems suitable to answer the question whether PROPPINs form multimers on membranes.

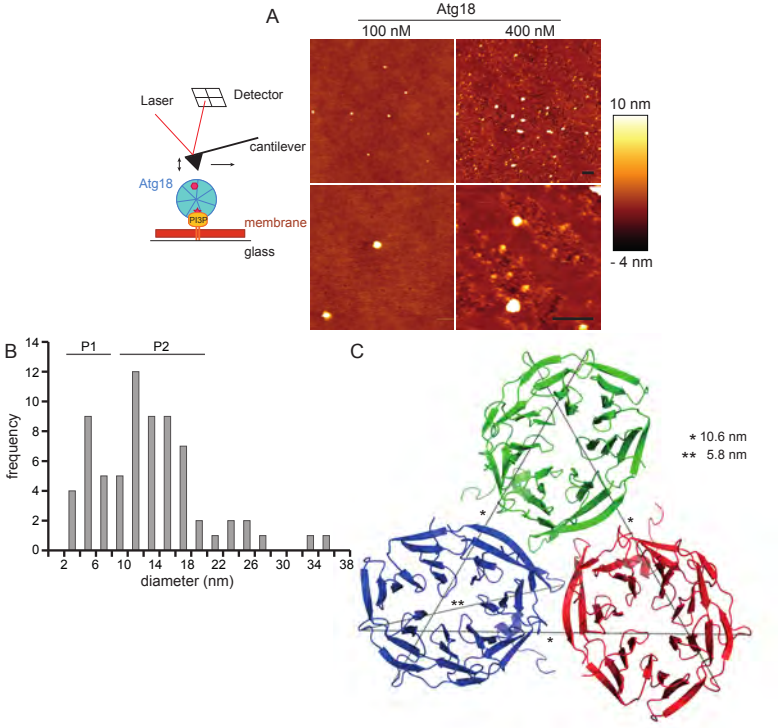

Figure 3.9: Establishing AFM experiments. The cartoon visualizes the principle of AFM measurements. Different concentrations of Atg18 were incubated with SLBs on plasma-cleaned glass slides containing 0.5 mol% PI(3)P. Membranes were probed with AFM in tapping mode. (A) When using 100 nM Atg18 well separated spots were observed on the membrane. The membrane was mostly intact with some small holes being detectable (left panel). For 400 nM Atg18 (right panel) membranes appeared more rough and protein spots of different sizes localize preferably to these rough membrane areas. (B) Size distribution of particles observed on membranes with two population being defined (P1, P2). (C) Symmetry-related molecules of the *K. lactis* Hsv2 crystal structure (PDB: 4AV8, [136]). Distances from crystal structures are depicted and correspond well to measured sizes. Scale bar = 200 nm

3.7 Establishing a Single Molecule Approach for Membrane Bound PROPPINs *In Vitro*

AFM is suited for high resolution imaging of the autophagic protein scaffold structure. Even though high speed AFM techniques are available two main reasons hamper the use of this technique to obtain temporal information on scaffold formation. First, fast repeated scanning might have an impact on membrane integrity without providing the possibility for real time observations. Second, proteins in solution frequently stick to the

tip reducing spatial resolution. To complement high spatial resolution of AFM experiments with dynamic measurements a single molecule total internal reflection fluorescence (TIRF) microscopy setup was established. The advantage of TIRF is, that reflection of the the laser beam on the glass surface evokes an evanescent energy field. This excitation energy drops exponentially with the distance to the surface. Thereby, only fluorophores in close proximity to the membrane are excited. This enables, on the one hand, detection of single molecules since background signals are strongly reduced. On the other hand, proteins bound to membranes can be observed since the membrane is immediately on top of the cover slide.

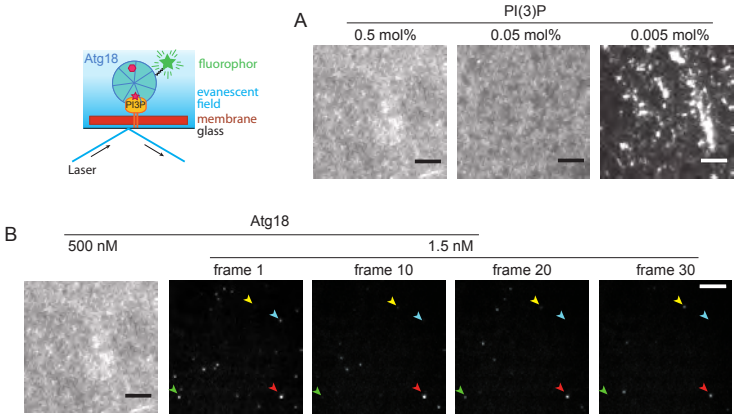

Figure 3.10: Single molecule TIRF of Atg18 bound to SLBs. The cartoon describes the experimental principle of TIRF microscopy and the setup used here. (A) Different concentrations of PI(3)P ranging from 0.5 mol% to 0.005 mol% were tested with constant amounts of Atg18. Decrease in total fluorescence signal was observed. For 0.005 mol% Atg18 clusters are formed. (B) Different concentrations of Atg18 were tested keeping PI(3)P concentration constant. An Atg18 concentration of 500 nM resulted in strong Atg18 signal covering the entire membrane (first panel). A concentration of 1.5 nM is suitable to detect single Atg18 spots with good separation (panels two to five). Repeated imaging reveals binding (yellow, green arrowhead) and unbinding (cyan, green arrowhead) events as well as stable binding (red arrowhead). The overall decrease in the number of fluorescent spots suggests fast bleaching. Scale bar = 5 μm

In these experiments conditions were established to obtain single, well separated spots of Atg18. First, SLBs with different concentrations of PI(3)P, ranging from 0.5 mol% to 0.005 mol%, in combination with constant concentrations of $Atg18^{Alexa633}$ were tested. For all PI(3)P concentrations Atg18 was inhomogeneously distributed on SLBs. On SLBs with 0.005 mol% PI(3)P large Atg18 clusters were observed. Even though the fluorescence signal intensity was decreased in membranes with lower PI(3)P concentrations, no single Atg18 spots could be observed for PI(3)P concentrations tested (Figure

3.10 A). The tendency of Atg18 to form clusters even at low PI(3)P concentrations suggests that PI(3)P clusters in membranes. To prevent Atg18-clustering, reduced Atg18 concentrations were used to avoid saturation of all available binding places. SLBs containing 0.5 mol% PI(3)P were incubated with different Atg18 concentrations ranging from 500 nM to 1.5 nM. While 500 nM Atg18 resulted in strong overall AlexaFluor633 signal, 1.5 nM Atg18 resulted in well separated single Atg18 spots (Figure 3.10 B, pannels one and two). Since fluorescence intensities differed among single spots it is likely that some Atg18 molecules bind as monomers whereas others bind as multimers. This is consitent with different Atg18 particle sizes observed in AFM experiments (Figure 3.9). A more detailed analysis is needed to clarify whether spots consist of one or several labeled Atg18 molecules. In addition, labeling efficiency of proteins used in this experiment was 41% raising the possibility that only a fraction of Atg18 molecules is labeled in such oligomeric assemblies. Therefore, use of proteins with a labeling efficiency of close to 100% is desireable. Repeated imaging of membranes incubated with 1.5 nM Atg18 showed that some spots were stably bound to membranes (red arrowhead, Figure 3.10 B, pannels two to five), while others disappeared and reappeared (green arrowhead). Overall a rapid decrease in the number of fluorescent spots was observed. This is caused by fast bleaching, raising the need for an efficient oxygen scavanging system. In addition, new binding events were detected during imaging (yellow arrow). Taken together initial AFM and TIRF experiments performed in this thesis are promising complementary systems to explore the detailed influence of PROPPINs on protein scaffold formation in high spatial and temporal resolution.

3.8 PROPPINs Localize to the PAS *In Vivo*

The *in vitro* data presented in this study clearly suggest a role of both PROPPINs, Atg18 and Atg21, in Atg8-lipidation. Furthermore, the *in vitro* effects of both PROPPINs were indistinguishable. According to previous reports, Atg18 belongs to the autophagic core machinery being essential for bulk autophagy and specific forms of autophagy [90, 138]. To the contrary, Atg21 has been proposed to only play a role in a specific form of autophagy, the Cvt-pathway [139]. Consequently, PROPPINs need to play different roles in formation of the phagophore at least in specific autophagy. Therefore, the function of Atg18 and Atg21 was investigated *in vivo*.

The PAS is characterized by localization of Atg proteins to punctate structures close to the vacuole. A commonly used marker for autophagosome biogenesis and the PAS is Atg8, because of its covalent association with the autophagosomal membrane [62]. To determine conditions in which PROPPINs localize to the PAS, Atg8 was used as PAS marker and PROPPINs were analyzed for colocalization with Atg8. Therefore,

cells ectopically expressing 2xmCherry-Atg8 and endogenously expressing PROPPIN-GFP fusion proteins (YS17 or YS18 with pC8) were imaged by confocal fluorescence microscopy during vegetative growth and starvation. As shown in Figure 3.11 A both PROPPINs as well as Atg8 formed puncta close to the vacuole under vegetative and starvation conditions. In addition to punctate localization, both PROPPINs localized to the vacuolar rim during vegetative growth. Interestingly, Atg18 localization to the vacuolar rim was lost under starvation conditions, while Atg21 still showed extensive staining of the vacuole (Appendix Figure A.10). This suggests a switch of Atg18 activity between vegetative and starvation conditions. An autophagy dependent Atg18-activation is consistent with previous data showing that both PROPPINs are required for ApeI processing under vegetative conditions, whereas Atg21 becomes dispensable upon starvation [139].

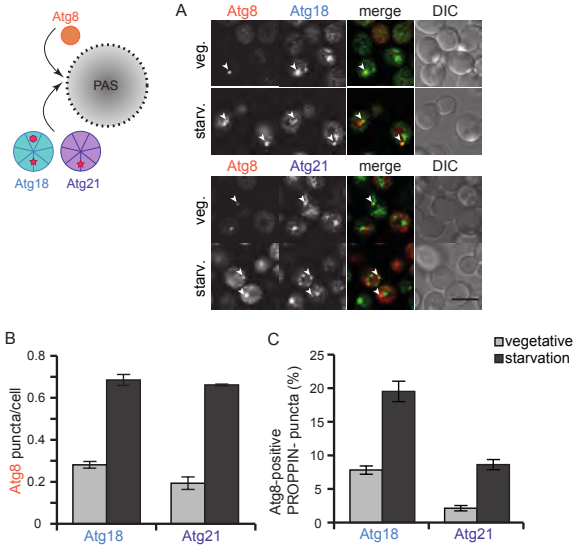

Figure 3.11: PROPPINs localize to the PAS under vegetative and starvation conditions. The cartoon visualizes the experimental setup. Atg18- or Atg21-GFP were expressed from their endogenous locus and 2xmCherry-Atg8 was overexpressed from a CEN-plasmid. Cells were imaged in mid-log phase and after 2 h starvation. (A) Pictures show PROPPINs colocalizing with Atg8 (arrowheads). (B, C) Quantification of (A). (B) Atg8-puncta formation is induced under starvation conditions in both PROPPIN-GFP tagged strains. (C) PROPPINs colocalize with Atg8 under vegetative and starvation conditions. Starvation enhances the frequency of Atg8-positive PROPPIN-puncta. The increase closely reflects the increase in overall Atg8 puncta. Scale bar = 5 μm. All quantifications are shown as mean ± SD of N = 3 independent experiments.

Atg8-puncta, representing forming autophagosomes, were quantified. Consistent with previous reports, the number of Atg8-puncta increased in both cell lines, from 0.28 ± 0.02 to 0.69 ± 0.03 puncta per cell in Atg18-GFP and from 0.19 ± 0.03 to 0.661 ± 0.004 puncta per cell in Atg21-GFP expressing cells (Figure 3.11 B) [212, 213]. This inidcates that PROPPIN-GFP fusion proteins were not affected in Atg8-recruitment and, therefore, autophagosome formation.

Quantification of the number of PROPPIN-puncta revealed that their frequency remains unchanged under vegetative and starvation conditions. For Atg18 1.4 ± 0.1 or 1.5 ± 0.1 puncta per cell were observed under vegetative and starvation conditions, respectively. Atg21 puncta were more frequent with 2.4 ± 0.3 puncta per cell under vegetative and 2.5 ± 0.1 puncta per cell under starvation conditions (Appendix Figure A.4 B). Colocalization of PROPPINs and Atg8 revealed that the frequency of Atg18-positive Atg8-puncta was constant under vegetative (39 ± 3%) and starvation (42 ± 2%) conditions. For Atg21-positive Atg8-puncta a small increase in colocalization was observed with 26 ± 3% in vegetative and 33 ± 3% under starvation conditions (Appendix Figure A.4 A). Consistent with an increase in Atg8-puncta number upon starvation, but constant fractions of PROPPIN-positive Atg8-puncta, the percentage of Atg8-positive PROPPIN-puncta increased upon starvation. For Atg18-GFP puncta 7.8 ± 0.6% and 20 ± 2% were Atg8-positive under vegetative and starvation conditions, respectively. Atg21-GFP puncta positive for Atg8 increased from 2.1 ± 0.4 in vegetative growth to 8.6 ± 0.8% upon starvation. The induction of autophagosome formation is, therefore, well reflected in an increase in the absolute amount of PROPPIN-Atg8-positive puncta, being a good indication that both PROPPINs are involved in autophagosome formation under vegetative and starvation conditions. Nevertheless, the low frequency of colocalization points towards a more transient PAS localization of PROPPINs compared to Atg8.

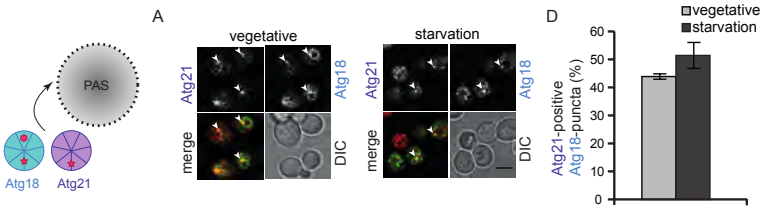

Figure 3.12: Atg18 and Atg21 colocalize under vegetative and starvation conditions. Atg18-GFP and Atg21-2xmCherry were expressed from their endogenous locus. Cells were imaged in mid-log phase and after 2 h starvation. (A) Pictures show representative images of colocalizing PROPPINs (arrowheads). (B) Quantification of (A). PROPPINs colocalize to the same extent under vegetative and starvation conditions. Scale bar = 5μm, bar graphs represent mean ± SD of N = 3 independent experiments.

To investigate whether both PROPPINs colocalize at punctate structures a yeast strain with genomically tagged Atg21-2xmCherry and Atg18-GFP (YS13) was imaged under vegetative and starvation conditions. Interestingly, 44 ± 1% and 51 ± 5% of Atg18 puncta colocalized with Atg21 puncta under vegetative and starvation conditions, respectively (Figure 3.12 B). The average number of double positive PROPPIN-puncta increased 1.5-fold from 0.60 ± 0.06 to 0.90 ± 0.05 puncta per cell upon starvation. In context with a similar increase in the number of Atg8-puncta upon starvation (Figure 3.11 A) it seems likely that both PROPPINs cooperate at the PAS under vegetative and starvation conditions. However, it cannot be completely excluded that double-positive PROPPIN-puncta and Atg8-positive PROPPIN-puncta are two distinct subsets. Still, the data presented above reveal that PROPPINs colocalize with its respective counterpart and both PROPPINs localize to the PAS under vegetative and starvation conditions. Upon starvation, Atg8-puncta per cell and the double-positive PROPPIN-puncta per cell increase suggesting both PROPPINs to be involved in autophagosome formation independent of nutrient supply.

3.9 Atg21 Regulates Atg8-Lipidation in Non-Specific Autophagy

All data presented so far reveal a strong similarity between Atg18 and Atg21 which would fit to the hypothesis that both PROPPINs serve the same function in different pathways. However, previous studies showed that both, Atg18 and Atg21 are crucial for the Cvt-pathway [138, 139]. This is consistent with the colocalization of PROPPINs with their counterpart and with Atg8 observed in this study. Thus, both PROPPINs potentially serve specific, non-redundant functions in autophagic pathways at least during vegetative growth. To investigate the specificity of PROPPIN-functions, it first had to be tested, whether the positive influence on Atg8-lipidation observed *in vitro* could also be detected *in vivo*. For this purpose, the specific contribution of individual PROPPINs to the pool of lipidated Atg8 was examined under vegetative and starvation conditions. Atg8–PE levels were determined by immuno-blotting in different yeast strains: wildtype, *ATG18*Δ, *ATG21*Δ or *ATG18*Δ*ATG21*Δ (YS1, YS8, YS7, YS10). Consistent with the literature, in all strains total Atg8 levels were induced upon starvation [89].
PROPPIN-dependent Atg8–PE formation was determined as decribed in Chapter 2.11.2. During vegetative growth small amounts of PROPPIN-dependent Atg8–PE are detected in wildtype cells. Deletion of either PROPPIN had no significant effect on Atg8–PE levels, although a tendency towards reduced levels was observed. As reported previously, Atg8–PE levels were induced upon starvation in wildtype cells. Consitent with our *in vitro* results, *ATG21* deletion caused a strong decrease in Atg8–PE levels compared to

the wildtype. In contrast, *ATG18* deletion even promoted Atg8–PE accumulation upon starvation (Figure 3.13 B), which is in good agreement with previous data [132], but was supprising in light of our *in vitro* findings. These data show that *in vivo* Atg21 is required for bulk Atg8-lipidation in starvation induced autophagy.

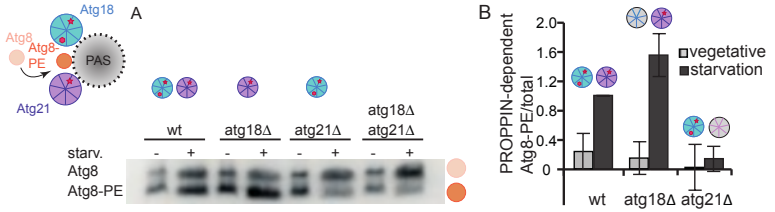

Figure 3.13: Atg21 facilitates bulk Atg8-lipidation in non-specific autophagy. Atg8–PE formation was examined by immuno-blotting under vegetative (-) and starvation (+) conditions in different yeast cells (wildtype, *ATG18*Δ, *ATG21*Δ and *ATG18*Δ*ATG21*Δ). (A) In all strains an increase of total Atg8 is observed upon starvation. Under starvation conditions Atg8–PE formation is increased in *atg18*Δ cells and decreased in *atg21*Δ cells. (B) Quantification of PROPPIN-dependent Atg8-lipidation. Shown is the normalized ratio of Atg8–PE and total Atg8 (Atg8 + Atg8–PE) corrected for PROPPIN-independent Atg8–PE levels detected in *atg18*Δ*atg21*Δ cells. Starvation leads to an Atg21-dependent induction of Atg8-lipidation. This induction is promoted in *atg18*Δ cells. No significant difference in Atg8-lipidation is observed between PROPPIN deletions and wildtype during vegetative growth. All quantifications are shown as mean ± SD of N = 3 independent experiments.

To explore whether the differences in Atg8-lipidation are correlating with autophagosome biogenesis GFP-Atg8-puncta formation was monitored in wildtype (wt, YS2), *atg18*Δ (YS14), *atg21*Δ (YS15) and *atg18*Δ*atg21*Δ (YS16) cells under vegetative and starvation conditions. Consistent with enhanced Atg8–PE formation upon starvation in wildtype cells the frequency of GFP-Atg8-puncta per cell increased from 0.22 ± 0.01 puncta per cell under vegetative to 0.50 ± 0.07 puncta per cell under starvation conditions (Figure 3.14 A, B). During quantification of Atg8-puncta it became obvious that bright and dim Atg8-puncta can be distinguished. Bright puncta represent autophagosomes close to completion, whereas dim puncta might represent unspecific phagophores that are either initiated but not elongated, completed but not fusing to the vacuole or Cvt-vesicles. Both, bright and dim puncta accounted for approximately 50% of total Atg8-puncta detected under vegetative (bright: 0.11 ± 0.02 puncta per cell; dim: 0.11 ± 0.01 puncta per cell) and starvation conditions (bright: 0.22 ± 0.04 puncta per cell; dim: 0.28 ± 0.04 puncta per cell; Appendix Figure A.5 A, B). This means that the ratio between autophagosomes in different stages of biogenesis stays constant. Consequently, either initation is the rate limiting step in autophagosome formation or all sequential steps in autophagosome formation are tightly interconnected to enable efficient autophagosome biogenesis and completion. In *atg18*Δ cells no effect on Atg8-puncta formation was observed under vegetative conditions compared to the wildtype with a total of 0.24 ± 0.05 puncta per cell (Figure 3.14 A, B). A more detailed analysis of bright and dim puncta

did not reveal a difference either (bright: 0.11 ± 0.04 puncta per cell; dim: 0.14 ± 0.01 puncta per cell). Taking into account, that Cvt-vesicles are not completed in *atg18*Δ cells [90] this suggests that Atg18 plays an additional role in phagophore initation under vegetative conditions, since a block of only late steps would lead to an accumulation of Atg8-puncta.

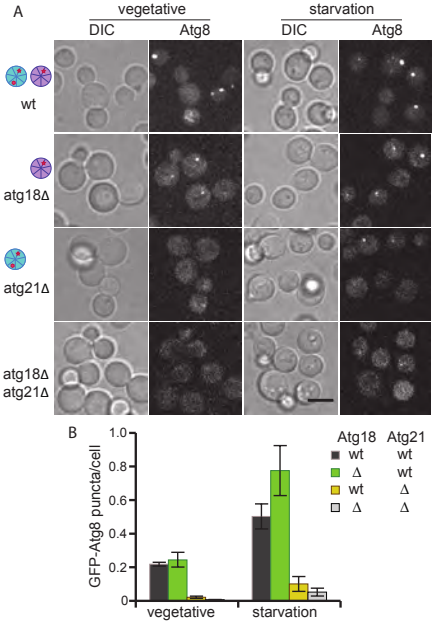

Figure 3.14: Atg21 directs Atg8-lipidation to the PAS under vegetative and starvation conditions. GFP-Atg8-puncta formation of wildtype (YS2), *atg18*Δ (YS14), *atg21*Δ (YS15) and *atg18*Δ*atg21*Δ (YS16) cells was examined by confocal fluorescence microscopy under vegetative and starvation conditions. (A) Representative images of GFP-Atg8 expressing cells under vegetative and starvation conditions. (B) Quantification of GFP-Atg8-puncta in (A). Starvation induces Atg8-puncta formation in wildtype cells. This induction is pronounced in *atg18*Δ cells. *ATG21* deletion strongly reduces GFP-Atg8-puncta formation under vegetative and starvation conditions. Scale bar = 5 μm. All quantifications are shown as mean ± SD of N = 3 independent experiments.

In contrast, upon starvation the overall number of Atg8-puncta was increased 1.6-fold in *atg18*Δ cells (0.78 ± 0.15 puncta per cell) compared to the wildtype (0.50 ± 0.07 puncta per cell). Interestingly, the number of bright Atg8-puncta per cell was almost unchanged (0.29 ± 0.08 puncta per cell), while dim Atg8-puncta were strongly increased (0.48 ± 0.07 puncta per cell) compared to the wildtype (0.28 ± 0.04 puncta per cell; Appendix Figure A.5 A, B). This suggests that autophagic membranes are still initiated in absence of Atg18, but are not elongated. Consitently, Suzuki *et al.* proposed that At18 and Atg2 are involved in membrane expansion at specific cargo [99].

In *atg21*Δ cells, formation of Atg8-puncta was largely impaired under vegetative (0.02 ± 0.01 puncta per cell) and starvation conditions (0.10 ± 0.04 puncta per cell; Figure 3.14 B). While bright puncta were completely abolished, few dim puncta (0.02 ± 0.01 puncta per cell) were observed under vegetative conditions (Appendix Figure A.5 A, B). Under starvation conditions bright puncta were almost completely abolished (0.02 ± 0.02 puncta per cell) and dim puncta were strongly reduced (0.08 ± 0.03 puncta per cell) to levels close to wildtype levels under vegetative conditions (0.11 ± 0.01 puncta per cell). This indicates that Atg21 is a critical factor for initation of Atg8-lipidation during autophagosome formation under both vegetative and starvation conditions. Deletion of both PROPPINs resulted in a phenotype similar to that of *atg21*Δ cells with the tendency to an even smaller number of Atg8-puncta in double deletion strains in both nutrient conditions (vegetative: 0.01 ± 0.00 puncta per cell; starvation: 0.05 ± 0.02). Taken together, these data show that Atg21 is the main driver of Atg8-lipidation at autophagosomes under vegetative and starvation conditions. It initiates Atg8-lipidation at the phagophore. Atg18 seems to be involved in autophagosome initation under vegetative conditions and elongation during starvation, leading to an accumulation of initiated phagophores upon *ATG18* deletion.

3.10 Atg18 and Atg21 Localize to Different Positions at Giant Cargo in Starvation

Biochemical and cell biological examination of PROPPIN-functions provide strong evidence that, although Atg18 and Atg21 share similar activities *in vitro*, they serve specific funtions under both vegetative and starvation conditions *in vivo*. This suggests that their activity is either spatially or temporally restricted during phagophore formation. To investigate spatial segregation of PROPPINs on phagophore membranes, cells containing giant autophagic cargo were used to map protein localization at the phagophore in more detail by fluorescence microscopy, as described recently [99]. PROPPIN localization was monitored after rapamycin treatment in cells expressing PROPPIN-GFP fusion proteins in presence or absence of their respective PROPPIN-counterpart (YS17: *atg18-gfp*; YS18: *atg21-gfp*; YS19 *atg18-gfp atg21*Δ; YS20 *atg21-gfp atg18*Δ). Additionally, these cells expressed 2xmCherry-Atg8 (pC8) and ApeI (pC11) from plasmids. Consistent with previous studies, Atg8 formed crescent shaped structures, representing the phagophore membrane, around giant cargo. Atg18 localized to the tips of these membrane crescents (Figure 3.15 A, upper panel) [99]. Quantification revealed that Atg18-puncta colocalized extensively with Atg8-crescents (93 ± 6%). The vast majority of Atg18-puncta localized to the tips of Atg8-crecents (83 ± 4%, Figure 3.15 A, B). This localization pattern of Atg18 supports the assumption derived from Atg8-puncta formation in Chapter 3.9, that

Atg18 might be involved in membrane expansion. Interestingly, Atg21 localized to crescent membrane structures as well (48 ± 13%), but not at their tips (Figure 3.15 A third and fourth panel, B). Atg21 rather localized to the middle of Atg8-crescents (31 ± 8%) and weak staining of the complete crescent was observed. These different localizations suggest distinct functions of Atg18 and Atg21 at the phagophore probably regulated by spatial separation.

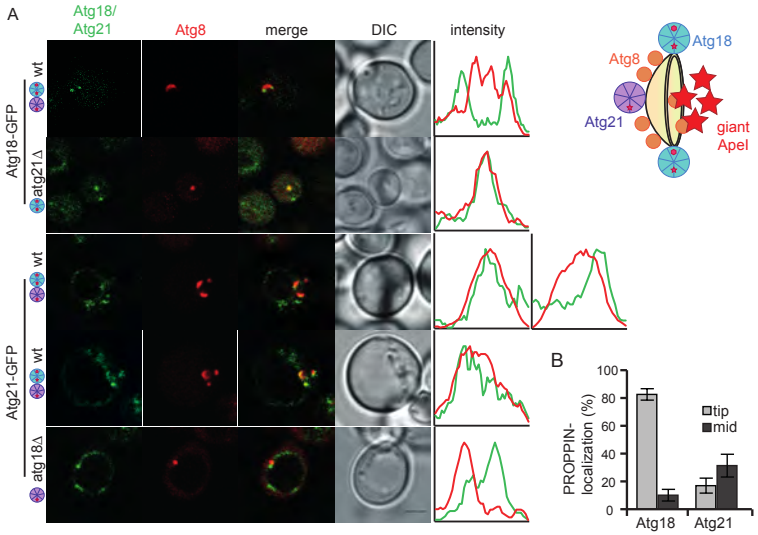

Figure 3.15: PROPPINs localize to different positions at giant cargo. The cartoon depicts giant cargo (red stars) surrounded by a growing phagophore membrane and the localization of PROPPINs and Atg8. PROPPIN localization was examined by fluorescence microscopy after rapamycin treatment in cells expressing PROPPIN-GFP fusion proteins in presence or absence of their respective PROPPIN-counterpart (YS17: *atg18-gfp*; YS18: *atg21-gfp*; YS19: *atg18-gfp atg21*Δ; YS20: *atg21-gfp atg18*Δ). Additionally, these cells expressed 2xmCherry-Atg8 (pC8) and ApeI (pC11) from plasmids. (A) Atg8 crescents are formed in wildtype cells. Single PROPPIN deletions result in formation of Atg8-puncta at giant cargo, but no expansion to Atg8-crescents is observed. Distinct localization of Atg18 and Atg21 at Atg8-positive crescents are detected. Atg18 localizes to crescent tips. Atg21 binds primarily to the middle and all over the crescent. (B) Quantification of PROPPIN localization on Atg8-crescents as in (A). Almost all Atg8-crescents bear Atg18 at their tips. Atg21 puncta localized to the body of Atg8-crescents or stains the complete crescent. Scale bar = 2 μm. All quantifications are shown as mean ± SD of N = 3 independent experiments.

Surprisingly, in both *atg18*Δ and *atg21*Δ cells no expanded Atg8-crescents were formed, but Atg8-puncta still localized to giant cargo (Figure 3.15 A, second and fifth panel). Consequently, both PROPPINs are needed to efficiently expand membranes around specific cargo, but both PROPPINs can target Atg8 to cargo under autophagy induced conditions. Furthermore, *ATG21* deletion reduced Atg8-puncta from 0.78 ± 0.19 puncta

per cell (wt) to 0.18 ± 0.09 puncta per cell, consistent with results obtained in non-specific autophagy. Interestingly, *ATG18* deletion also reduced Atg8-puncta from 0.64 ± 0.09 puncta per cell to 0.32 ± 0.06 puncta per cell (Appendix Figure A.6 A). This implies that Atg18 plays an important role in targeting Atg8-lipidation to cargo under autophagy induced conditions. In addition, colocalization of PROPPINs with Atg8 was quantified in presence and absence of respective PROPPIN-counterparts. While 57 ± 8% of Atg8-puncta were Atg18-positive in the wildtype background colocalization was only slightly reduced in *atg21*Δ cells (45 ± 4%). In contrast, the percentage of Atg21-positive Atg8-puncta was strongly reduced from 41 ± 2% in the wildtype to 24 ± 4% in *atg18*Δ cells (Appendix Figure A.6 B). Taken together, phagophore formation at specific cargo and Atg21-recruitment to the PAS seem to depend at least partially on Atg18. The different functions of PROPPINs could be a result of their distinct localization at the autophagosomal membrane.

3.11 PROPPINs Cooperate in Different Autophagy Pathways

To investigate how the observed differences in PROPPIN localization translate into distinct functions during the biogenesis of autophagosomes, three different autophagy assays were performed (Figure 3.16). Non-specific autophagy was quantified using the Pho8Δ60 assay (Chapter 2.11.3) that measures autophagy-mediated transport of cytoplasmic Pho8Δ60 to the vacuole. A similar principle was used to quantify mitophagy by expressing mitochodria-targeted (mt)Pho8Δ60. ApeI processing was quantified to determine flux through Cvt-pathway which can be observed during vegetative growth. Under starvation conditions ApeI processing is commonly used to examine bulk autophagy [202].

A comprehensive analysis of reported PROPPIN mutants was performed to obtain information regarding contributions and requirements of each PROPPIN to specific and non-specific autophagy. For Atg18 a PI(3)P-binding defective mutant has been reported (Atg18$^{\Delta PI3P}$, pC6) [131]. Another mutant is deficient in Atg2 binding (Atg18$^{\Delta Atg2}$, pC5) [137]. In addition, a double mutant binding neither PI(3)P nor Atg2 (Atg18$^{\Delta Atg2/\Delta PI3P}$, pC7) was used. In case of Atg21 only a PI(3)P-binding deficient mutant has been described (Atg21$^{\Delta PI3P}$, pC10). All possible permutations of these PROPPIN mutants and their deletions were tested. For this purpose, an *S. cerevisiae atg18*Δ *atg21*Δ strain (Pho8Δ60, ApeI: YS3; mtPho8Δ60: YS6) was supplemented with CEN plasmids overexpressing variants of one or both PROPPINs (Atg18: wt = pC4, ΔAtg2 = pC5, ΔPI3P = pC6, ΔAtg2/ΔPI3P = pC7; Atg21: wt = pC9 and ΔPI3P = pC10). To resolve the influence of PROPPIN overexpression on autophagic function, wildtype (Pho8Δ60, ApeI:

YS4; mtPho8Δ60: YS5) cells and strains with single deletions of *ATG18* (Pho8Δ60, ApeI: YS9; mtPho8Δ60: YS27) or *ATG21* (Pho8Δ60, ApeI: YS25; mtPho8Δ60: YS26) were used.

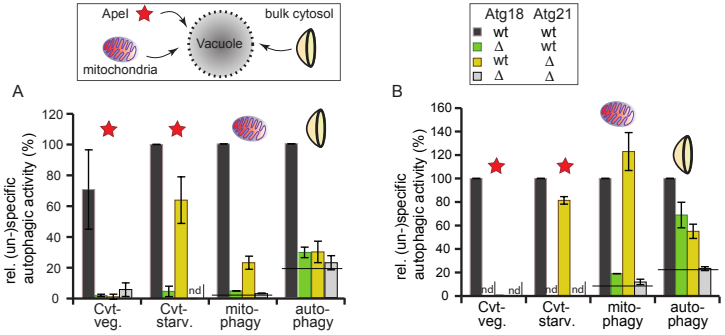

Figure 3.16: PROPPINs excert distinct functions in different autophagic pathways. Cartoons visualize the experimental setup with different cargos. Wildtype (wt), *atg18*Δ, *atg21*Δ, *atg18*Δ*atg21*Δ cells as well as *atg18*Δ*atg21*Δ cells complemented with PROPPIN-variants (see text) were grown to mid-log phase and starved for 4 h (Cvt and autophagy) or 24 h (mitophagy). (A) Genomic deletions of *ATG18* or both PROPPINs completely abolish autophagic processes. Atg21 is essential for the Cvt-pathway during vegetative growth, but becomes dispensable under starvation. Mitophagy is strongly reduced and bulk autophagy is not detectable in *atg21*Δ cells. (B) Double deletion strains(YS3, YS6), complemented with PROPPINs from CEN plasmids. ApeI processing is not altered by overexpression of PROPPINs (see (A)). In mitophagy Atg18 overexpression fully compensates loss of Atg21. In bulk autophagy overexpression of the complementary PROPPIN causes partial activity. All quantifications are shown as mean ± SD of N = 3 independent experiments. nd = not detectable.

ApeI processing was examined by Western Blotting under vegetative and starvation conditions (Chapter 2.11.3). Under vegetative conditions ApeI processing was dependent on both Atg18 and Atg21, irrespective of their expression level (Figure 3.16 A, B). This is in good agreement with previous studies showing that both PROPPINs are required for the Cvt-pathway [90, 139, 214]. Interestingly, mutational analysis revealed that Atg18 binding to either PI(3)P or Atg2 is necessary and sufficient for ApeI processing. Full Cvt-activity required, however, PI(3)P- and Atg2-recognition by Atg18 (Figure 3.17 A). Moreover, Atg21 PI(3)P-binding was crucial for ApeI processing (Appendix Figure A.8 A). Consequently, in the Cvt-pathway Atg21 is functional only when recruited to the PAS by PI(3)P. Atg18 needs PI(3)P and Atg2 as localization determinants for full activity. These data suggest, that under vegetative conditions both PROPPINs need to cooperate to enable formation of functional Cvt-vesicles. In contrast, under starvation, Atg21 becomes dispensable for ApeI processing (Figure 3.16 A,B), whereas PI(3)P or Atg2 binding of Atg18 remained necessary and sufficient for partial activity (Figure 3.17 A, Appendix Figure A.7). This suggests different mechanisms of Cvt-vesicle formation under vegetative and starvation conditions. Atg18-activity might require Atg21 during vegetative growth, but under starvation Atg18 could be active by itself. Importantly,

the efficient transport of ApeI requires Atg8–PE to be present at the conave face of the phagophore to efficiently tether cargo and membrane. Since this transport is still working in *atg21*Δ cells another factor has to enable formation of Atg8–PE at the concave face of autophagosomes.

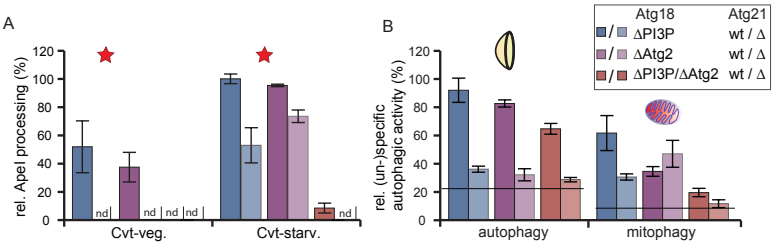

Figure 3.17: Analysis of Atg18 variants in different autophagy pathways. Autophagic assays were perforemd as described in the main text. (A) Influence of Atg18 PI(3)P- or Atg2-binding mutants on Cvt-pathway. Under vegetative conditions PI(3)P- or Atg2- binding of Atg18 are sufficient for partial Cvt-activity in presence of Atg21. Upon starvation Atg21 is dispensable and Atg18 targeting by either PI(3)P or Atg2 restore full ApeI-processing. (B) Influence of PI(3)P- or Atg2- binding mutants on autophagy and mitophagy. In autophagy, Atg21 can compensate for PI(3)P- or Atg2-binding deficiency of Atg18. Remarkably, Atg18 essentially needs PI(3)P- and Atg2-binding to compensate for *ATG21* deletion in bulk autophagy. Effects of PI(3)P- or Atg2-binding Atg18 mutants is more pronounced in mitophagy than in ApeI processing. All quantifications are shown as mean ± SD of N = 3 independent experiments. nd = not detectable.

Mitophagy and non-sepcific autophagy were quantified using the Pho8Δ60 assay as described in Chapter 2.11.3. Mitophagy, which was monitored after starvation, was completely blocked in *atg18*Δ and *atg18*Δ*atg21*Δ cells and strongly diminished in *atg21*Δ cells (Figure 3.16 A). Overexpression of wildtype Atg18, however, restored mitophagic activity in *atg18*Δ*atg21*Δ cells (Figure 3.16 B). This implies that the amount of Atg18 plays a critical role during autophagic transport of specific cargo. Consitent with the observation that Atg18 facilitates Atg8-lipidation *in vitro* and to some extent *in vivo* and the reported function of Atg8 to bind cargo-adpators [22], the amount of lipidated Atg8 could play a critical role for autophagic transport of specific cargo. Therefore, Atg18- and Atg21-levels were analyzed expressing respective PROPPINs genomically or overexpressing them from CEN-plasmids. Interestingly, endogenous Atg21 levels exceed Atg18 levels by a factor of four [215]. Testing the expression levels of PROPPIN-GFP fusions endogenously or overexpressed from CEN-plasmids revealed a 3- to 4-fold increased expression from CEN-plasmids compared to genomic expression (Appendix Figure A.8). Thereby, overexpression results in Atg18 levels comparable to endogenous Atg21 levels. Consequently, the dose-dependent compensation of Atg18 for Atg21 supports the notion that Atg18 expression levels are an important determinant for degradation of large specific cargo. Importantly, in cells expressing $Atg18^{\Delta PI3P}$ or $Atg18^{\Delta Atg2}$ reduction in mitophagic activity was more pronounced compared to ApeI processing (Figure 3.17 A,

B). This means that interaction of Atg18 with its localization determinants PI(3)P and Atg2 is more important in mitophagy as opposed to ApeI processing. This again supports the notion that cargo selection and efficient membrane expansion around specific cargo depends on fully functional Atg18.

Surprisingly, non-selective autophagy was almost completely abolished in all PROPPIN deletions and overexpression of the respective PROPPIN counterpart could only partially restore Pho8Δ60 activity. PI(3)P-binding mutants of both PROPPINs ($Atg18^{\Delta PI3P}$, $Atg21^{\Delta PI3P}$) as well as $Atg18^{\Delta Atg2}$ showed only minor reduction in Pho8Δ60 activity (Figure 3.17 B, Appendix Figure A.7 C). This is consitent with a previous study showing that $Atg18^{\Delta PI3P}$ is active in autophagy in presence of Atg21. Remarkably, Atg18 essentially needed PI(3)P- and Atg2-binding to compensate for *ATG21* deletion in non-specific autophagy (Appendix Figure A.7 C). A possible reason would be that Atg18 is recruited to the PAS by PI(3)P and Atg2 in non-specific autophagy. In specific autophagy, however, an additional localization signal such as cargo or cargo adaptors might be involved. Atg18 has been previously discussed to be involved in autophagosome completion, being critical for fusion with the vacuole [148]. Therefore, our finding that Atg21 overexpression restored Pho8Δ60 delivery to the vacuole was surprising. It seems likely that autophagy-independent, but Atg21-dependent pathways are capable to deliver bulk cytoplasm to the vacuole. Taken together, these data suggest that Atg18 and Atg21 are both critical for Cvt-vesicle formation during vegetative growth. Under starvation conditions, however, Atg18 is crucial, but Atg21 is dispensable for selective degradation of autophagic cargo.

3.12 Atg21 Regulates Number and Size of Autophagosomes

Atg21 was the major initator of Atg8-lipidation under starvation conditions and Atg18 led to an accumulation of GFP-Atg8 puncta. Since previous studies demonstrated that the amount of Atg8–PE directly correlates with phagophore-size [89] the influence of Atg21-mediated Atg8-lipidation on autophagosome size was investigated by electron microscopy (EM). Moreover, in aggreement with previous reports [138], results obtained by functional assays suggest that in *atg18*Δ cells neither ApeI nor bulk cytoplasm is delivered to the vacuole. In contrast, in *atg18*Δ*atg21*Δ cells overexpressing Atg21 partial recovery of Pho8Δ60 delivery to the vacuole was observed. Therefore, another open question was whether Atg21 overexpression could restore delivery of autophagic bodies into the vacuole.

To answer these questions EM was applied. Determining the number of autophagic bodies in the vacuole allows for the analysis of successful autophagic cargo delivery.

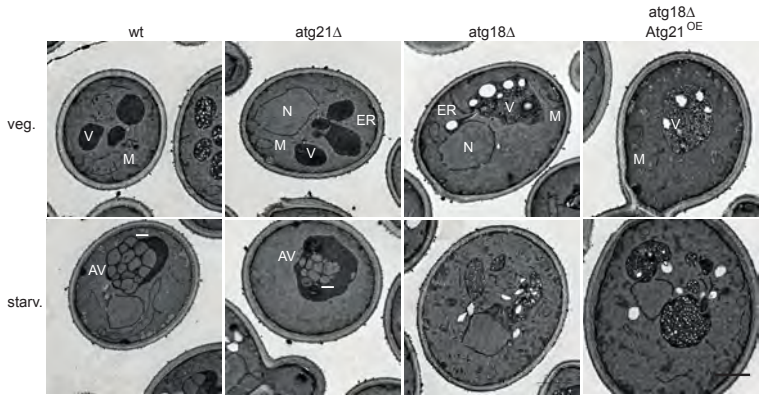

Figure 3.18: Electron microscopy of starvation induced autophagosomes. Wildtype (wt, YS21), *atg18*Δ (YS22), *atg21*Δ (YS23) and atg21Δatg18Δ cells overexpressing Atg21 (atg18ΔAtg21^{OE}, YS24 with pC9) in a *pep4*Δ background were imaged by electron microscopy. Under vegetative conditions vacuoles do not contain autophagic bodies. *atg18*Δ cells accumulate vesicles of low electron density in the vacuole. Upon starvation wt and *atg21*Δ cells accumulate autophagic vesicles (AV) in the vacuole. AVs in *atg21*Δ cells appear to be less and smaller. In cells lacking Atg18, no autophagic vesicles are observed in the vacuole independent of Atg21 expression levels. Scale bar = 1 μm, AV = autopahgic vesicle, ER = endoplasmic reticulum, M = mitochondria, N = nucleus, V = vacuole

To accumulate autophagic bodies in vacuoles, their degradation was inhibited by delting the protease Pep4. Wildtype (WT, YS21), *ATG18*Δ (YS22), *ATG21*Δ (YS23) and *ATG18*Δ*ATG21*Δ overexpressing Atg21 (*atg18*ΔAtg21^{OE}, YS24 with pC9) were imaged under vegetative growth and starvation conditions. During vegetative growth most vacuoles did not contain autophagic bodies in wt and *atg21*Δ cells. Still some small vesicles were observed in wt cells with a diameter of 240 ± 60 nm (Appendix Figure A.9). In cells lacking Atg18, spheres with low electron density were observed frequently in vacuoles. Since lipids are not fixed in the staining procedure used for electron microscopy but extracted during the procedure [203], electron transparent vesicles are likely to be lipid droplets. Upon starvation autophagic vesicles (AVs) accumulated exclusively in wt and *atg21*Δ cells (Figure 3.18 lower panel). Vacuoles in cells lacking Atg18 appeared more fragmented compared to wt and *atg21*Δ cells and contained inhomogeneous small vesicles of low electron density. The nature of these small vesicles was not determined.
The accumulation of AVs in *atg21*Δ cells was not surprising, since specific cargo was still transported to the vacuole. Because of the obvious difference in size and number of AVs both parameters were quantified. For that purpose diameters and numbers of autophagic vesicles in vacuoles were determined using ImageJ. The frequency of AVs

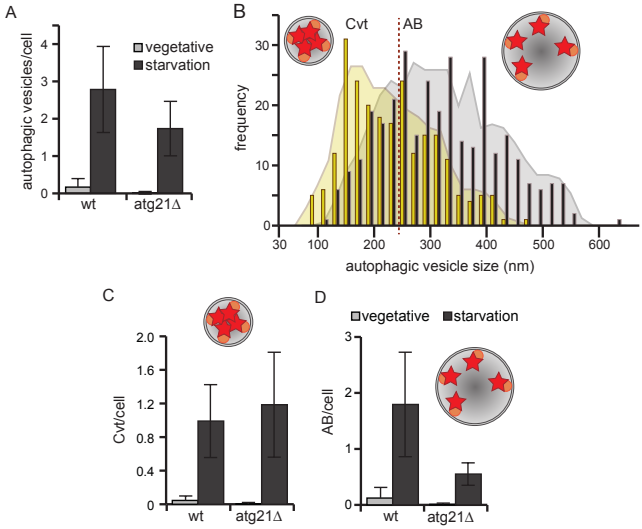

Figure 3.19: Atg21 determines the size of autophagosomes. Autophagic vesicles as shown in Figure 3.18 were quantified for wt and *atg21*Δ cells. (A) Quantification of total AVs per cell. Only a small reduction of autophagic vesicles was observed in *atg21*Δ cells compared to the wildtype. (B) Size distribution of AVs from wt and *atg21*Δ cells. The size distribution of AVs is shifted to smaller sizes in *atg21*Δ cells compared to the wildtype. The cut-off for discrimination between Cvt-vesicles and autophagic bodies is indicated by the dotted red line. (C) Quantification of Cvt-vesicles per cell. No significant difference is observed for *atg21*Δ cells compared to wt. (D) Quantification of ABs per cell. A strong reduction of autophagic bodies per cell is detected in *atg21*Δ cells compared to wt. mean ± SD of ten samples with a total of >110 cells per condition

per vacuole was strongly induced by starvation in wt and *atg21*Δ cells. However, while in wt cells 3 ± 1 AVs per cell were formed, only 2 ± 1 AV per cell were counted in *atg21*Δ cells (Figure 3.19 A). More importantly, the size distribution of AVs in *atg21*Δ cells was markedly shifted to smaller sizes compared to the wildtype (Figure 3.19 B). In the literature the size of Cvt-vesicles has been reported to be 140-150 nm [94] while autophagic bodies range from 300-900 nm [95]. Interestingly, in *atg21*Δ cells a moving median of size histograms displayed a peak at 160-180 nm whereas the peak of wt cells was at 300 nm. Consitent with literature values a diameter of 250 nm was used as a cut-off (dotted red line) to classify AVs as Cvt-vesicles (<250 nm) or autophagic bodies (ABs, >250 nm). Quantification of both vesicle types per vacuole revealed that the number of Cvt-vesicles does not change upon *ATG21* deletion (Figure 3.19 C). In contrast, ABs are strongly reduced (Figure 3.19 D). This is consistent with data obtained in functional assays that ApeI representing small, specific cargo is efficiently transported to the vacuole in *atg21*Δ cells, whereas bulk cytoplasm and mitochondria are almost completely excluded. Consequently, Atg21 appears to be a critical factor in starvation

induced autophagy that determines phagophore size by Atg8-lipidation. Thereby, Atg21 enables efficient degradation of large autophagic cargo and bulk cytoplasm while small specific cargo is still degraded in *atg21*Δ cells.

3.13 Atg18 Facilitates Formation of a Cargo-Tethering Atg8–PE Pool

As mentioned before, Atg8–PE has at least two functions in autophagy. First, it determines the size of autophagosomes, probably by formation of a protein scaffold at the convex face of the growing membrane [21, 89]. Second, the concave pool of Atg8–PE is used to tightly connect cargo to the phagophore [22]. *In vitro* data presented in this study clearly pointed towards a redundant function of Atg18 and Atg21 to facilitate Atg8-lipidation by membrane recruitment of its E3-ligase Atg12–Atg5-Atg16. *In vivo*, however, Atg8–PE formation was oppositely affected by *ATG18* and *ATG21* deletion. While deletion of *ATG21* drastically reduced Atg8-lipidation, an *atg18*Δ strain accumulated Atg8–PE. Surprisingly, in *atg21*Δ cells small specific cargo (ApeI) was still efficiently degraded via autophagy. Efficient autophagic degradation of bigger cargo was dependent on Atg18 overexpression in cells lacking Atg21. Therefore, it seems likely that Atg18 plays a crucial role in selection of specific cargo during starvation. To test this hypothesis wildtype (wt, YS2), *atg21*Δ (YS15) and *atg18*Δ*atg21*Δ cells with overexpression of Atg18 (*atg21*ΔAtg18^{OE}, YS16 with pC4) expressing GFP-Atg8 and forming giant ApeI cargo (pC11) were investigated by fluorescence microscopy after rapamycin treatment.

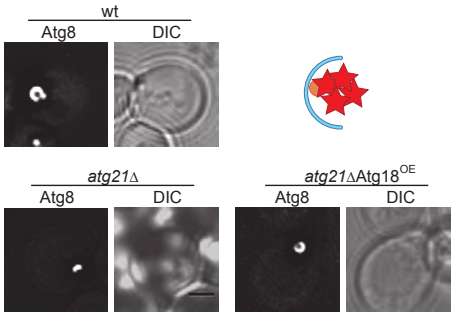

Figure 3.20: Atg18 facilitates formation of Atg8-crescents around giant cargo. Atg8-crescents observed on giant ApeI aggregates (stars) are depicted schematically. The crescents with maximal sizes observed for each strain are shown. In wt and *atg21*ΔAtg18^{OE} cells, Atg8 forms crescents around giant cargo. In *atg21*Δ cells, only small Atg8-crescents were observed very rarely. Scale bar = 2 μm

In wt cells crescent shaped Atg8 structures were frequently observed. These crescents

could mostly be colocalized to cargo aggregates visible in DIC images and resemble the growing autophagosomal membrane which is presumably directly attached to cargo via Atg8 (Figure 3.20). In contrast to wt and as observed before (Chapter 3.10), deletion of *ATG21* prevented formation of Atg8 crescents almost entirely. This is consistent with findings reported in this thesis, demonstrating that Atg21 is the major initiator of Atg8-lipidation under starvation conditions (Figure 3.13), that delivery of large cargo to the vacuole is strongly impaired in *atg21*Δ cells (Figure 3.16 A) and that autophagosome size is reduced in *atg21*Δ cells (Figure 3.19 B). Taken together these data point towards a role of Atg21 in efficient expansion of the phagophore in selective and non-selective autophagy probably mediated by facilitating Atg8-lipidation.

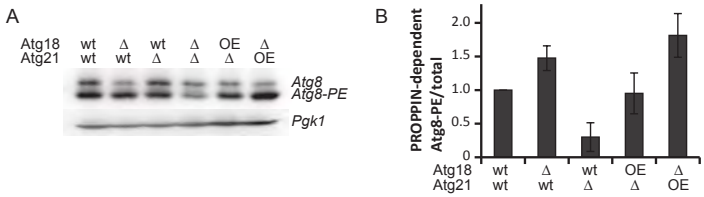

Figure 3.21: Atg18 facilitates Atg8-lipidation in cells with giant cargo. (A) Atg8–PE assay in presence of giant cargo. Different cells expressing wildtype PROPPINs (wt), single deletions (*atg18*Δ, *atg21*Δ) or overexpressing one PROPPIN and deletion of its counterpart (*atg21*ΔAtg18^{OE}, *atg18*ΔAtg21^{OE}) were examined for Atg8–PE formation after rapamycin treatment. (B) Quantification of (A) showing PROPPIN-dependent Atg8–PE formation. As in non-specific autophagy, *ATG18* deletion leads to an accumulation of Atg8–PE, whereas *ATG21* deletion reduces Atg8–PE formation. Overexpression of Atg18 can compensate for *ATG21* deletion and Atg21 overexpression further promotes Atg8-lipidation. Bars show mean ± SD of N = 3 independent experiments.

Interestingly, overexpression of Atg18 in cells lacking Atg21 (*atg21*ΔAtg18^{OE}) restored the formation of Atg8-positive crescents to some extent (Figure 3.20). To investigate whether membrane expansion in wt and *atg21*ΔAtg18^{OE} cells was similar, the length of the largest Atg8-crescents observed in each strain was determined. Notably, only one crescent shaped membrane was found in *atg21*Δ cells. The maximal length of observed crescents was 1.9 μm in wt cells, 1.4 μm in *atg21*ΔAtg18^{OE} cells and 0.8 μm in *atg21*Δ cells. These data show that Atg18 can restore membrane expansion around large specific cargo in cells lacking Atg21, explaining the Atg18-dose dependency of mitophagy in *atg21*Δ cells observed before (Figure 3.16 A, B).

A possible mechanism for Atg18 to restore membrane expansion around large cargo in absence of Atg21 is to facilitate Atg8-lipidation, most probably an Atg8-pool binding cargo-adaptors. To confirm this hypothesis Atg8–PE formation was monitored as described before, but using cells overexpressing ApeI (pC11) to generate excess of giant cargo. Atg8–PE formation was assessed in wildtype (wt, YS1), *atg18*Δ (YS8), *atg21*Δ (YS7), *atg18*Δ*atg21*Δ (YS10) and *atg18*Δ*atg21*Δ cells overexpressing either Atg18 (*atg21*ΔAtg18^{OE}, YS10 with pC4) or Atg21 (*atg18*ΔAtg21^{OE}, YS10 with pC9)

after rapamycin treatment. As in previous experiments (Figure 3.13 A), deletion of *ATG18* or *ATG21* had opposite effects on Atg8-lipidation. Overexpression of Atg18 in cells lacking Atg21 (*atg21*ΔAtg18^{OE}) was, however, sufficient to restore Atg8-lipidation (Figure 3.21 A, B). And Atg21 overexpression in cells lacking Atg18 led to a more pronounced phenotype compared to *atg18*Δ cells with endogenous Atg21 expression. Taken together these data strongly suggest, that Atg18 catalyzes formation of an Atg8–PE pool tethering cargo to the autophagosomal membrane. This function enables efficient degradation of specific autophagy cargo even in absence of Atg21.

3.14 Pho8Δ60 is Partially Delivered to the Vacuole in an Atg21-/MVB-Dependent Manner

Autophagy assays monitoring specific and non-specific cargo delivery to the vacuole revealed that overexpression of Atg21 partially restores cytoplasmic Pho8Δ60 delivery to the vacuole in cells lacking Atg18 (Figure 3.16 B). However, consitent with previous findings that Atg18 is essential to complete autophagosome formation [148], no autophagic vesicles were observed in the vacuole of these cells by electron micoscopy (Figure 3.18). Consequently, an alternative pathway has to deliver cytoplasmic material to the vacuole in an autophagy-independent, but Atg21-dependent manner. Atg21 has previously been reported to localize to endosomes [88] and MVBs are formed by inward budding of small vesicles, including cytoplasmic material [65]. Furthermore, MVB pathway and autophagy have recently been shown to act in a coordinated fashion during starvation [216]. Therefore, it seems likely that some cytoplasmic material is delivered to the vacuole by the MVB-pathway.

To investigate a possible contribution of the MVB-pathway to deliver cytoplasm to the vacuole, the Pho8Δ60 assay was applied to cells either expressing Vps4 or lacking Vps4, since *VPS4* deletion blocks the MVB-pathway [216]. To further examine the contribution of PROPPINs in MVB-dependent delivery of cytoplasmic cargo to the vacuole wildtype cells (vps4wt: YS4; *vps4*Δ: YS28), *atg18*Δ cells overexpressing Atg21 (vps4wt: YS9 with pC9; *vps4*Δ: YS29 with pC9) and *atg21*Δ cells overexpressing Atg18 (vps4wt: YS25 with pC4; *vps4*Δ: YS30 with pC4) were used.

As expected Pho8Δ60 activity was induced upon starvation and strains overexpressing one PROPPIN, but lacking the respective PROPPIN counterpart still exhibited strong activity. In yeast strains expressing both PROPPINs *VPS4* deletion did not cause a significant difference in Pho8Δ60 delivery to the vacuole compared to the wildtype. In *atg21*ΔAtg18^{OE} cells Pho8Δ60 activity was slightly reduced compared to cells expressing both PROPPINs, but additional deletion of *VPS4* did not further decrease Pho8Δ60 delivery to the vacuole. In contrast, in cells overexpressing Atg21 in absence of *ATG18*

blocking the MVB-pathway reduced delivery of cytoplasmic material to the vacuole. This suggests on the one hand, that contribution of the MVB pathway to cytoplasm-to-vacuole transport is detectable only if autophagy is impaired. On the other hand, Atg21 is required for this MVB-dependent delivery of cytoplasm. Furthermore, the residual Pho8Δ60 activity observed in *vps4*Δ*atg18*ΔAtg21^{OE} cells suggests that additional pathways exist delivering cytoplasm to the vacuole under starvation conditions.

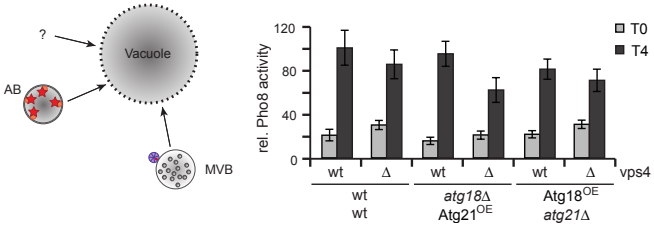

Figure 3.22: MVB-pathway dependent delivery of cytoplasmic material to the vacuole. The role of the MVB-pathway in cytoplasm-to-vacuole transport under starvation conditions was assessed using three pairs of yeast strains. In Pho8Δ60 strains the MVB-pathway was either unperturbed (wt) or blocked by deletion of *VPS4* (*vps4*Δ). In these strains either both PROPPINs were expressed or one PROPPIN was deleted and its counterpart was overexpressed (*atg18*ΔAtg21^{OE}, *atg21*ΔAtg18^{OE}). In wt and *atg21*ΔAtg18^{OE} cells the MVB-pathway has no significant influence on delivery of cytoplasmic material to the vacuole. Overexpression of Atg21 in *atg18*Δ cells (*atg18*ΔAtg21^{OE}) results in transport of cytoplasm to the vacuole by the MVB-pathway. Bar graphs represent mean ± SD of three independent experiments.

Discussion

Autophagy is a major catabolic pathway which delivers cytoplasmic material as well as whole organelles to the vacuole for degradation. Consistent with its importance in developmental processes, energy homeostasis and cellular response to cytotoxic stress and nutrient deprivation, autophagy is highly conserved throughout eukaryotic cells [62, 217]. Under vegetative conditions non-selective autophagy runs at a basal level to recycle cytoplasm and selective autophagy serves as a quality control mechanism by delivering dysfunctional organelles to the vacuole [62]. Yeast additionally delivers proenzymes (e.g. ApeI) to the vacuole under vegetative conditions by a process that appears to be a variation of specific autophagy, the Cvt-pathway [93]. Upon starvation it is believed that ApeI is randomly engulfed by autophagosomes together with bulk cytoplasm for vacuole delivery [93]. A critical protein involved in autophagic processes is Atg8. This Ub-like protein is covalently attached to autophagosomal membranes by a Ub-like conjugation machinery consisting of Atg proteins [112, 162, 163]. The unique characteristic of Atg8 is its covalent linkage to phosphatidylethanolamine (PE) [45]. Interestingly, Atg8–PE serves two main functions depending on its localization at the autophagosomal membrane. First, it has been reported that Atg8 determines the size of autophagosomes, probably by formation of a protein scaffold at the convex face of the autophagosomal membrane [21, 89]. The second function depends on Atg8–PE localization to the concave face of the phagophore. This Atg8–PE pool ensures tight binding of specific cargo to the growing autophagosomal membrane, excluding cytoplasmic material [22]. To facilitate tight interaction of cargo and membrane, cargo-adaptors like Atg19 directly interact with Atg8 via a conserved Atg8-interaction motif (AIM) [22, 165]. How these distinct pools of Atg8–PE are generated remains elusive. But recently Atg21, a PROPPIN family member, has been shown to recruit the Ub-like conjugation machinery to the phagophore to initiate Atg8-lipidation under vegetative conditions.

4.1 PROPPIN Functions in Autophagosome Formation

In *S. cerevisiae* three proteins (Atg18, Atg21 and Hsv1) belong to the PROPPIN family of proteins forming a β-propeller that binds phosphoinositides [130, 140]. Atg18 and Atg21 have been shown to be involved in different autophagic pathways [90, 138, 139] while Hsv1 is involved only in PMN, a specific form of microautophagy degrading superfluous parts of the nucleus [82]. Localization of Atg18 and Atg21 to the PAS and endosomes was shown to depend on PI(3)P formation by PI3K complex I [123, 140, 218]. Furthermore, PI3K activity is crucial for PAS targeting of Atg8 and for autophagic

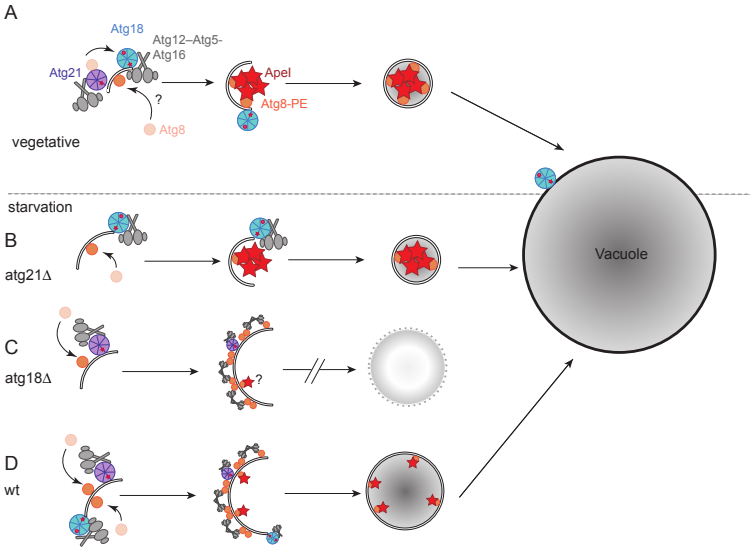

Figure 4.1: PROPPINs in the formation of different autophagic vesicles. (A) Atg21 is essential for Cvt-vesicle initiation and Atg18-activity at the PAS under vegetative conditions. Consequently, cooperation of both PROPPINs is essential to tightly bind ApeI to Cvt-membranes and complete Cvt-vesicles for delivery to the vacuole. (B-D) Under starvation conditions the requirements for PROPPIN proteins are altered. (B) In absence of Atg21 (atg21Δ), Atg18 is sufficient for efficient delivery of small specific cargo to the vacuole and results in formation of small, Cvt-like vesicles. Transport of large specific cargo and bulk cytoplasm is, however, impaired in *atg21*Δ cells. Consequently, Atg18 is proposed to generate an Atg8–PE pool tethering cargo to phagophore membranes. (C) Atg21, in absence of Atg18 (atg18Δ), catalyzes bulk Atg8-lipidation at autophagosomes, but autophagosomes cannot be closed without functional Atg18. Together with data from *atg21*Δ cells this suggests that Atg21 generates the Atg8–PE pool needed for phagophore expansion. (D) In wildtype cells both PROPPIN functions are combined to form large autophagosomes with two Atg8–PE pools for efficient phagophore expansion and specific cargo binding. At later steps Atg18 excerts further functions enabling autophagosome maturation or closure. The concerted action of both PROPPINs is needed for full functionality of Cvt-vesicles under vegetative and autophagosomes under starvation conditions.

flux [112, 219]. Accordingly, in mammalian cells WIPI-2, an Atg18 homolog, has been reported to promote lipidation of the human Atg8 homolog LC3 under starvation conditions [150]. In contrast, early studies on yeast Atg21 suggested a positive influence on Atg8–PE formation under starvation conditions. Nevertheless, they reported Atg21 to be dispensable for autophagic flux [132, 139]. A recent study demonstrated that Atg21 recruits the Atg12–Atg5-Atg16 complex to the PAS in vegetative growth [155]. For Atg18 only late actions, including Atg9-recycling and autopagosome closure have been proposed so far [90, 123]. If and how PROPPINs cooperate in autophagic pathways remained, however, poorly understood.

In this thesis, *in vitro* reconstitution of the autophagic Atg8-lipidation reaction in absence or presence of PROPPINs provides strong evidence that both Atg18 and Atg21 facilitate Atg8-lipidation *in vitro*. Consequently, similar functions of both PROPPINs were assumed and tested *in vivo*. These experiments revealed that both PROPPINs cooperate in selective and non-selective autophagy under vegetative and starvation conditions (see Figure 4.1). Whereas both PROPPINs are essential for ApeI processing by the Cvt-pathway (Figure 4.1 A), Atg21 becomes dispensable for selective autophagy during starvation (Figure 4.1 B, C, D). These differential requirements depend on specific PROPPIN-functions at the phagophore. Atg21 is essential to initiate Cvt-vesicle formation under vegetative conditions and facilitates bulk Atg8-lipidation at the PAS under starvation conditions. Thereby, Atg21 determines the size of autophagosomes (Figure 4.1 C). In contrast, Atg18 is sufficient to generate an Atg8–PE pool that tethers specific cargo to the phagophore (Figure 4.1 B), thereby, enabling efficient cargo recruitment to autophagosomes. To form large autophagosomes capable to deliver specific cargo and bulk cytoplasm to the vacuole, cooperation of both PROPPINs is essential (Figure 4.1 D).

4.2 PROPPINs Promote Atg8-Lipidation by Atg12–Atg5-Atg16 Recruitment *In Vitro*

To gain detailed mechanistical insights into PROPPIN function, both Atg18 and Atg21 were purified from *E. coli*. Even though it had been reported that PROPPINs tend to form soluble aggregates [135, 136] SEC profiles (Figure 3.1 C) and DLS measurements (Appendix Figure A.1) suggested Atg18 and Atg21 to be monomeric. Next, PI(3)P-binding of Atg18 and Atg21 was investigated using fluorescence labeled model membranes (GUVs) and PROPPINs in a fluorescence microscopy based assay. Recombinant PROPPINs were found to bind GUVs in a PI(3)P-dependent manner, confirming that both proteins are functional (Figure 3.2). Furthermore, PIP-dependent membrane binding of Atg18 was characterized in more detail by Biacore measurements and immobilized LUVs as model membranes (Figure 3.3 and Appendix Figures A.1 and A.2). Atg18 was found to bind PI(3)P and PI(3,5)P_2 with its FRRG-motif, but some residual binding was observed for Atg18^{FKKG}. These results are consistent with previous findings that Atg18 and Atg21 localization depends on their FRRG-motif *in vivo* [133] and that depletion of PI(3)P and PI(3,5)P_2 leads to a loss of detectable localization of Atg18 to the PAS, endosomes or the vacuole [131, 218].

Interestingly, previous studies did not observe binding of PROPPINs to PI(3,5)P_2 *in vitro* [132, 133]. In these reports binding was assessed using fusion proteins with MBP- or GST-tags, which might alter binding due to steric reasons. Furthermore, PIP strip

assays used in these studies have the disadvantage that lipids are not used in their native membrane environment. Therefore, interaction analysis of proteins with lipids is more reliable when performed with model membrane systems such as large unilamellar vesicles (LUVs), giant unilamellar vesicles (GUVs) or supported lipid bilayers (SLBs). Two other studies used Biacore measurements on immobilized LUVs to investigate PIP binding of Atg18. Both found interaction with PI(3,5)P_2 but not PI(3)P containing vesicles [131, 220]. Importantly, in these studies LUVs were prepared from phosphatidylcholin and PIPs only. In an experiment using GUVs with identical lipid composition, Atg18 binding was not detectable (data not shown). Consequently, PROPPIN binding critically depends on PI(3)P and PI(3,5)P_2, but other lipids seem to be needed for efficient binding as well. One possible explanation is that PROPPINs contain a loop region that is supposed to be inserted into membranes [135–137]. Inserting this loop might be critical to bind PI(3)P-containing membranes due to lower affinity of PROPPINs for PI(3)P compared to PI(3,5)P_2. Therefore, a more fluid membrane might facilitate loop insertion, resulting in enhanced binding. Taken together the data presented in this thesis are consistent with previous studies showing that Atg18 and Atg21 localize to the PAS, endosomes and the vacuole in a PI(3)P- and PI(3,5)P_2-dependent manner and confirm that purified PROPPINs are functional.

With functional PROPPINs in hand, their influence on Atg8-lipidation was tested. For this purpose, the Atg8-lipidation machinery was purified as described previously [21]. Two membrane systems (GUVs and SLBs) containing PI(3)P were incubated with the Atg8-lipidation machinery in absence or presence of Atg18 or Atg21. In both membrane systems Atg8-lipidation was promoted by PROPPINs (Figure 3.6). This positive influence on Atg8-lipidation was evoked by PROPPIN-dependent recruitment of Atg12–Atg5-Atg16 to PI(3)P-containing membranes (Figure 3.4). Consistent with these data, two papers were published recently during this study. First, the previously reported function of WIPI-2 to enhance LC3-lipidation in mammalian cells was refined. WIPI-2B interacts with Atg16L1 to direct LC3-lipidation to the PAS [151]. Second, in *S. cerevisae* it was proposed that Atg21 interacts with Atg16 under vegetative conditions, thereby, enhancing Atg8-lipidation and GFP-Atg8 localization to the PAS [155]. Since it cannot be ruled out that interaction observed by co-immunoprecipitations is indirect, *in vitro* data in this thesis are the first proof that Atg12–Atg5-Atg16 interacts with PROPPINs. Another study reported membrane binding of Atg12–Atg5-Atg16 *in vitro* [221]. Consistent with these findings weak, inhomogeneous binding of Atg12–Atg5-Atg16 was observed as well (Figure 3.4). The stronger binding observed by Romanov et. al might be caused by highly charged lipid mixtures used in their study.

To explore the function of PROPPINs on Atg8-lipidation in more detail two complementary methods were established. For both systems SLBs containing PI(3)P were prepared on plasma-cleaned glass slides. First, Atg18 bound to SLBs was visualized by atomic

force microscopy (AFM). Experiments were optimized such that well-separated Atg18-particles were observed on SLBs (Figure 3.9 A). Two different populations of particles with sizes of 5 ± 2 nm and 13 ± 3 nm were detected. Interestingly, these sizes were similar to that of Atg18-mono- (5.8 nm) or trimers (10.6 nm), respectively (Figure 3.9 B, C). Analyzing symmetry related molecules of Hsv2 crystal structures, a PROPPIN family protein, and considering particle dimensions observed in AFM experiments it seems likely that Atg18 forms trimers [135, 136]. Interestingly, β-propellers, which are conserved among all canonical coats, are involved in trimerization and thus assembly of cage components and in connecting cargo at sites of vesicle budding [211, 222, 223]. This indicates that Atg18 might be involved in assembling the autophagic membrane scaffold as well, or functions as nucleator for scaffold formation. Second, TIRF microscopy was used to establish single molecule detection of membrane bound Atg18. Single, well separated spots of Atg18 were detectable (Figure 3.10 B). Time traces of these spots showed stable puncta not moving on the membrane. This is in good aggreement with AFM results, since in AFM experiments discrete particles were detected, that were not dragged by the AFM tip. Consistent with these results PIPs seem to be immobile in SLBs as was observed by a FRAP experiment on SLBs containing fluorescently labeled PI(3,5)P_2 (data not shown). During TIRF time traces, Atg18-puncta appeared or disappeared. The newly appearing and reappearing spots can be assigned to binding events, whereas disappearing spots might either be caused by detachment from the membrane or bleaching of fluorescent dyes. Furthermore, the signal intensity varied among different spots, consistent with distinct particle sizes observed in AFM experiments. Thus stepwise bleaching of single spots might reveal the number of fluorescently labeled proteins per spot.

Taken together our *in vitro* data strongly suggest that PROPPINs possess redundant activities in promoting Atg8-lipidation. To understand how the different reported phenotypes of single PROPPIN deletions are evoked, extensive *in vivo* experiments were employed.

4.3 Cooperation of PROPPINs in Different Autophagic Pathways

Previous studies concerning the influence of PROPPIN proteins on autophagic processes suggested that Atg18 is a member of the autophagic core machinery, involved in various autophagic processes [90, 132, 138, 148]. In contrast, Atg21 was reported to only be essential for the Cvt-pathway in *S. cerevisiae* [139]. The molecular functions suggested for Atg18 are limited to late processes of autophagosome formation, including Atg9 trafficking and Cvt-vesicle closure [90, 123]. Atg21 has, however, been reported to target

the Ub-like conjugation machinery to the PAS under vegetative conditions [155] and to promote Atg8-lipidation under starvation conditions [132, 143]. Despite these findings, it is commonly believed that Atg21 is not essential for starvation induced, non-selective autophagy.

Fluorescence microscopy based experiments demonstrated that both Atg18 and Atg21 localize to the PAS under vegetative and starvation conditions (Figure 3.11). Atg8-positive PROPPIN-puncta were more frequently observed under starvation conditions resembling the increase of Atg8-puncta upon starvation. The low frequency of PROPPIN-Atg8 colocalization suggests a more transient binding of PROPPINs to the PAS compared to Atg8. Furthermore, the frequency of PROPPIN-puncta per cell did not change upon starvation, indicating an additional function for PROPPINs in a pathway distinct from autophagy. Consistently, endosomal localization had been proposed for both, Atg18 and Atg21 [140]. Besides punctate structures, Atg18 and Atg21 could be detected at the vacuolar rim. Consistent with previous studies, Atg18 vacuole binding was lost during starvation [95]. This suggests the presence of a mechanism regulating Atg18 localization in response to nutrient supply. In contrast, Atg21 was detected at the vacuole independent of nutritional conditions. In addition to PAS localization, the colocalization of Atg18 and Atg21 revealed that ~50% of Atg18-puncta colocalized with Atg21 during vegetative growth and starvation. These puncta were often detected in proximity of the vacuole, indicating that they might represent the PAS or late endosomes. Taken together these results point towards an activity of both PROPPINs in autophagic processes under vegetative and starvation conditions, but other processes might be coordinated by PROPPINs as well. In this thesis *in vitro* experiments suggested a similar function of PROPPINs in facilitating Atg8-lipidation. Colocalization experiments *in vivo* proposed that both PROPPINs cooperate in autophagy during vegetative growth and starvation. To shed light on the exact requirements of yeast PROPPINs for different autophagic pathways a comprehensive analysis was performed determining the influence of PROPPIN mutants and deletions on vacuole delivery of different autophagic cargos. These experiments revealed that both PROPPINs are needed for delivery of specific cargo under vegetative conditions (Figure 3.16). In contrast, observation of Atg8-puncta formation, a measure of phagophore biogenesis, revealed that Atg21 is essential to initiate Cvt-vesicle formation, while deletion of *ATG18* had no obvious effect on Atg8-puncta formation (Figure 3.14). If Atg18 would act exclusively in autophagosome completion, as it has been proposed [88, 133, 214], an accumulation of Atg8-puncta would be expected, since autophagic membranes would accumulate over time. The discrepancy between the expected accumulation and the observed constant number of Atg8-puncta suggests an additional function of Atg18 in earlier steps of autophagosome formation counteracting accumulation of incomplete autophagosomes. One such function might be that Atg18 and Atg21 protect Atg8 from premature cleavage by Atg4 as has been proposed in a previous study[148]. Besides this

function of Atg18, *in vitro* data presented in this thesis suggest that Atg18 facilitates Atg8-lipidation, a key step in phagophore expansion and thus upstream of autophagosome completion. Taken together, both PROPPINs cooperate and are essential for the Cvt-pathway. While Atg21 is essential for initiation of Atg8-lipidation at the PAS. Atg18 appears to have two functions. The data presented in this work suggest Atg18 to promote Atg8–PE formation in addition to its proposed function in autophagosome closure [90].

In contrast, under starvation conditions Atg21 became dispensable for ApeI delivery, but not for mitophagy and bulk autophagy (Figure 3.16). Interestingly, the requirements for Atg21 correlate with Atg18 redistribution from the vacuole to the PAS, whereas Atg21 localization is not altered upon starvation (Appendix Figure A.10) [95]. This suggests that Atg18-activity is initiated by Atg21 during vegetative growth, but through other factors during starvation. Considering current knowledge about PROPPINs different candidates are to be discussed, including PIPs, proteins like Atg2, and the Vac14 complex, upstream Atg proteins as well as post-translational modifications. PI(3)P and PI(3,5)P_2 were demonstrated to be determinants for PROPPIN localization to PAS, endosomes and vacuole [88, 131]. Nevertheless, PIPs are unlikely to cause the switch in Atg18 localization and function because of two reasons. First, according to Biacore measurements Atg18-binding to PI(3)P and PI(3,5)P_2 is comparable ruling out that Atg18 could be redistributed to the PAS simply by enhanced PI(3)P levels. Second, Atg21 remains bound to the vacuole excluding the possibility that Atg18 might be dispersed from the vacuole by a lack of PI(3,5)P_2. Atg2, a protein interacting with Atg18, has been shown to be essential for both Cvt-pathway and specific and non-specific autophagy under starvation conditions [145, 214]. Previous studies identified Atg18 mutants impaired in Atg2-binding to reduce Cvt-activity as well as specific and non-specific autophagy under starvation conditions [137, 212]. Using overexpression of Atg18 variants in *atg18*Δ*atg21*Δ cells, functional assays in this thesis propose that Atg18 does not require Atg2-binding to rescue ApeI processing in *atg21*Δ cells under starvation conditions as opposed to mitophagy and bulk autophagy (Figure A.7). Together this indicates that Atg2 does not cause a general switch in PROPPIN requirements, but rather decides about the size of cargo transported to the vacuole in absence of Atg21 during starvation. Consistently, a role for Atg2 in membrane expansion has been proposed recently [99]. The Vac14 complex is another interaction partner of Atg18, which might sequester Atg18 at the vacuole during vegetative growth, but might release it upon starvation [154]. However, since the overall number of Atg18-puncta remains constant under vegetative and starvation conditions (Appendix Figure A.4 B), it is unlikely that release of Atg18 from the vacuole and subsequent relocalization to the PAS is the sole reason for the observed switch in PROPPIN requirements upon starvation. It is plausible that a yet uncharacterized

interaction partner of Atg18 alters its activity. Furthermore, post-translational modification is a common regulatory mechanism, which has not been studied extensively for Atg18. Finally, the different requirements for PROPPINs during vegetative growth and starvation might be caused by upstream factors in autophagosome formation. Atg17 is critical for PAS-formation in non-selective autophagy by recruiting Atg9 [112]. Atg11, however, is discussed to replace Atg17 in selective autophagy [121]. Furthermore, Atg1 kinase activity has been suggested to be involved in membrane expansion at giant cargo under autophagy induced conditions [99]. Interestingly, Atg1 kinase activity is inudced under starvation conditions [84]. Importantly, a recent study revealed that Atg1 directly phsophorylates Atg9, thereby, facilitating Atg18 recruitment to the PAS. Since Atg1 kinase activity is induced upon starvation this is a likely mechanism to cause different PROPPIN requirements during vegetative and starvation conditions.

In line with results of functional assays showing degradation of small, specific cargo, electron microscopy images revealed that *atg21*Δ cells still accumulate autophagic vesicles upon starvation (Figure 3.18). However, these vesicles are smaller than in wildtype cells. Furthermore, *atg21*Δ cells were impaired in expansion of autophagosomal membranes at giant ApeI aggregates (Figure 3.15 A). Consistently, small cargo like ApeI is transported to the vacuole independent of Atg21, while delivery of large cargo and bulk cytoplasm requires Atg21. Atg18 is essential for delivery of all kinds of autophagic cargo to the vacuole, but not for GFP-Atg8 puncta formation during vegetative and starvation conditions. This confirms that Atg18 is not essential for PAS-formation and thus autophagy initiation, but plays a critical role in autophagosome expansion, completion or fusion with the vacuole [90]. Consistently, Atg18 is required for the expansion of phagophore membranes at giant ApeI cargo and overexpression of Atg18, to adjust its expression levels to that of Atg21, compensates for Atg21. Furthermore, small cargo (ApeI) is transported to the vacuole in *atg21*Δ cells expressing endogenous levels of Atg18, while efficient mitophagy in *atg21*Δ cells requires Atg18 overexpression. This implies that Atg18 mediates Atg8-lipidation, which tethers autophagic membranes to cargo.

Analysis of PROPPIN mutants revealed that under vegetative conditions PI(3)P binding of Atg21 via its FRRG-motif is essential for the Cvt-pathway (Appendix Figure A.7). Consequently, PI(3)P is either the sole PAS recruitment factor for Atg21 under vegetative conditions, or it is required for correct orientation at the membrane. Furthermore, overexpression of Atg21$^{\Delta PI(3)P}$ did not rescue its phenotype under vegetative conditions, suggesting that Atg21$^{\Delta PI(3)P}$ does not display residual PIP binding as proposed by previous *in vitro* studies [133]. In contrast, during starvation Atg21$^{\Delta PI(3)P}$ did not alter cargo delivery to the vacuole. Consequently, PI(3)P is not the only PAS recruitment factor for Atg21 under starvation conditions. This is, at least for specific autophagy, supported by further data, since deletion of *ATG18* resulted in strong reduction of Atg8-puncta at giant ApeI cargo (Appendix Figure A.6 B). Atg21, therefore, seems to be recruited

partially by Atg18 during starvation.

For Atg18, PI(3)P- or Atg2-binding were sufficient for residual activity in ApeI maturation during vegetative growth. Mutation of both binding sites ($Atg18^{\Delta PI3P\Delta Atg2}$), however, completely blocked the Cvt-pathway. Two conclusions can be drawn from these experiments for vegetative conditions. First, PI(3)P and Atg2 are complementary factors ensuring correct localization of Atg18 to the forming Cvt vesicle. Second, PI(3)P and Atg2 are the sole factors for functional localization of Atg18, since mutation of both binding sites ($Atg18^{\Delta PI3P\Delta Atg2}$) results in complete loss of function. During starvation PI(3)P- or Atg2-binding mutants of Atg18 have only minor effects on autophagic degradation of small specific cargo and bulk cytoplasm. For large specific cargo, binding of both interaction partners is more relevant (Appendix Figure A.7). Nevertheless, $Atg18^{\Delta PI3P\Delta Atg2}$ completely blocks specific autophagy. This implies two possible interpretations. First, an additional localization factor might ensure PAS recruitment of Atg18 under starvation conditions and PI(3)P or Atg2 binding would be essential for the correct orientation of Atg18 on the membrane. Second, PI(3)P and Atg2 could be the sole PAS-determinants for Atg18, but enhanced activity of Atg18 during starvation can compensate for reduced PAS localization in single mutants ($Atg18^{\Delta PI3P}$ and $Atg18^{\Delta Atg2}$). Given the fact that both single mutants could not be detected at the PAS in previous studies [88, 133, 137] the second hypthesis is more likely. The actual cause of enhanced Atg18 activity, however, remains to be identified. As discussed above starvation-sepcific interaction-partners as well as post-translational modifications of Atg18 or an interaction partner are possible switches. These are likely to be caused by distinct upstream signalling during vegetative growth and starvation.

In contrast to a previous study, yeast strains overexpressing $Atg18^{FKKG}$ and $Atg21^{FKKG}$ exhibited delivery of bulk cytoplasm to the vacoule [148]. Nair *et al.* used native promoters, thus Atg18 and Atg21 expression levels were considerably lower. Therefore, residual activity was caused most likely by overexpression. A possible explanation for this discrepancy is that the mutants are not completely devoid of PI(3)P binding and that the residual binding is sufficient when proteins are overexpressed. Consistently, very weak residual binding of $Atg18^{\Delta PI3P}$ was observed on GUVs containing PI(3)P (data not shown). Taken together, PROPPIN requirements for functional autophagic pathways differ between vegetative growth and starvation conditions. This is most probably caused by a switch in Atg18 activity, since Atg21 becomes dispensable for specific autophagy only upon starvation.

4.4 PROPPINs Might Catalyze the Formation of Distinct Atg8–PE Pools

The function of Atg21 in the Cvt-pathway has been identified recently, but its role in unspecific autophagy remained poorly understood. The molecular funtion of Atg18 is even less well characterized and why Atg18 is critical for all types of autophagy, whereas Atg21 is dispensable for non-selective autophagy remained unknown. This work set out to characterize both proteins *in vitro* and *in vivo*. *In vitro* data suggested that both PROPPINs can facilitate Atg8-lipidation by recruitment of Atg12–Atg5-Atg16. This is supported by two recent studies. One showed that the human Atg18 homolog WIPI-2B initiates LC3-lipidation (Atg8 homolog) by direct interaction with Atg16L1 [151]. The second study showed that Atg21 initiates Atg8-lipidation at the PAS under vegetative conditions by interaction with Atg16 [155]. Therefore, the potential of PROPPINs to facilitate Atg8-lipidation was investigated in detail.

Examination of Atg8–PE and Atg8-puncta formation revealed that Atg21 initiates Atg8-lipidation at the PAS during starvation (Figure 3.13 and Figure 3.14), which is required to produce autophagosomes that capture cytoplasmic material non-selectively (Figure 3.16 A). Atg18, on the other hand, was sufficient for vacuolar delivery of small specific cargo (ApeI, Figure 3.16 A). Its expression level, furthermore, directly correlated with cargo size, with large cargo being delivered to the vacuole in *atg21*Δ cells when Atg18 was overexpressed (Figure 3.16 B). Consistently, Atg8-containing membranes were impaired in expanding around giant ApeI cargo in *atg21*Δ cells (Figure 3.15), suggesting that phagophore expansion depends on Atg21. Electron microscopy confirmed this hypothesis, since autophagic vesicles that accumulated in the vacuoles of *atg21*Δ cells were smaller than in wildtype cells (Figure 3.19 B). This implies that, Atg21 mediates bulk Atg8-lipidation and that the amount of Atg8–PE correlates with autophagosome size. Moreover, Atg21 is dispensable for formation of Cvt-like vesicles and mitophagy critically depends on Atg18 expression levels. Consequently, the Atg8-pool that tethers cargo does not depend on Atg21. Therefore, it is likely that Atg21 mediates formation of a convex Atg8–PE pool. This is consistent with previous reports demonstrating that Atg8 levels determine the size of autophagosomes [89]. Atg12–Atg5-Atg16 have been demonstrated to localize to the convex face of the autophagosome where it can form a scaffold with Atg8 *in vitro* [21, 224]. Atg21 also supplies Atg8 for specific autophagy since Atg8-mediated capturing of mitochondria and giant ApeI works in wildtype but not in *atg21*Δ cells.

In contrast to Atg21, Atg18 is essential for transport of any autophagic cargo, consistent with previous reports on Atg18 [90, 139]. This might be attributed to its proposed late function in autophagosome formation [90]. Based on the observed localization of

Atg18 to phagophore tips [99] and its function to recruit Atg12–Atg5-Atg16 to membranes, two Atg18-dependent mechanisms seem likely to mediate phagophore closure. First, Atg12–Atg5-Atg16 has been reported to tether membranes [221]. Consequently, Atg12–Atg5-Atg16 recruited to the tips of the phagophore membrane by Atg18 might facilitate membrane tethering fusion to complete autophagosomes. Second, Atg8 has been suggested to tether membranes and to facilitate hemifusion [91]. Therefore, Atg8 localized to phagophore tips might facilitate membrane fusion to close the phagophore. Nevertheless, autophagosome closure seems not to be the only function of Atg18. Lipidation of Atg8 was enhanced in *atg18*Δ cells during starvation, but only dim Atg8-puncta accumulated under these conditions. This indicates an impairment in phagophore expansion, consistent with data presented in this study and by another lab demonstrating that membranes do not expand around giant ApeI cargo (Figure 3.15) [99]. On the other hand, Atg18 has been proposed to protect Atg8–PE from premature cleavage [148] which could explain accumulation of dim Atg8-puncta in *atg18*Δ cells as well. In cells harbouring giant cargo Atg8-lipidation was reduced in *atg21*Δ cells (Figure 3.20), but Cvt-like vesicles were still formed (Figure 3.16 A, and Figure 3.19). Upon overexpression of Atg18 mitophagy could be fully rescued in *atg21*Δ cells. These data imply that Atg18 is sufficient for production of an Atg8-pool that tethers the phagophore membrane to specific cargo. Consistently, Atg18 overexpression in *atg21*Δ cells facilitated expansion of membrane crescents around giant cargo and Atg8–PE levels were elevated to wild-type levels (Figure 3.21). Taken together these data strongly suggest, that Atg18 and Atg21 generate distinct Atg8-pools at the phagophore important for cargo selection and phagophore expansion. However, PROPPIN activity and their mode of cooperation differ in distinct types of autophagy. As discussed above, upstream factors of autophagy and post-translational modifications are likely candidates to cause these differences. Furthermore, distinct binding partners of PROPPINs might alter their activity. This needs to be further investigated.

4.5 Potential Involvement of PROPPINs in Alternative Pathways Delivering Cytoplasm to the Vacuole

Pho8Δ60 data demonstrate that overexpression of Atg21 in absence of Atg18 can partially rescue delivery of bulk cytoplasm into the vacuole (Figure 3.16 B). However, electron microscopy revealed that no autophagic bodies are transported to the vacuole (Figure 3.18). Consequently, alternative routes must exist to deliver cytoplasmic material to the vacuole. One obvious candidate is the MVB-pathway, since it has been reported that cytoplasmic proteins are transported into ILVs in an ESCRT- and Atg-protein-dependent manner [225]. In this study a microautophagy-like process was identified that delivers

soluble cytoplamic proteins to the vesicles of MVBs [225]. Therefore, the influence of Atg21-dependent, MVB-mediated delivery of cytoplasmic material to the vacuole was tested. Data demonstrate that some cytoplasmic material is delivered to the vacuole in an MVB-dependent manner (Figure 3.22). MVB-dependent delivery of cytoplasm to the vacuole could only be detected in absence of functional autophagy and in presence of Atg21 overexpression. Elevated Atg21 levels might induce the MVB-pathway, since it has been shown to localize to endosomes [140]. Nevertheless, vacuolar transport of cytoplasmic material was not completely abolished by a block of the MVB-pathway. Therefore, additional pathways might exist that transport cytoplasm to the vacuole and depend on Atg21. In electron microscopy experiments an accumulation of small vesicles in vacuoles was observed in *atg18*Δ cells some of which might represent ILVs, whereas the majority rather seemed to be small lipid droplets. Additionally, large lipid droplets accumulated in *atg18*Δ cells under starvation conditions and numbers of lipid dorplets correlated with Atg21 expression levels. Thus, Atg21 might be additionally involved in lipophagy. This implies that Atg21 might not be exclusively needed for autophagy, but for other transport pathways. Consequently, the pathways by which Atg21-mediated transport of cytoplasmic material is facilitated needs further investigation.

Taken together data presented in this thesis reveal a clear cut difference in the functions of Atg18 and Atg21. Atg21 initiates bulk Atg8-lipidation by recruitment of Atg12–Atg5-Atg16 and controls phagophore expansion probably by scaffold formation on the convex face of the membrane. Thereby, Atg21 controls the size of autphagosomes. Atg18, on the other hand, is important for late steps in autophagy and in addition facilitates cargo tethering presumably by promoting the formation of a concave Atg8-PE pool.

Outlook

In this thesis an unexpected division of labor of the two yeast PROPPINs, Atg18 and Atg21, was observed which leads to a better understanding of critical steps in autophagy, including the switch between selective and non-selective types of autophagy. It was demonstrated that both PROPPINs localize to the PAS under vegetative and starvation conditions. Additionally, PORPPINs colocalize under both conditions to similar extents. This suggests a cooperative action of PROPPINs in Cvt-vesicle and autophagosome formation. However, it is not clear whether double-positive PROPPIN-puncta localize to the PAS. Microscopic observation of triple-labeled yeast cells could answer this question. In addition to PROPPINs, upstream factors such as Atg1 or Atg13 could be fused to a fluorescent protein as a PAS marker. Atg17, another component of the Atg1 kinase complex, is not well suited for these experiments since it is critical for PAS formation in non-selective autophagy by recruitment of Atg9 [112], whereas Atg11 is discussed to replace Atg17 in selective autophagy [121]. Timecourse experiments with triple labeled yeast has the potential to reveal sequential or parallel recruitment of PROPPINs to the PAS.

Using the giant ApeI assay it was detected that both PROPPINs localize to autophagosomal membranes expanding around giant cargo. Interestingly, differential localization was observed, with Atg18 being localized at the tips and Atg21 being distributed over the complete membrane. Super-resolution imaging of PROPPINs would reveal a more detailed picture of their localization since resolution limits can be pushed down to 20 nm [226].

Data presented in this thesis strongly suggest that both PROPPINs mediate Atg8-lipidation resulting in phagophore expansion and cargo tethering. Based on extensive *in vivo* experiments it seems likely that Atg21 mainly mediates Atg8-lipidation at the convex phase which is involved in membrane expansion [89]. Atg18, on the other hand, is sufficient to generate cargo tethering Atg8–PE, which is supposed to be localized at the concave face of the phagophore [22]. A direct proof for this hypothesis could be obtained by immuno-electron microscopy. Atg8 could be tagged with GFP or an HA tag for immuno-detection. To monitor the Atg8–PE amount at the concave and convex face of the phagophore, autophagosomes could be accumulated in the cytoplasm by blocking their fusion with the vacuole. Possible candidates would be *vam3*Δ or *vpt7*Δ strains [143, 227]. In addition to conventional electron microscopy, the quick-freeze and freeze-fracture labeling could be used to dissect Atg8 membrane distribution [228]. It is likely that Atg18 and Atg21 do not exclusively form one Atg8–PE pool, but with strong preference. This could also be directly prooven by these immuno-electron microscopy

studies.

Consistent with previous studies [139, 143], ApeI processing assays in this study suggest that upon starvation ApeI processing requires only Atg18, whereas both PROPPINs are essential for ApeI processing in vegetative growth. Additionally, relocalization of Atg18 from the vacuolar rim to the PAS was observed under starvation conditions. Therefore, an intriguing question is what causes this molecular switch between vegetative and starvation conditions. A possible mode of regulation would be post-translational modifications of PROPPINs, dependent on growth conditions. Interestingly, a study in *P. pastoris* revealed that Atg18 phosphorylation regulates vacuole binding [144]. Furthermore, several phsosphorylation sites, specific for nutirent conditions, have been proposed for Atg18 in *S. cerevisiae*, but none of those was reported to have a strong influence on autophagy [229]. An approach to directly investigate post-translational regulation of Atg18 and Atg21 would be mass-spectrometry of immuno-enriched Atg18 and Atg21 under vegetative or starvation conditions. On the other hand, a different set or post-translational modification of interaction partners might cause the functional difference. Consistently, Atg18 has been reported recently, to interact with phosphorylated Atg9. This phosphorlation depends on Atg1 kinase activity, which is induced upon starvation [119]. Consequently, CoIP and mass-spectrometry based identification of interaction partners might shed light on the mechanistic switch from Cvt to autophagy. In order not to miss transient interaction partners, crosslinking of proteins prior to immunoprecipitation could be applied.

In vitro smTIRF and AFM experiments provide a solid basis to further investigate the mechanistical influence of PROPPINs on Atg8-lipidation and scaffold formation. AFM can be used to detect how the protein scaffold forms in absence and presence of PROPPINs with high spatial resolution. Therefore, lipidation reactions have to be performed in absence and presence of PROPPINs and need to be stopped at distinct timepoints. Imaging of different reaction setups could reveal differences in coat formation. With the complementary approach of smTIRF, one can observe lipidation in real time. With this setup, it would be interesting to see whether the protein scaffold spreads radially from a PROPPIN spot. But additional information can be retreaved from this system. First, it would be possible to monitor residence times and the distribution of PROPPINs at the membrane. This would allow for a conclusion if PROPPINs only initiate scaffold formation or if they are integral part of the scaffold. To gain these informations, first a more detailed characterization of single fluorescent spots has to be obtained, the number of PROPPINs per spot should be determined by stepwise bleaching of dye molecules. To minimize bleaching, oxigen scavangeing systems and Trolox can be used and time traces of single molecules up to 90 min have been achieved [230].

Interestingly, PROPPINs have been suggested to play an important role in stabilizing Atg proteins on the autophagosome [156]. More specifically, Atg8 recycling from the

autophagosome preceeds fusion with the vacuole and Atg18 and Atg21 have been suggested to protect Atg8 from premature cleavage by Atg4 [148]. Therefore, the influence of PROPPINs on Atg8 recycling by Atg4 should be tested *in vitro* using model membranes and purified proteins.

Using AFM, particles were observed on the membrane that seem to represent multimers. Interestingly, symmetry related molecules in the crystal structure of Hsv2 suggest trimer formation of PROPPINs. In general, β-propellers are common domains for protein-oligomerization [135, 136]. One example includes the trimer formation of COPI-subunits on membranes [211]. Consequently, it would be possible to investigate trimer formation of PROPPINs on membranes using AFM. Complementary *in vivo* functional assays with trimerization incompetent mutants would then clarify the functional implications of PROPPIN trimerization.

It is known that two Atg8-pools exist on phagophores [22, 89]. According to the data presented in this thesis Atg18 is important for efficient transport of specific cargo most probably by generating Atg8–PE at the concave face of the phagophore. An important question is how these two Atg8-pools are being generated. One hypothesis would be that the concave and convex face are defined by PROPPINs, with Atg21 defining the convex face and leading to Atg8 scaffold formation. Atg18 could, maybe in concert with an additional interaction partner, prevent scaffold formation and, thereby, ensure Atg8 to be available for cargo-adaptor interaction. Apart from these possibilities, in *D. melanogaster* Atg18 has been suggested to bind Atg9 and p62; thereby, it might facilitate selective degradation of ubiquitinated proteins [231]. Furthermore, WD40 β-propellers have been identified as ubiquitin sensors that regulate protein turnover [232]. And finally, in canonical protein coats β-propellers have been reported to mediate interactions between cargo and coat components [5, 7]. Consequently, it is tempting to speculate that prior to Atg8-lipidation Atg18 binding to adaptor proteins could provide an efficient way to initiate Atg8–PE formation at membranes in close proximity of specific cargo. *In vitro* studies using GUVs and purified proteins as well as CoIP experiments in combination with mass spectrometric analysis might reveal such interaction.

A function of Atg18 not yet investigated in detail is its involvement in autophagosome closure [90]. A recent study demonstrated that Atg18 localizes to the tips of phagophore membranes expanding around giant cargo [99]. In this thesis it was demonstrated that Atg18 recruits Atg12–Atg5-Atg16 to membranes and facilitates Atg8-lipidation. Interestingly, Atg12–Atg5-Atg16 as well as Atg8 have been proposed to tether membranes [91, 221]. It would be interesting to see if these proteins mediate autophagosome sealing and whether this function depends on Atg18.

Studies in mammalian cells claim WIPI-2B to be an Atg18 homolog [150, 151]. In contrast, results of yeast experiments presented in this thesis and in other studies [155] rather suggest a functional homology between Atg21 and WIPI-2B. Using mammalian

homologs in yeast to rescue autophagy-impaired mutants has been performed sucessfully [233]. Therefore, one possible attempt to clarify which yeast PROPPIN is the functional homolog of WIPI-2B would be to replace *ATG18* or *ATG21* by *WIPI-2B* and monitor different types of autophagy. Still, it needs to be considered that the protein folding machinery differs from mammalian cells. Consequently, a conclusion can only be drawn from experiments where rescue is observed.

Finally, it has been shown before that Atg18-Atg2 form a constitutive complex of ~450 kDa [88] corresponding to a dimer of Atg18-Atg2. In this thesis and in other studies it was showen that Atg18-Atg2 localize to the tips of growing autophagosomes and both are needed for membrane expansion [99]. Furthermore, Atg18 binds to phosphorylated Atg9 [119]. These results make it tempting to speculate that the Atg18-Atg2 complex is involved in the formation of contact sites between phagophore and ER exit sites and the vacuole. A characteriization of these contact sites in *atg2*Δ cells would shed light on the function of Atg2. To gain further knowledge about this complex it would be interesting to map the interaction site of Atg2 with Atg18. A potential candidate is glycine 83 in Atg2, which has been shown to be critical for Atg2-PAS localization [145]. Alternatively, soluble Atg2 fragments, obtained in an expression screen during this thesis could be used as competition factors to narrow down the binding site of Atg18 and Atg2.

Bibliography

[1] Szul, T. and Sztul, E. “COPII and COPI Traffic at the ER-Golgi Interface”. In: *Physiology* 26.5 (2011), pp. 348–364.

[2] Cai, H., Reinisch, K., and Ferro-Novick, S. “Coats, Tethers, Rabs, and SNAREs Work Together to Mediate the Intracellular Destination of a Transport Vesicle”. In: *Developmental Cell* 12.5 (2007), pp. 671–682.

[3] Nair, U., Jotwani, A., Geng, J., Gammoh, N., Richerson, D., Yen, W.-L., Griffith, J., Nag, S., Wang, K., Moss, T., Baba, M., McNew, J. a., Jiang, X., Reggiori, F., Melia, T. J., and Klionsky, D. J. “SNARE proteins are required for macroautophagy.” In: *Cell* 146.2 (2011), pp. 290–302.

[4] Lynch-Day, M. a., Bhandari, D., Menon, S., Huang, J., Cai, H., Bartholomew, C. R., Brumell, J. H., Ferro-Novick, S., and Klionsky, D. J. “Trs85 directs a Ypt1 GEF, TRAPPIII, to the phagophore to promote autophagy.” In: *Proceedings of the National Academy of Sciences of the United States of America* 107.17 (2010), pp. 7811–7816.

[5] Beck, R., Rawet, M., Ravet, M., Wieland, F. T., and Cassel, D. “The COPI system: molecular mechanisms and function.” In: *FEBS letters* 583.17 (2009), pp. 2701–9.

[6] Brandizzi, F. and Barlow, C. “Organization of the ER–Golgi interface for membrane traffic control”. In: *Nature Reviews Molecular Cell Biology* 14.6 (2013), pp. 382–392.

[7] Faini, M., Beck, R., Wieland, F. T., and Briggs, J. a. G. “Vesicle coats: structure, function, and general principles of assembly.” In: *Trends in cell biology* 23.6 (2013), pp. 279–88.

[8] Park, S.-Y., Yang, J.-S., Schmider, A. B., Soberman, R. J., and Hsu, V. W. “Coordinated regulation of bidirectional COPI transport at the Golgi by CDC42”. In: *Nature* 521 (2015), pp. 529–531.

[9] Edeling, M. a., Mishra, S. K., Keyel, P. a., Steinhauser, A. L., Collins, B. M., Roth, R., Heuser, J. E., Owen, D. J., and Traub, L. M. “Molecular switches involving the AP-2 β2 appendage regulate endocytic cargo selection and clathrin coat assembly”. In: *Developmental Cell* 10.3 (2006), pp. 329–342.

[10] Knuehl, C., Chen, C. Y., Manalo, V., Hwang, P. K., Ota, N., and Brodsky, F. M. “Novel binding sites on Clathrin and adaptors regulate distinct aspects of coat assembly”. In: *Traffic* 7.12 (2006), pp. 1688–1700.

[11] Bi, X., Mancias, J. D., and Goldberg, J. “Insights into COPII Coat Nucleation from the Structure of Sec23-Sar1 Complexed with the Active Fragment of Sec31”. In: *Developmental Cell* 13.5 (2007), pp. 635–645.

[12] Hara-Kuge, S., Kuge, O., Orci, L., Amherdt, M., Ravazolla, M., Wieland, F. T., and Rothman, J. E. “En Bloc Incorporation of Coatomer Subunits during the Assembly of COP-coated Vesicles”. In: *Journal of Cell Biology* 124.6 (1994), pp. 883–892.

[13] Brodsky, F. M. “Diversity of Clathrin Function: New Tricks for an Old Protein”. In: *Annual Review of Cell and Developmental Biology* 28.1 (2012), pp. 309–336.

[14] Reider, A. and Wendland, B. “Endocytic adaptors–social networking at the plasma membrane.” In: *Journal of cell science* 124.10 (2011), pp. 1613–1622.

[15] Rohde, G., Wenzel, D., and Haucke, V. “A phosphatidylinositol (4,5)-bisphosphate binding site within mu2-adaptin regulates clathrin-mediated endocytosis.” In: *Journal of Cell Biology* 158.2 (2002), pp. 209–214.

[16] Jackson, L. P., Kelly, B. T., McCoy, A. J., Gaffry, T., James, L. C., Collins, B. M., Höning, S., Evans, P. R., and Owen, D. J. “A large-scale conformational change couples membrane recruitment to cargo binding in the AP2 clathrin adaptor complex”. In: *Cell* 141.7 (2010), pp. 1220–1229.

[17] Ohno, H., Stewart, J., Fournier, M. C., Bosshart, H., Rhee, I., Miyatake, S., Saito, T., Gallusser, A., Kirchhausen, T., and Bonifacino, J. S. “Interaction of tyrosine-based sorting signals with clathrin-associated proteins.” In: *Science* 269.5232 (1995), pp. 1872–1875.

[18] Haar, E. ter, Harrison, S. C., and Kirchhausen, T. “Peptide-in-groove interactions link target proteins to the beta-propeller of clathrin.” In: *Proceedings of the National Academy of Sciences of the United States of America* 97.3 (2000), pp. 1096–1100.

[19] Kang, D. S., Kern, R. C., Puthenveedu, M. a., Zastrow, M. von, Williams, J. C., and Benovic, J. L. “Structure of an arrestin2-clathrin complex reveals a novel clathrin binding domain that modulates receptor trafficking”. In: *Journal of Biological Chemistry* 284.43 (2009), pp. 29860–29872.

[20] Fotin, A., Cheng, Y., Sliz, P., Grigorieff, N., Harrison, S. C., Kirchhausen, T., and Walz, T. “Molecular model for a complete clathrin lattice from electron cryomicroscopy.” In: *Nature* 432.7017 (2004), pp. 573–579.

[21] Kaufmann, A., Beier, V., Franquelim, H. G., and Wollert, T. “Molecular Mechanism of Autophagic Membrane-Scaffold Assembly and Disassembly”. In: *Cell* 156.3 (2014), pp. 469–481.

[22] Sawa-Makarska, J., Abert, C., Romanov, J., Zens, B., Ibiricu, I., and Martens, S. "Cargo binding to Atg19 unmasks additional Atg8 binding sites to mediate membrane–cargo apposition during selective autophagy". In: *Nature Cell Biology* 16 (2014), pp. 425–433.

[23] Campelo, F. and Malhotra, V. "Membrane fission: the biogenesis of transport carriers." In: *Annual review of biochemistry* 81 (2012), pp. 407–27.

[24] McCullough, J., Colf, L. a., and Sundquist, W. I. "Membrane Fission Reactions of the Mammalian ESCRT Pathway." In: *Annual review of biochemistry* 82 (2013), pp. 663–92.

[25] Faelber, K., Held, M., Gao, S., Posor, Y., Haucke, V., Noé, F., and Daumke, O. "Structural insights into dynamin-mediated membrane fission." In: *Structure* 20.10 (2012), pp. 1621–8.

[26] Klein, D. E., Lee, A., Frank, D. W., Marks, M. S., and Lemmon, M. a. "The pleckstrin homology domains of dynamin isoforms require oligomerization for high affinity phosphoinositide binding". In: *Journal of Biological Chemistry* 273.42 (1998), pp. 27725–27733.

[27] Shupliakov, O., Löw, P., Grabs, D., Gad, H., Chen, H., David, C., Takei, K., De Camilli, P., and Brodin, L. "Synaptic vesicle endocytosis impaired by disruption of dynamin-SH3 domain interactions." In: *Science* 276.5310 (1997), pp. 259–263.

[28] Soulet, F., Yarar, D., Leonard, M., and Schmid, S. L. "SNX9 Regulates Dynamin Assembly and Is Required for Efficient Clathrin-mediated Endocytosis". In: *Molecular biology of the cell* 16.1 (2005), pp. 2058–2067.

[29] Hinshaw, J. E. and Schmid, S. L. "Dynamin self-assembles into rings suggesting a mechanism for coated vesicle budding." In: *Nature* 374.6518 (1995), pp. 190–192.

[30] Mears, J. a., Ray, P., and Hinshaw, J. E. "A Corkscrew Model for Dynamin Constriction". In: *Structure* 15.10 (2007), pp. 1190–1202.

[31] Stowell, M. H., Marks, B., Wigge, P., and McMahon, H. T. "Nucleotide-dependent conformational changes in dynamin: evidence for a mechanochemical molecular spring." In: *Nature cell biology* 1.1 (1999), pp. 27–32.

[32] Roux, A., Uyhazi, K., Frost, A., and De Camilli, P. "GTP-dependent twisting of dynamin implicates constriction and tension in membrane fission." In: *Nature* 441.7092 (2006), pp. 528–531.

[33] Bashkirov, P. V., Akimov, S. A., Evseev, A. I., Schmid, S. L., Zimmerberg, J., and Frolov, V. A. "A partnership between dynamin and lipids defines dynamics and intermediates of membrane fission". In: *Cell* 135.7 (2008), pp. 1276–1286.

[34] Lee, M. C., Orci, L., Hamamoto, S., Futai, E., Ravazzola, M., and Schekman, R. “Sar1p N-Terminal Helix Initiates Membrane Curvature and Completes the Fission of a COPII Vesicle”. In: *Cell* 122.4 (2005), pp. 605–617.

[35] Adolf, F., Herrmann, A., Hellwig, A., Beck, R., Brügger, B., and Wieland, F. T. “Scission of COPI and COPII vesicles is independent of GTP hydrolysis.” In: *Traffic* 14.8 (2013), pp. 922–32.

[36] Yu, I.-M. and Hughson, F. M. “Tethering factors as organizers of intracellular vesicular traffic.” In: *Annual review of cell and developmental biology* 26 (2010), pp. 137–156.

[37] Wang, W., Sacher, M., and Ferro-Novick, S. “TRAPP stimulates guanine nucleotide exchange on Ypt1p”. In: *Journal of Cell Biology* 151.2 (2000), pp. 289–295.

[38] Morozova, N., Liang, Y., Tokarev, A. a., Chen, S. H., Cox, R., Andrejic, J., Lipatova, Z., Sciorra, V. a., Emr, S. D., and Segev, N. “TRAPPII subunits are required for the specificity switch of a Ypt-Rab GEF.” In: *Nature cell biology* 8.11 (2006), pp. 1263–1269.

[39] Cai, H., Yu, S., Menon, S., Cai, Y., Lazarova, D., Fu, C., Reinisch, K., Hay, J. C., and Ferro-Novick, S. “TRAPPI tethers COPII vesicles by binding the coat subunit Sec23.” In: *Nature* 445.7130 (2007), pp. 941–944.

[40] Jang, S. B., Kim, Y. G., Cho, Y. S., Suh, P. G., Kim, K. H., and Oh, B. H. “Crystal structure of SEDL and its implications for a genetic disease spondyloepiphyseal dysplasia tarda”. In: *Journal of Biological Chemistry* 277.51 (2002), pp. 49863–49869.

[41] Kakuta, S., Yamamoto, H., Negishi, L., Kondo-Kakuta, C., Hayashi, N., and Ohsumi, Y. “Atg9 vesicles recruit vesicle-tethering proteins Trs85 and Ypt1 to the autophagosome formation site”. In: *Journal of Biological Chemistry* 287.53 (2012), pp. 44261–44269.

[42] Wang, J., Menon, S., Yamasaki, A., Chou, H.-T., Walz, T., Jiang, Y., and Ferro-Novick, S. “Ypt1 recruits the Atg1 kinase to the preautophagosomal structure.” In: *Proceedings of the National Academy of Sciences of the United States of America* 110.24 (2013), pp. 9800–5.

[43] Tan, D., Cai, Y., Wang, J., Zhang, J., Menon, S., Chou, H.-T., Ferro-Novick, S., Reinisch, K. M., and Walz, T. “The EM structure of the TRAPPIII complex leads to the identification of a requirement for COPII vesicles on the macroautophagy pathway.” In: *Proceedings of the National Academy of Sciences of the United States of America* (2013), pp. 2–7.

[44] McEwan, D. G., Popovic, D., Gubas, A., Terawaki, S., Suzuki, H., Stadel, D., Coxon, F. P., Miranda de Stegmann, D., Bhogaraju, S., Maddi, K., Kirchof, A., Gatti, E., Helfrich, M. H., Wakatsuki, S., Behrends, C., Pierre, P., and Dikic, I. "PLEKHM1 Regulates Autophagosome-Lysosome Fusion through HOPS Complex and LC3/GABARAP Proteins". In: *Molecular Cell* 57.1 (2014), pp. 39–54.

[45] Ichimura, Y., Kirisako, T., Takao, T., Satomi, Y., Shimonishi, Y., Ishihara, N., Mizushima, N., Tanida, I., Kominami, E., Ohsumi, M., Noda, T., and Ohsumi, Y. "A ubiquitin-like system mediates protein lipidation." In: *Nature* 408.6811 (2000), pp. 488–492.

[46] Jiang, P., Nishimura, T., Sakamaki, Y., Itakura, E., Hatta, T., Natsume, T., and Mizushima, N. "The HOPS complex mediates autophagosome-lysosome fusion through interaction with syntaxin 17." In: *Molecular biology of the cell* 25.8 (Feb. 2014), pp. 1327–1337.

[47] Lobingier, B. T., Nickerson, D. P., Lo, S. Y., and Merz, A. J. "SM proteins Sly1 and Vps33 co-assemble with Sec17 and SNARE complexes to oppose SNARE disassembly by Sec18". In: *eLife* 2014.3 (2014), pp. 1–22.

[48] Malsam, J., Kreye, S., and Söllner, T. H. "Membrane traffic in the secretory pathway: Membrane fusion: SNAREs and regulation". In: *Cellular and Molecular Life Sciences* 65.18 (2008), pp. 2814–2832.

[49] Söllner, T., Whiteheart, S. W., Brunner, M., Erdjument-Bromage, H., Geromanos, S., Tempst, P., and Rothman, J. E. "SNAP receptors implicated in vesicle targeting and fusion". In: *Nature* 362 (1993), pp. 318–324.

[50] Fasshauer, D., Sutton, R. B., Brunger, a. T., and Jahn, R. "Conserved structural features of the synaptic fusion complex: SNARE proteins reclassified as Q- and R-SNAREs." In: *Proceedings of the National Academy of Sciences of the United States of America* 95.26 (1998), pp. 15781–15786.

[51] Söllner, T., Bennett, M. K., Whiteheart, S. W., Scheller, R. H., and Rothman, J. E. "A protein assembly-disassembly pathway in vitro that may correspond to sequential steps of synaptic vesicle docking, activation, and fusion." In: *Cell* 75.3 (1993), pp. 409–418.

[52] Dulubova, I., Sugita, S., Hill, S., Hosaka, M., Fernandez, I., Südhof, T. C., and Rizo, J. "A conformational switch in syntaxin during exocytosis: Role of munc18". In: *EMBO Journal* 18.16 (1999), pp. 4372–4382.

[53] Shen, J., Tareste, D. C., Paumet, F., Rothman, J. E., and Melia, T. J. "Selective Activation of Cognate SNAREpins by Sec1/Munc18 Proteins". In: *Cell* 128.1 (2007), pp. 183–195.

[54] Stenmark, H. “Rab GTPases as coordinators of vesicle traffic.” In: *Nature reviews. Molecular cell biology* 10.8 (2009), pp. 513–525.

[55] Pfeffer, S. R. “Structural clues to rab GTPase functional diversity”. In: *Journal of Biological Chemistry* 280.16 (2005), pp. 15485–15488.

[56] Mizuno-Yamasaki, E., Rivera-Molina, F., and Novick, P. “GTPase Networks in Membrane Traffic”. In: *Annual Review of Biochemistry* 81.1 (2012), pp. 637–659.

[57] Semerdjieva, S., Shortt, B., Maxwell, E., Singh, S., Fonarev, P., Hansen, J., Schiavo, G., Grant, B. D., and Smythe, E. “Coordinated regulation of AP2 uncoating from clathrin-coated vesicles by rab5 and hRME-6”. In: *Journal of Cell Biology* 183.3 (2008), pp. 499–511.

[58] Arai, S., Noda, Y., Kainuma, S., Wada, I., and Yoda, K. “Ypt11 Functions in Bud-Directed Transport of the Golgi by Linking Myo2 to the Coatomer Subunit Ret2”. In: *Current Biology* 18.13 (2008), pp. 987–991.

[59] Guo, W., Roth, D., Walch-Solimena, C., and Novick, P. “The exocyst is an effector for Sec4P, targeting secretory vesicles to sites of exocytosis”. In: *EMBO Journal* 18.4 (1999), pp. 1071–1080.

[60] Finley, D., Ulrich, H. D., Sommer, T., and Kaiser, P. “The ubiquitin-proteasome system of Saccharomyces cerevisiae”. In: *Genetics* 192.2 (2012), pp. 319–360.

[61] Apaja, P. M. and Lukacs, G. L. “Protein Homeostasis at the Plasma Membrane.” In: *Physiology* 29.4 (2014), pp. 265–277.

[62] Nakatogawa, H., Suzuki, K., Kamada, Y., and Ohsumi, Y. “Dynamics and diversity in autophagy mechanisms: lessons from yeast.” In: *Nature reviews. Molecular cell biology* 10.7 (2009), pp. 458–67.

[63] Finley, D., Sadis, S., Monia, B. P., Boucher, P., Ecker, D. J., Crooke, S. T., and Chau, V. “Inhibition of proteolysis and cell cycle progression in a multiubiquitination-deficient yeast mutant.” In: *Molecular and cellular biology* 14.8 (1994), pp. 5501–5509.

[64] Schrader, E. K., Harstad, K. G., and Matouschek, A. “Targeting proteins for degradation.” In: *Nature chemical biology* 5.11 (2009), pp. 815–822.

[65] Klumperman, J. and Raposo, G. “The Complex Ultrastructure of the Endolysosomal System”. In: *Cold Spring Harbor perspectives in biology* 6 (2014), pp. 1–22.

[66] Wandinger-Ness, A. and Zerial, M. “Rab Proteins and the Compartmentalization of the Endosomal System”. In: *Cold Spring Harbor perspectives in biology* 6 (2014), pp. 1–25.

[67] Smythe, E. and Warren, G. “The mechanism of receptor-mediated endocytosis.” In: *European journal of biochemistry / FEBS* 202.3 (1991), pp. 689–699.

[68] McMahon, H. T. and Boucrot, E. “Molecular mechanism and physiological functions of clathrin-mediated endocytosis.” In: *Nature reviews. Molecular cell biology* 12.8 (2011), pp. 517–533.

[69] Wollert, T. and Hurley, J. H. “Molecular Mechanism of Multivesicular Body Biogenesis by ESCRT Complexes”. In: *Nature* 464.7290 (2010), pp. 864–869.

[70] Ashford, T. P. and Porter, K. R. “PublisCytoplasmic components in hepatic lysosomes”. In: *Journal of Cell Biology* 12 (1962), pp. 198–202.

[71] Kraft, C., Reggiori, F., and Peter, M. “Selective types of autophagy in yeast”. In: *Biochimica et Biophysica Acta - Molecular Cell Research* 1793.9 (2009), pp. 1404–1412.

[72] Kaushik, S., Bandyopadhyay, U., Sridhar, S., Kiffin, R., Martinez-Vicente, M., Kon, M., Orenstein, S. J., Wong, E., and Cuervo, A. M. “Chaperone-mediated autophagy at a glance.” In: *Journal of cell science* 124.4 (2011), pp. 495–9.

[73] Dice, J. F. “Peptide Sequences that target cytosolic proteins for lysosomal proteolysis”. In: *Trends in Biochemical Sciences* 15.8 (1990), pp. 305–309.

[74] Chiang, H. L., Terlecky, S. R., Plant, C. P., and Dice, J. F. “A role for a 70-kilodalton heat shock protein in lysosomal degradation of intracellular proteins.” In: *Science* 246.4928 (1989), pp. 382–385.

[75] Cuervo, a. M. and Dice, J. F. “A receptor for the selective uptake and degradation of proteins by lysosomes.” In: *Science* 273.5274 (1996), pp. 501–503.

[76] Bandyopadhyay, U., Kaushik, S., Varticovski, L., and Cuervo, A. M. “The chaperone-mediated autophagy receptor organizes in dynamic protein complexes at the lysosomal membrane.” In: *Molecular and cellular biology* 28.18 (2008), pp. 5747–5763.

[77] Salvador, N., Aguado, C., Horst, M., and Knecht, E. “Import of a Cytosolic Protein into Lysosomes by Chaperone-Mediated Autophagy Depends on its Folding State”. In: *Journal of Biological Chemistry* 275.35 (2000), pp. 27447–56.

[78] Cuervo, A. M., Dice, J. F., and Knecht, E. “A population of rat liver lysosomes responsible for the selective uptake and degradation of cytosolic proteins”. In: *Journal of Biological Chemistry* 272.9 (1997), pp. 5606–5615.

[79] Park, C., Suh, Y., and Cuervo, A. M. “Regulated degradation of Chk1 by chaperone-mediated autophagy in response to DNA damage”. In: *Nature Communications* 6 (2015), p. 6823.

[80] Li, W.-w., Li, J., and Bao, J.-k. “Microautophagy: lesser-known self-eating.” In: *Cellular and molecular life sciences* 69.7 (2012), pp. 1125–36.

[81] Farré, J. C. and Subramani, S. “Peroxisome turnover by micropexophagy: An autophagy-related process”. In: *Trends in Cell Biology* 14.9 (2004), pp. 515–523.

[82] Krick, R., Muehe, Y., Prick, T., Bremer, S., Schlotterhose, P., Eskelinen, E., Millen, J., Goldfarb, D. S., and Thumm, M. "Piecemeal Microautophagy of the Nucleus Requires the Core Macroautophagy Genes". In: *Molecular Biology of the Cell* 19 (2008), pp. 4492–4505.

[83] Hamasaki, M., Shibutani, S. T., and Yoshimori, T. "Up-to-date membrane biogenesis in the autophagosome formation". In: *Current Opinion in Cell Biology* (2013), pp. 1–6.

[84] Kamada, Y., Funakoshi, T., Shintani, T., Nagano, K., Ohsumi, M., and Ohsumi, Y. "Tor-mediated induction of autophagy via an Apg1 protein kinase complex". In: *Journal of Cell Biology* 150.6 (2000), pp. 1507–1513.

[85] Yamamoto, H., Kakuta, S., Watanabe, T. M., Kitamura, A., Sekito, T., Kondo-Kakuta, C., Ichikawa, R., Kinjo, M., and Ohsumi, Y. "Atg9 vesicles are an important membrane source during early steps of autophagosome formation". In: *Journal of Cell Biology* 198.2 (2012), pp. 219–233.

[86] Jao, C. C., Ragusa, M. J., Stanley, R. E., and Hurley, J. H. "A HORMA domain in Atg13 mediates PI 3-kinase recruitment in autophagy." In: *Proceedings of the National Academy of Sciences of the United States of America* 110.14 (2013), pp. 5486–91.

[87] Obara, K., Noda, T., Niimi, K., and Ohsumi, Y. "Transport of phosphatidylinositol 3-phosphate into the vacuole via autophagic membranes in Saccharomyces cerevisiae." In: *Genes to cells : devoted to molecular & cellular mechanisms* 13.6 (2008), pp. 537–47.

[88] Obara, K., Sekito, T., Niimi, K., and Ohsumi, Y. "The Atg18-Atg2 complex is recruited to autophagic membranes via phosphatidylinositol 3-phosphate and exerts an essential function." In: *The Journal of biological chemistry* 283.35 (2008), pp. 23972–80.

[89] Xie, Z., Nair, U., and Klionsky, D. J. "Atg8 controls phagophore expansion during autophagosome formation". In: *Molecular biology of the cell* 19 (2008), pp. 3290–3298.

[90] Guan, J., Stromhaug, P. E., George, M. D., Habibzadegah-Tari, P., Bevan, A., Dunn, W. a., and Klionsky, D. J. "Cvt18/Gsa12 is required for cytoplasm-to-vacuole transport, pexophagy, and autophagy in Saccharomyces cerevisiae and Pichia pastoris." In: *Molecular biology of the cell* 12.12 (2001), pp. 3821–38.

[91] Nakatogawa, H., Ichimura, Y., and Ohsumi, Y. "Atg8, a ubiquitin-like protein required for autophagosome formation, mediates membrane tethering and hemifusion." In: *Cell* 130.1 (2007), pp. 165–78.

[92] Weidberg, H., Shpilka, T., Shvets, E., Abada, A., Shimron, F., and Elazar, Z. "LC3 and GATE-16 N termini mediate membrane fusion processes required for autophagosome biogenesis." In: *Developmental cell* 20.4 (2011), pp. 444–54.

[93] Umekawa, M. and Klionsky, D. J. "The Cytoplasm-to-Vacuole Targeting Pathway: A Historical Perspective." In: *International journal of cell biology* 2012 (2012), p. 142634.

[94] Baba, M., Osumi, M., Scott, S. V., Klionsky, D. J., and Ohsumi, Y. "Two distinct pathways for targeting proteins from the cytoplasm to the vacuole/lysosome". In: *Journal of Cell Biology* 139.7 (1997), pp. 1687–1695.

[95] Jr, R. T., Chen, P.-H., Chou, C.-C., Patel, J., Jin, S. V., and Taylor, R. "KCS1 deletion in Saccharomyces cerevisiae leads to a defect in translocation of autophagic proteins and reduces autophagosome formation". In: *Autophagy* 8.9 (2012), pp. 1300–11.

[96] Feng, Y., Yao, Z., and Klionsky, D. J. "How to control self-digestion: transcriptional, post-transcriptional, and post-translational regulation of autophagy". In: *Trends in Cell Biology* 25.6 (2015), pp. 354–363.

[97] Choi, A. M., Ryter, S. W., and Levine, B. "Autophagy in Human Health and Disease". In: *New England Journal of Medicine* 368.7 (2013), pp. 651–662.

[98] Suzuki, K., Kirisako, T., Kamada, Y., Mizushima, N., Noda, T., and Ohsumi, Y. "The pre-autophagosomal structure organized by concerted functions of APG genes is essential for autophagosome formation." In: *The EMBO journal* 20.21 (2001), pp. 5971–81.

[99] Suzuki, K., Akioka, M., Kondo-Kakuta, C., Yamamoto, H., and Ohsumi, Y. "Fine mapping of autophagy-related proteins during autophagosome formation in Saccharomyces cerevisiae". In: *Journal of cell science* 126 (2013), pp. 2534–2544.

[100] Sekito, T., Kawamata, T., Ichikawa, R., Suzuki, K., and Ohsumi, Y. "Atg17 recruits Atg9 to organize the pre-autophagosomal structure". In: *Genes to Cells* 14.5 (2009), pp. 525–538.

[101] Noda, T., Kim, J., Huang, W. P., Baba, M., Tokunaga, C., Ohsumi, Y., and Klionsky, D. J. "Apg9p/Cvt7p is an integral membrane protein required for transport vesicle formation in the Cvt and autophagy pathways." In: *The Journal of cell biology* 148.3 (2000), pp. 465–80.

[102] Mari, M., Griffith, J., Rieter, E., Krishnappa, L., Klionsky, D. J., and Reggiori, F. "An Atg9-containing compartment that functions in the early steps of autophagosome biogenesis". In: *Journal of Cell Biology* 190.6 (2010), pp. 1005–1022.

[103] Graef, M., Friedman, J. R., Graham, C., Babu, M., and Nunnari, J. "ER exit sites are physical and functional core autophagosome biogenesis components". In: *Molecular Biology of the Cell* 24.18 (2013), pp. 2918–2931.

[104] Vaart, A. van der, Griffith, J., and Reggiori, F. "Exit from the Golgi Is Required for the Expansion of the Autophagosomal Phagophore in Yeast Saccharomyces cerevisiae". In: *Molecular biology of the cell* 21 (2010), pp. 2270–2284.

[105] Axe, E. L., Walker, S. a., Manifava, M., Chandra, P., Roderick, H. L., Habermann, A., Griffiths, G., and Ktistakis, N. T. "Autophagosome formation from membrane compartments enriched in phosphatidylinositol 3-phosphate and dynamically connected to the endoplasmic reticulum". In: *Journal of Cell Biology* 182.4 (2008), pp. 685–701.

[106] Hayashi-Nishino, M., Fujita, N., Noda, T., Yamaguchi, A., Yoshimori, T., and Yamamoto, A. "A subdomain of the endoplasmic reticulum forms a cradle for autophagosome formation." In: *Nature cell biology* 11.12 (2009), pp. 1433–1437.

[107] Mizushima, N., Yoshimori, T., and Ohsumi, Y. "The role of Atg proteins in autophagosome formation." In: *Annual review of cell and developmental biology* 27 (2011), pp. 107–32.

[108] Ge, L., Melville, D., Zhang, M., and Schekman, R. "The ER-Golgi intermediate compartment is a key membrane source for the LC3 lipidation step of autophagosome biogenesis". In: *eLife* 2 (2013), e00947–e00947.

[109] Sohda, M., Misumi, Y., Ogata, S., Sakisaka, S., Hirose, S., Ikehara, Y., and Oda, K. "Trans-Golgi protein p230/golgin-245 is involved in phagophore formation." In: *Biochemical and biophysical research communications* 456.1 (Nov. 2014), pp. 275–281.

[110] Ge, L., Zhang, M., and Schekman, R. "Phosphatidylinositol 3-kinase and COPII generate LC3 lipidation vesicles from the ER-Golgi intermediate compartment". In: *eLife* 3 (2014), e04135.

[111] Araki, Y., Ku, W.-C., Akioka, M., May, a. I., Hayashi, Y., Arisaka, F., Ishihama, Y., and Ohsumi, Y. "Atg38 is required for autophagy-specific phosphatidylinositol 3-kinase complex integrity". In: *The Journal of Cell Biology* 203.2 (2013), pp. 299–313.

[112] Suzuki, K., Kubota, Y., Sekito, T., and Ohsumi, Y. "Hierarchy of Atg proteins in pre-autophagosomal structure organization." In: *Genes to cells* 12.2 (2007), pp. 209–18.

[113] Kabeya, Y., Kamada, Y., Baba, M., Tkikawa, H., Sasaki, M., and Ohsumi, Y. "Atg17 Functions in Cooperation with Atg1 and Atg13 in Yeast Autophagy". In: *Molecular biology of the cell* 16 (2005), pp. 2544–2553.

[114] Kamada, Y., Yoshino, K.-i., Kondo, C., Kawamata, T., Oshiro, N., Yonezawa, K., and Ohsumi, Y. "Tor directly controls the Atg1 kinase complex to regulate autophagy." In: *Molecular and cellular biology* 30.4 (2010), pp. 1049–1058.

[115] Kraft, C., Kijanska, M., Kalie, E., Siergiejuk, E., Lee, S. S., Semplicio, G., Stoffel, I., Brezovich, A., Verma, M., Hansmann, I., Ammerer, G., Hofmann, K., Tooze, S., and Peter, M. "Binding of the Atg1/ULK1 kinase to the ubiquitin-like protein Atg8 regulates autophagy". In: *The EMBO Journal* 31.18 (2012), pp. 3691–3703.

[116] Fujioka, Y., Suzuki, S. W., Yamamoto, H., Kondo-Kakuta, C., Kimura, Y., Hirano, H., Akada, R., Inagaki, F., Ohsumi, Y., and Noda, N. N. "Structural basis of starvation-induced assembly of the autophagy initiation complex." In: *Nature structural & molecular biology* October 2013 (2014), pp. 1–12.

[117] Ragusa, M. J., Stanley, R. E., and Hurley, J. H. "Architecture of the Atg17 Complex as a Scaffold for Autophagosome Biogenesis". In: *Cell* 151.7 (2012), pp. 1501–1512.

[118] Cheong, H., Nair, U., Geng, J., and Klionsky, D. J. "The Atg1 Kinase Complex Is Involved in the Regulation of Protein Recruitment to Initiate Sequestering Vesicle Formation for Nonspecific Autophagy in Saccharomyces cerevisiae". In: *Molecular biology of the cell* 19 (2008), pp. 668–681.

[119] Papinski, D., Schuschnig, M., Reiter, W., Wilhelm, L., Barnes, C. a., Majolica, A., Hansmann, I., Pfaffenwimmer, T., Kijanska, M., Stoffel, I., Lee, S. S., Brezovich, A., Lou, J. H., Turk, B. E., Aebersold, R., Ammerer, G., Peter, M., and Kraft, C. "Early Steps in Autophagy Depend on Direct Phosphorylation of Atg9 by the Atg1 Kinase." In: *Molecular cell* (2014), pp. 1–13.

[120] Backues, S. K., Orban, D. P., Bernard, A., Singh, K., Cao, Y., and Klionsky, D. J. "Atg23 and Atg27 act at the early stages of Atg9 trafficking in S. cerevisiae." In: *Traffic* (2014).

[121] He, C., Song, H., Yorimitsu, T., Monastyrska, I., Yen, W. L., Legakis, J. E., and Klionsky, D. J. "Recruitment of Atg9 to the preautophagosomal structure by Atg11 is essential for selective autophagy in budding yeast". In: *Journal of Cell Biology* 175.6 (2006), pp. 925–935.

[122] Jin, M., He, D., Backues, S. K., Freeberg, M. a., Liu, X., Kim, J. K., and Klionsky, D. J. "Transcriptional regulation by pho23 modulates the frequency of autophagosome formation." In: *Current Biology* 24.12 (2014), pp. 1314–22.

[123] Reggiori, F., Tucker, K. a., Stromhaug, P. E., and Klionsky, D. J. "The Atg1-Atg13 complex regulates Atg9 and Atg23 retrieval transport from the pre-autophagosomal structure." In: *Developmental cell* 6.1 (2004), pp. 79–90.

[124] Tan, D., Cai, Y., Wang, J., Zhang, J., Menon, S., Chou, H.-T., Ferro-Novick, S., Reinisch, K. M., and Walz, T. "The EM structure of the TRAPPIII complex leads to the identification of a requirement for COPII vesicles on the macroautophagy pathway." In: *Proceedings of the National Academy of Sciences of the United States of America* 110.48 (2013), pp. 19432–7.

[125] Popovic, D. and Dikic, I. "TBC 1D5 and the AP2 complex regulate ATG9 trafficking and initiation of autophagy". In: *EMBOreports* 15.4 (2014), pp. 323–453.

[126] Longatti, A. and Tooze, S. A. "Vesicular trafficking and autophagosome formation." In: *Cell death and differentiation* 16.7 (2009), pp. 956–965.

[127] Jao, C. C., Ragusa, M. J., Stanley, R. E., and Hurley, J. H. "A HORMA domain in Atg13 mediates PI 3-kinase recruitment in autophagy." In: *Proceedings of the National Academy of Sciences of the United States of America* 110.14 (2013), pp. 5486–91.

[128] Itakura, E., Kishi, C., Inou, K., and Mizushima, N. "MyoD expression marks the onset of skeletal myogenesis in Myf-5 mutant mice." In: *Molecular Biology of the Cell* 19 (2008), pp. 5360–5372.

[129] Matsunaga, K., Morita, E., Saitoh, T., Akira, S., Ktistakis, N. T., Izumi, T., Noda, T., and Yoshimori, T. "Autophagy requires endoplasmic reticulum targeting of the PI3-kinase complex via Atg14L". In: *Journal of Cell Biology* 190.4 (2010), pp. 511–521.

[130] Georgakopoulos, T., Koutroubas, G., Vakonakis, I., Tzermia, M., Prokova, V., Voutsina, A., and Alexandraki, D. "Functional analysis of the Saccharomyces cerevisiae YFR021w/YGR223c/YPL100w ORF family suggests relations to mitochondrial/peroxisomal functions and amino acid signalling pathways." In: *Yeast* 18.12 (2001), pp. 1155–71.

[131] Dove, S. K., Piper, R. C., McEwen, R. K., Yu, J. W., King, M. C., Hughes, D. C., Thuring, J., Holmes, A. B., Cooke, F. T., Michell, R. H., Parker, P. J., and Lemmon, M. a. "Svp1p defines a family of phosphatidylinositol 3,5-bisphosphate effectors." In: *The EMBO journal* 23.9 (2004), pp. 1922–33.

[132] Strømhaug, P. E., Reggiori, F., Guan, J., Wang, C.-w., and Klionsky, D. J. "Atg21 Is a Phosphoinositide Binding Protein Required for Efficient Lipidation and Localization of Atg8 during Uptake of Aminopeptidase I by Selective Autophagy". In: *Molecular biology of the cell* 15 (2004), pp. 3553–3566.

[133] Krick, R., Tolstrup, J., Appelles, A., Henke, S., and Thumm, M. "The relevance of the phosphatidylinositolphosphat-binding motif FRRGT of Atg18 and Atg21 for the Cvt pathway and autophagy." In: *FEBS letters* 580.19 (2006), pp. 4632–8.

[134] Busse, R. A., Scacioc, A., Krick, R., Pérez-Lara, Á., Thumm, M., and Kühnel, K. "Characterization of PROPPIN-Phosphoinositide Binding and Role of Loop 6CD in PROPPIN-Membrane Binding". In: *Biophysical Journal* 108.9 (2015), pp. 2223–2234.

[135] Baskaran, S., Ragusa, M. J., Boura, E., and Hurley, J. H. "Two-Site Recognition of Phosphatidylinositol 3-Phosphate by PROPPINs in Autophagy." In: *Molecular cell* (2012), pp. 1–10.

[136] Krick, R., Busse, R. A., Scacioc, A., Stephan, M., Janshoff, A., and Thumm, M. "Structural and functional characterization of the two phosphoinositide binding sites of PROPPINs , a β-propeller protein family". In: *Proceedings of the National Academy of Sciences* 109.30 (2012), E2042–E2049.

[137] Watanabe, Y., Kobayashi, T., Yamamoto, H., Hoshida, H., Akada, R., Inagaki, F., Ohsumi, Y., and Noda, N. N. "Structure-based analyses reveal distinct binding sites for Atg2 and phosphoinositides in Atg18." In: *The Journal of biological chemistry* (2012), pp. 16–18.

[138] Barth, H., Meiling-Wesse, K., Epple, U. D., and Thumm, M. "Autophagy and the cytoplasm to vacuole targeting pathway both require Aut10p". In: *FEBS Letters* 508.1 (2001), pp. 23–28.

[139] Barth, H., Meiling-Wesse, K., Epple, U. D., and Thumm, M. "Mai1p is essential for maturation of proaminopeptidase I but not for autophagy." In: *FEBS letters* 512.1-3 (2002), pp. 173–9.

[140] Krick, R., Henke, S., Tolstrup, J., and Thumm Michael. "Dissecting the localization and function of Atg18 , Atg21 and Ygr223c". In: *Autophagy* 4.7 (2008), pp. 896–910.

[141] Xie, Z. and Klionsky, D. J. "Autophagosome formation: core machinery and adaptations." In: *Nature cell biology* 9.10 (2007), pp. 1102–9.

[142] Zutphen, T. van, Todde, V., Boer, R. de, Kreim, M., Hofbauer, H. F., Wolinski, H., Veenhuis, M., Klei, I. J. van der, and Kohlwein, S. D. "Lipid droplet autophagy in the yeast Saccharomyces cerevisiae." In: *Molecular biology of the cell* 25.2 (2014), pp. 290–301.

[143] Meiling-Wesse, K., Barth, H., Voss, C., Eskelinen, E.-L., Epple, U. D., and Thumm, M. "Atg21 is required for effective recruitment of Atg8 to the preautophagosomal structure during the Cvt pathway." In: *The Journal of biological chemistry* 279.36 (2004), pp. 37741–50.

[144] Tamura, N., Oku, M., Ito, M., Noda, N. N., Inagaki, F., and Sakai, Y. "Atg18 phosphoregulation controls organellar dynamics by modulating its phosphoinositide-binding activity." In: *The Journal of cell biology* 202.4 (2013), pp. 685–98.

[145] Shintani, T., Suzuki, K., Kamada, Y., Noda, T., and Ohsumi, Y. "Apg2p functions in autophagosome formation on the perivacuolar structure." In: *The Journal of biological chemistry* 276.32 (2001), pp. 30452–60.

[146] Rieter, E., Vinke, F., Bakula, D., Cebollero, E., Ungermann, C., Proikas-Cezanne, T., and Reggiori, F. "Atg18 function in autophagy is regulated by specific sites within its β-propeller". In: *Journal of cell science* 126.2 (2012), pp. 593–604.

[147] Kobayashi, T., Suzuki, K., and Ohsumi, Y. "Autophagosome formation can be achieved in the absence of Atg18 by expressing engineered PAS-targeted Atg2." In: *FEBS letters* 586.16 (2012), pp. 2473–8.

[148] Nair, U., Cao, Y., Xie, Z., and Klionsky, D. J. "Roles of the lipid-binding motifs of Atg18 and Atg21 in the cytoplasm to vacuole targeting pathway and autophagy." In: *The Journal of biological chemistry* 285.15 (2010), pp. 11476–88.

[149] Proikas-Cezanne, T., Waddell, S., Gaugel, A., Frickey, T., Lupas, A., and Nordheim, A. "WIPI-1alpha (WIPI49), a member of the novel 7-bladed WIPI protein family, is aberrantly expressed in human cancer and is linked to starvation-induced autophagy." In: *Oncogene* 23.58 (2004), pp. 9314–25.

[150] Polson, H. E. J., Lartigue, J. de, Rigden, D. J., Reedijk, M., Urbé, S., Clague, M. J., and Tooze, S. a. "Mammalian Atg18 (WIPI2) localizes to omegasome-anchored phagophores and positively regulates LC3 lipidation." In: *Autophagy* 6.4 (2010), pp. 506–522.

[151] Dooley, H. C., Razi, M., Polson, H. E., Girardin, S. E., Wilson, M. I., and Tooze, S. A. "WIPI2 Links LC3 Conjugation with PI3P, Autophagosome Formation, and Pathogen Clearance by Recruiting Atg12–5-16L1". In: *Molecular Cell* 200 (2014), pp. 1–15.

[152] Efe, J. A., Botelho, R. J., and Emr, S. D. "Atg18 Regulates Organelle Morphology and Fab1 Kinase". In: *Molecular Biology of the Cell* 18 (2007), pp. 4232–4244.

[153] Zieger, M. and Mayer, A. "Yeast vacuoles fragment in an asymmetrical two-phase process with distinct protein requirements." In: *Molecular biology of the cell* 23.17 (2012), pp. 3438–49.

[154] Jin, N., Chow, C. Y., Liu, L., Zolov, S. N., Bronson, R., Davisson, M., Petersen, J. L., Zhang, Y., Park, S., Duex, J. E., Goldowitz, D., Meisler, M. H., and Weisman, L. S. "VAC14 nucleates a protein complex essential for the acute interconversion of PI3P and PI(3,5)P(2) in yeast and mouse." In: *The EMBO journal* 27.24 (2008), pp. 3221–34.

[155] Juris, L., Montino, M., Rube, P., Schlotterhose, P., Thumm, M., and Krick, R. "PI 3 P binding by Atg 21 organises Atg 8 lipidation". In: *EMBO Journal* 13.7 (2015), pp. 955–73.

[156] Cebollero, E., Vaart, A. van der, Zhao, M., Rieter, E., Klionsky, D. J., Helms, J. B., and Reggiori, F. "Phosphatidylinositol-3-Phosphate Clearance Plays a Key Role in Autophagosome Completion." In: *Current biology* 22 (July 2012), pp. 1–9.

[157] Noda, N. N. and Inagaki, F. "Mechanisms of Autophagy". In: *Annual Review of Biophysics* 44 (2014), pp. 101–22.

[158] Mizushima, N., Noda, T., Yoshimori, T., Tanaka, Y., Ishii, T., George, M. D., Klionsky, D. J., Ohsumi, M., and Ohsumi, Y. "A protein conjugation system essential for autophagy." In: *Nature* 395.6700 (1998), pp. 395–8.

[159] Shintani, T., Mizushima, N., Ogawa, Y., Matsuura, A., Noda, T., and Ohsumi, Y. "Apg10p, a novel protein-conjugating enzyme essential for autophagy in yeast". In: *EMBO Journal* 18.19 (1999), pp. 5234–5241.

[160] Kuma, A., Mizushima, N., Ishihara, N., and Ohsumi, Y. "Formation of the ˜350-kDa Apg12-Apg5.Apg16 multimeric complex, mediated by Apg16 oligomerization, is essential for autophagy in yeast". In: *Journal of Biological Chemistry* 277.21 (2002), pp. 18619–18625.

[161] Kirisako, T., Ichimura, Y., Okada, H., Kabeya, Y., Mizushima, N., Yoshimori, T., Ohsumi, M., Takao, T., Noda, T., and Ohsumi, Y. "The reversible modification regulates the membrane-binding state of Apg8/Aut7 essential for autophagy and the cytoplasm to vacuole targeting pathway." In: *The Journal of cell biology* 151.2 (2000), pp. 263–76.

[162] Hanada, T., Noda, N. N., Satomi, Y., Ichimura, Y., Fujioka, Y., Takao, T., Inagaki, F., and Ohsumi, Y. "The Atg12-Atg5 conjugate has a novel E3-like activity for protein lipidation in autophagy." In: *The Journal of biological chemistry* 282.52 (2007), pp. 37298–302.

[163] Fujita, N., Itoh, T., Omori, H., Fukuda, M., Noda, T., and Yoshimori, T. "The Atg16L Complex Specifies the Site of LC3 Lipidation for Membrane Biogenesis in Autophagy". In: *Moecular Biology of the Cell* 19 (2008), pp. 2092–2100.

[164] Kirisako, T., Baba, M., Ishihara, N., Miyazawa, K., Ohsumi, M., Yoshimori, T., Noda, T., and Ohsumi, Y. "Formation Process of Autophagosome Is Traced with Apg8 / Aut7p in Yeast". In: *Journal of Cell Biology* 147.2 (1999), pp. 435–446.

[165] Suzuki, K., Kondo, C., Morimoto, M., and Ohsumi, Y. "Selective transport of alpha-mannosidase by autophagic pathways: Identification of a novel receptor, Atg34p". In: *Journal of Biological Chemistry* 285.39 (2010), pp. 30019–30025.

[166] Scott, S. V., Guan, J., Hutchins, M. U., Kim, J., and Klionsky, D. J. "Cvt19 is a receptor for the cytoplasm-to-vacuole targeting pathway." In: *Molecular cell* 7.6 (2001), pp. 1131–41.

[167] Klionsky, D. J., Baehrecke, E. H., Brumell, J. H., Chu, C. T., Codogno, P., Cuervo, A. M., Debnath, J., Deretic, V., Elazar, Z., Eskelinen, E.-L., Finkbeiner, S., Fueyo-Margareto, J., Gewirtz, D., Jäättelä, M., Kroemer, G., Levine, B., Melia, T. J., Mizushima, N., Rubinsztein, D. C., Simonsen, A., Thorburn, A., Thumm, M., and Tooze, S. a. "A comprehensive glossary of autophagy-related molecules and processes (2nd edition)." In: *Autophagy* 7.11 (Nov. 2011), pp. 1273–94.

[168] Burnett, S. F., Farré, J.-C., Nazarko, T. Y., and Subramani, S. "Peroxisomal Pex3 activates selective autophagy of peroxisomes via interaction with pexophagy receptor, Atg30". In: *Journal of Biological Chemistry* 290.13 (2015), pp. 8623–31.

[169] Farré, J.-C., Burkenroad, A., Burnett, S. F., and Subramani, S. "Phosphorylation of mitophagy and pexophagy receptors coordinates their interaction with Atg8 and Atg11." In: *EMBO reports* 14.5 (2013), pp. 441–9.

[170] Mochida, K., Oikawa, Y., Kimura, Y., Kirisako, H., Hirano, H., Ohsumi, Y., and Nakatogawa, H. "Receptor-mediated selective autophagy degrades the endoplasmic reticulum and the nucleus". In: *Nature* 522 (2015), pp. 359–362.

[171] Lu, K., Psakhye, I., and Jentsch, S. "Autophagic clearance of PolyQ proteins mediated by ubiquitin-Atg8 adaptors of the conserved CUET protein family". In: *Cell* 158.3 (2014), pp. 549–563.

[172] Bento, C. F., Puri, C., Moreau, K., and Rubinsztein, D. C. "The role of membrane-trafficking small GTPases in the regulation of autophagy." In: *Journal of cell science* 126.Pt 5 (2013), pp. 1059–69.

[173] Gutierrez, M. G., Munafó, D. B., Berón, W., and Colombo, M. I. "Rab7 is required for the normal progression of the autophagic pathway in mammalian cells." In: *Journal of cell science* 117.Pt 13 (2004), pp. 2687–2697.

[174] Wurmser, A. E., Sato, T. K., and Emr, S. D. "New component of the vacuolar class C-Vps complex couples nucleotide exchange on the Ypt7 GTPase to SNARE-dependent docking and fusion". In: *Journal of Cell Biology* 151.3 (2000), pp. 551–562.

[175] Diao, J., Liu, R., Rong, Y., Zhao, M., Zhang, J., Lai, Y., Zhou, Q., Wilz, L. M., Li, J., Vivona, S., Pfuetzner, R. a., Brunger, A. T., and Zhong, Q. "ATG14 promotes membrane tethering and fusion of autophagosomes to endolysosomes". In: *Nature* 520.7548 (2015), pp. 563–6.

[176] Durán, R. V., Oppliger, W., Robitaille, A. M., Heiserich, L., Skendaj, R., Gottlieb, E., and Hall, M. N. "Glutaminolysis activates Rag-mTORC1 signaling." In: *Molecular cell* 47.3 (2012), pp. 349–58.

[177] Bonfils, G., Jaquenoud, M., Bontron, S., Ostrowicz, C., Ungermann, C., and De Virgilio, C. "Leucyl-tRNA Synthetase Controls TORC1 via the EGO Complex". In: *Molecular Cell* 46.1 (2012), pp. 105–110.

[178] Abada, A. and Elazar, Z. "Getting ready for building: signaling and autophagosome biogenesis." In: *EMBO reports* 15.8 (2014), pp. 839–852.

[179] Hu, G., McQuiston, T., Bernard, A., Park, Y.-D., Qiu, J., Vural, A., Zhang, N., Waterman, S. R., Blewett, N. H., Myers, T. G., Maraia, R. J., Kehrl, J. H., Uzel, G., Klionsky, D. J., and Williamson, P. R. "A conserved mechanism of TOR-dependent RCK-mediated mRNA degradation regulates autophagy". In: *Nature Cell Biology* 17.7 (2015), pp. 930–942.

[180] Dunlop, E. a. and Tee, a. R. "mTOR and autophagy: A dynamic relationship governed by nutrients and energy." In: *Seminars in cell & developmental biology* 36 (Aug. 2014), pp. 121–9.

[181] Bernard, A., Jin, M., González-Rodríguez, P., Füllgrabe, J., Delorme-Axford, E., Backues, S. K., Joseph, B., and Klionsky, D. J. "Rph1/KDM4 Mediates Nutrient-Limitation Signaling that Leads to the Transcriptional Induction of Autophagy". In: *Current Biology* 25.5 (2015), pp. 546–555.

[182] Tang, J., Di, J., Cao, H., Bai, J., and Zheng, J. "p53-mediated autophagic regulation: A prospective strategy for cancer therapy". In: *Cancer Letters* 363.2 (2015), pp. 101–107.

[183] Hu, D., Wu, J., Wang, W., Mu, M., Zhao, R., Xu, X., Chen, Z., Xiao, J., Hu, F., Yang, Y., and Zhang, R. "Autophagy regulation revealed by SapM-induced block of autophagosome-lysosome fusion via binding RAB7". In: *Biochemical and Biophysical Research Communications* 461.2 (2015), pp. 401–407.

[184] Castrejón-Jiménez, N. S., Leyva-Paredes, K., Hernández-González, J. C., Luna-Herrera, J., and García-Pérez, B. E. "The role of autophagy in bacterial infections". In: *BioScience Trends* 9.3 (2015), pp. 149–159.

[185] Jackson, W. T. "Viruses and the autophagy pathway". In: *Virology* 479-480 (2015), pp. 1–7.

[186] Yang, Z., Goronzy, J. J., and Weyand, C. M. "Autophagy in autoimmune disease". In: *Journal of Molecular Medicine* 93 (2015), pp. 707–717.

[187] Rubinsztein, D. C., Bento, C. F., and Deretic, V. "Therapeutic targeting of autophagy in neurodegenerative and infectious diseases". In: *Journal of Experimental Medicine* 212.7 (2015), pp. 979–990.

[188] Rui, Y.-N., Xu, Z., Patel, B., Chen, Z., Chen, D., Tito, A., David, G., Sun, Y., Stimming, E. F., Bellen, H. J., Cuervo, A. M., and Zhang, S. "Huntingtin functions as a scaffold for selective macroautophagy". In: *Nature Cell Biology* 17.3 (2015), pp. 262–275.

[189] Cicchini, M., Karantza, V., and Xia, B. "Molecular Pathways: Autophagy in Cancer - A Matter of Timing and Context". In: *Clinical cancer research* 21.3 (2000), pp. 498–504.

[190] Chen, Y., Li, X., Guo, L., Wu, X., He, C., Zhang, S., Xiao, Y., Yang, Y., and Hao, D. "Combining radiation with autophagy inhibition enhances suppression of tumor growth and angiogenesis in esophageal cancer". In: *Molecular Medicine Reports* (2015), pp. 1645–1652.

[191] Poklepovic, A. and Gewirtz, D. a. "Outcome of early clinical trials of the combination of hydroxychloroquine with chemotherapy in cancer". In: *Autophagy* 10.8 (2014), pp. 1478–1480.

[192] Nakatogawa, H. and Ohsumi, Y. "SDS-PAGE Techniques to Study Ubiquitin-Like Conjugation Systems in Yeast Autophagy". In: *Methods in Molecular Biology* 832 (2012), pp. 519–529.

[193] Niedenthal, R. K., Riles, L., Johnston, M., and Hegemann, J. H. "Green fluorescent protein as a marker for gene expression and subcellular localization in budding yeast." In: *Yeast* 12.8 (1996), pp. 773–786.

[194] Janke, C., Magiera, M. M., Rathfelder, N., Taxis, C., Reber, S., Maekawa, H., Moreno-Borchart, A., Doenges, G., Schwob, E., Schiebel, E., and Knop, M. "A versatile toolbox for PCR-based tagging of yeast genes: new fluorescent proteins, more markers and promoter substitution cassettes." In: *Yeast* 21.11 (2004), pp. 947–62.

[195] Mendl, N., Occhipinti, A., Müller, M., Wild, P., Dikic, I., and Reichert, A. S. "Mitophagy in yeast is independent of mitochondrial fission and requires the stress response gene WHI2." In: *Journal of cell science* 124.Pt 8 (2011), pp. 1339–1350.

[196] Scholz, J., Besir, H., Strasser, C., and Suppmann, S. "A new method to customize protein expression vectors for fast, efficient and background free parallel cloning." In: *BMC biotechnology* 13.12 (2013).

[197] Sikorski, R. S. and Hieter, P. "A system of shuttle vectors and yeast host strains designed for efficient manipulation of DNA in Saccharomyces cerevisiae." In: *Genetics* 122.1 (1989), pp. 19–27.

[198] Guimaraes, R. S., Delorme-Axford, E., Klionsky, D. J., and Reggiori, F. "Assays for the biochemical and ultrastructural measurement of selective and nonselective types of autophagy in the yeast Saccharomyces cerevisiae." In: *Methods* 75 (2014), pp. 141–50.

[199] Esteban-Martínez, L. and Boya, P. "Autophagic flux determination in vivo and ex vivo". In: *Methods* (2015), pp. 1–8.

[200] Schneider, C. a., Rasband, W. S., and Eliceiri, K. W. "NIH Image to ImageJ: 25 years of image analysis". In: *Nature Methods* 9.7 (2012), pp. 671–675.

[201] Noda, T. and Klionsky, D. J. "The quantitative Pho8Delta60 assay of nonspecific autophagy." In: *Methods in enzymology*. 1st ed. Vol. 451. 08. Elsevier Inc., 2008, pp. 33–42.

[202] Delorme-Axford, E., Guimaraes, R. S., Reggiori, F., and Klionsky, D. J. "The yeast Saccharomyces cerevisiae: an overview of methods to study autophagy progression." In: *Methods* 75 (2014), pp. 3–12.

[203] Wright, R. "Transmission electron microscopy of yeast." In: *Microscopy research and technique* 51.6 (2000), pp. 496–510.

[204] Tan, S. "A modular polycistronic expression system for overexpressing protein complexes in Escherichia coli." In: *Protein expression and purification* 21.1 (2001), pp. 224–234.

[205] Angelova, M. I. and Dimitrov, D. S. "Liposome Electro formation". In: *Faraday Discuss. Chem. Soc.* 81 (1986), pp. 303–311.

[206] Cooper, M. a., Hansson, a., Löfås, S., and Williams, D. H. "A vesicle capture sensor chip for kinetic analysis of interactions with membrane-bound receptors." In: *Analytical biochemistry* 277.2 (2000), pp. 196–205.

[207] Phair, R. D., Gorski, S. a., and Misteli, T. "Measurement of Dynamic Protein Binding to Chromatin In Vivo, Using Photobleaching Microscopy". In: *Methods in Enzymology* 375.2000 (2004), pp. 393–414.

[208] Yildiz, A. and Vale, R. D. "Total Internal Reflection Fluorescence Microscopy". In: *Cold Spring Harbor Protocols* 9 (2015), pp. 801–810.

[209] Whited, A. M. and Park, P. S.-H. "Atomic force microscopy: a multifaceted tool to study membrane proteins and their interactions with ligands." In: *Biochimica et biophysica acta* 1838.1 Pt A (2014), pp. 56–68.

[210] Wollert, T., Wunder, C., Lippincott-schwartz, J., and James, H. "Membrane Scission by the ESCRT-III Complex". In: *Nature* 458.7235 (2009), pp. 172–177.

[211] Lee, C. and Goldberg, J. "Structure of Coatomer Cage Proteins and the Relationship among COPI, COPII, and Clathrin Vesicle Coats". In: *Cell* 142.1 (2010), pp. 123–132.

[212] Rieter, E., Vinke, F., Bakula, D., Cebollero, E., Ungermann, C., Proikas-Cezanne, T., and Reggiori, F. "Atg18 function in autophagy is regulated by specific sites within its β-propeller." In: *Journal of cell science* 126.Pt 2 (2013), pp. 593–604.

[213] Williams, R. a. M., Mottram, J. C., and Coombs, G. H. "Distinct Roles in Autophagy and Importance in Infectivity of the Two ATG4 Cysteine Peptidases of Leishmania major." In: *The Journal of biological chemistry* 288.5 (2013), pp. 3678–90.

[214] Barth, H. and Thumm, M. "A genomic screen identifies AUT8 as a novel gene essential for autophagy in the yeast Saccharomyces cerevisiae." In: *Gene* 274.1-2 (2001), pp. 151–6.

[215] Ghaemmaghami, S., Huh, W.-K., Bower, K., Howson, R. W., Belle, A., Dephoure, N., O'Shea, E. K., and Weissman, J. S. "Global analysis of protein expression in yeast." In: *Nature* 425.6959 (2003), pp. 737–41.

[216] Müller, M., Schmidt, O., Angelova, M., Faserl, K., Weys, S., Kremser, L., Pfaffenwimmer, T., Dalik, T., Kraft, C., Trajanoski, Z., Lindner, H., and Teis, D. "The coordinated action of the MVB pathway and autophagy ensures cell survival during starvation". In: *eLife* 4 (2015), pp. 1–25.

[217] Hale, A. N., Ledbetter, D. J., Gawriluk, T. R., and Rucker, E. B. "Autophagy regulation and role in development". In: *Autophagy* 9.7 (2013), pp. 951–972.

[218] Obara, K. and Ohsumi, Y. "Dynamics and function of PtdIns(3)P in autophagy". In: *Autophagy* 4.7 (2008), pp. 952–954.

[219] Kihara, a., Noda, T., Ishihara, N., and Ohsumi, Y. "Two distinct Vps34 phosphatidylinositol 3-kinase complexes function in autophagy and carboxypeptidase Y sorting in Saccharomyces cerevisiae." In: *The Journal of cell biology* 152.3 (2001), pp. 519–30.

[220] Narayan, K. and Lemmon, M. a. "Determining selectivity of phosphoinositide-binding domains." In: *Methods* 39.2 (2006), pp. 122–33.

[221] Romanov, J., Walczak, M., Ibiricu, I., Schüchner, S., Ogris, E., Kraft, C., and Martens, S. "Mechanism and functions of membrane binding by the Atg5-Atg12/Atg16 complex during autophagosome formation." In: *The EMBO journal* (2012), pp. 1–14.

[222] Fath, S., Mancias, J. D., Bi, X., and Goldberg, J. "Structure and Organization of Coat Proteins in the COPII Cage". In: *Cell* 129.7 (2007), pp. 1325–1336.

[223] Jackson, L. P., Lewis, M., Kent, H. M., Edeling, M. a., Evans, P. R., Duden, R., and Owen, D. J. "Molecular Basis for Recognition of Dilysine Trafficking Motifs by COPI". In: *Developmental Cell* 23.6 (2012), pp. 1255–1262.

[224] Mizushima, N., Yamamoto, a., Hatano, M., Kobayashi, Y., Kabeya, Y., Suzuki, K., Tokuhisa, T., Ohsumi, Y., and Yoshimori, T. "Dissection of autophagosome formation using Apg5-deficient mouse embryonic stem cells." In: *The Journal of cell biology* 152.4 (2001), pp. 657–68.

[225] Sahu, R., Kaushik, S., Clement, C. C., Cannizzo, E. S., Scharf, B., Follenzi, A., Potolicchio, I., Nieves, E., Cuervo, A. M., and Santambrogio, L. "Microautophagy of cytosolic proteins by late endosomes." In: *Developmental cell* 20.1 (2011), pp. 131–9.

[226] Almada, P., Culley, S., and Henriques, R. "PALM and STORM: Into large fields and high-throughput microscopy with sCMOS detectors". In: *Methods* (2015).

[227] Reggiori, F., Wang, C. W., Stromhaug, P. E., Shintani, T., and Klionsky, D. J. "Vps51 is part of the yeast Vps fifty-three tethering complex essential for retrograde traffic from the early endosome and Cvt vesicle completion". In: *Journal of Biological Chemistry* 278.7 (2003), pp. 5009–5020.

[228] Cheng, J., Fujita, A., Yamamoto, H., Tatematsu, T., Kakuta, S., Obara, K., Ohsumi, Y., and Fujimoto, T. "Yeast and mammalian autophagosomes exhibit distinct phosphatidylinositol 3-phosphate asymmetries." In: *Nature communications* 5 (2014), p. 3207.

[229] Feng, W., Zhang, W., Wang, H., Ma, L., Miao, D., Liu, Z., Xue, Y., Deng, H., and Yu, L. "Analysis of phosphorylation sites on autophagy proteins". In: *Protein & Cell* 6.9 (2015), pp. 698–701.

[230] Hengesbach, M., Kim, N.-K., Feigon, J., and Stone, M. D. "Single-molecule FRET reveals the folding dynamics of the human telomerase RNA pseudoknot domain." In: *Angewandte Chemie (International ed. in English)* 51.24 (2012), pp. 5876–9.

[231] Nagy, P., Hegedűs, K., Pircs, K., Varga, Á., and Juhász, G. "Different effects of Atg2 and Atg18 mutations on Atg8a and Atg9 trafficking during starvation in Drosophila." In: *FEBS letters* 588.3 (2014), pp. 408–13.

[232] Pashkova, N., Gakhar, L., Winistorfer, S. C., Yu, L., Ramaswamy, S., and Piper, R. C. "WD40 Repeat Propellers Define a Ubiquitin-Binding Domain that Regulates Turnover of F Box Proteins". In: *Molecular Cell* 40.3 (2010), pp. 433–443.

[233] Lu, K., Psakhye, I., and Jentsch, S. "Autophagic Clearance of PolyQ Proteins Mediated by Ubiquitin-Atg8 Adaptors of the Conserved CUET Protein Family". In: *Cell* (2014), pp. 1–15.

Appendix

Table A.1: DLS measurements of Atg18

Radius (nm)	**M.W. (kDa)**	**Polydispersity**	**Fraction (%)**
3.52	44.2	0.0556	83
3.62	53.1	0.1900	85
3.78	59.5	0.1800	89
3.59	47.4	0.0855	83
4.39	129.0	0.3660	90
4.02	70.5	0.1620	100
3.51	45.3	0.1270	85
3.24	34.9	0.0952	94
3.26	35.2	0.0875	98
4.31	86.2	0.1501	94

Table A.2: Adjusted R^2 values of fits on Biacore data.

	Adj. R^2					
	PI(3)P		PI(3,5)P_2		PI(4,5)P_2	
	$Atg18^{wt}$	$Atg18^{FKKG}$	$Atg18^{wt}$	$Atg18^{FKKG}$	$Atg18^{wt}$	$Atg18^{FKKG}$
#1	0.944	0.978	0.989	0.995	0.993	0.999
#2	0.984	0.902	0.986	0.976	0.966	0.993
#3	0.899	0.985	0.995	0.990	0.991	0.998

Table A.3: Dissociation constants and R_{max} values obtained for Atg18 binding to LUVs with specific PIPs in Biacore measurements.

	PI(3)P				PI(3,5)P_2				PI(4,5)P_2			
	Atg18^{wt}		Atg18^{FKKG}		Atg18^{wt}		Atg18^{FKKG}		Atg18^{wt}		Atg18^{FKKG}	
	K_D (nM)	ΔK_D (nM)	K_D (nM)	ΔK_D (nM)	K_D (nM)	ΔK_D (nM)	K_D (nM)	ΔK_D (nM)	K_D (nM)	ΔK_D (nM)	K_D (nM)	ΔK^D (nM)
#1	170	30	360	60	26	2	80	20	190	50	180	20
#2	280	30	300	20	42	3	140	20	460	30	260	20
#3	430	40	450	20	100	20	230	20	600	70	430	20
mean ± stdev of means	300 ± 100		370 ± 60		60 ± 30		150 ± 60		400 ± 200		300 ± 100	
	R_{max} (RU)	ΔR_{max} (RU)	R_{max} (RU)	ΔR_{max} (RU)	R_{max} (RU)	ΔR_{max} (RU)	R_{max} (RU)	ΔR_{max} (RU)	R_{max} (RU)	ΔR_{max} (RU)	R_{max} (RU)	ΔR_{max} (RU)
#1	390	20	135	6	445	3	290	10	210	10	265	7
#2	360	10	89	2	432	5	266	7	199	4	211	5
#3	341	9	74	1	430	10	255	5	182	7	192	3
mean ± stdev of means	370 ± 20		100 ± 30		436 ± 6		270 ± 20		200 ± 10		220 ± 30	

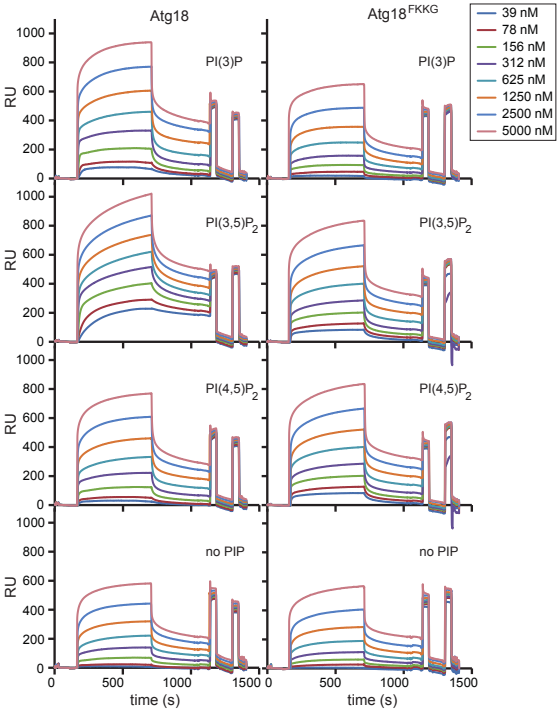

Figure A.1: Atg18 membrane binding to LUVs with different PIPs - raw data. Atg18 wildtype (left panel) and Atg18^{FKKG} (right panel) were probed for lipid binding specificity using Biacore. Each flow cell of an L1 chip was loaded with comparable amounts of distinct LUVs each containing 3 mol% of a specific PIP or no PIPs. Atg18 wildtype or Atg18^{FKKG} were injected to imobilized LUVs in a concentration series from 39 nM to 5 μM. Binding was observed for each type of LUVs, but PI(3)P and PI(3,5)P_2 provided additional binding places for Atg18 as can be seen by the increased signal. Binding of Atg18 to PI(3)P and PI(3,5)P_2 was dependent on its FRRG-motif.

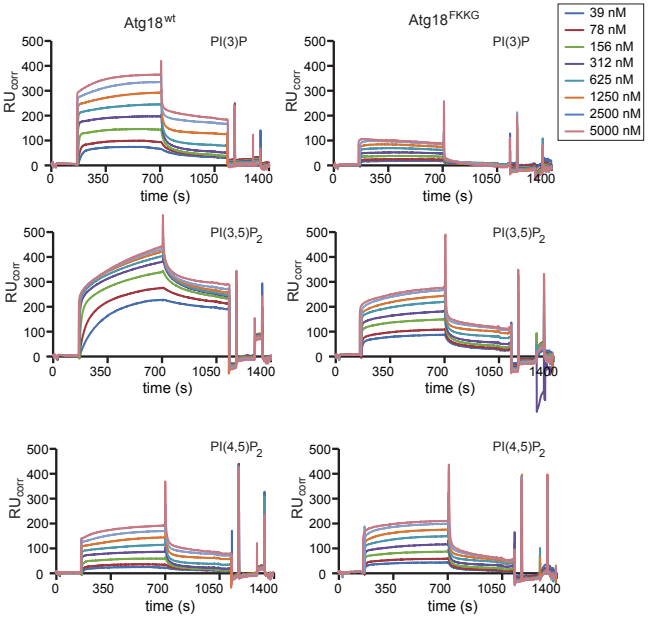

Figure A.2: Atg18 membrane binding to LUVs with different PIPs - corrected. Binding signals shown in Figure A.1 were corrected for binding by subtraction of signals obtained for LUVs without PIPs. A saturation of binding places is observed for increasing concentrations of Atg18. For PI(3)P and PI(3,5)P_2 containing LUVs binding of Atg18 depends partially on its FKKG-motif indicating a binding of Atg18 to these PIPs. For LUVs with PI(4,5)P_2 comparable amounts of Atg18^{wt} and Atg18^{FKKG} bind LUVs.

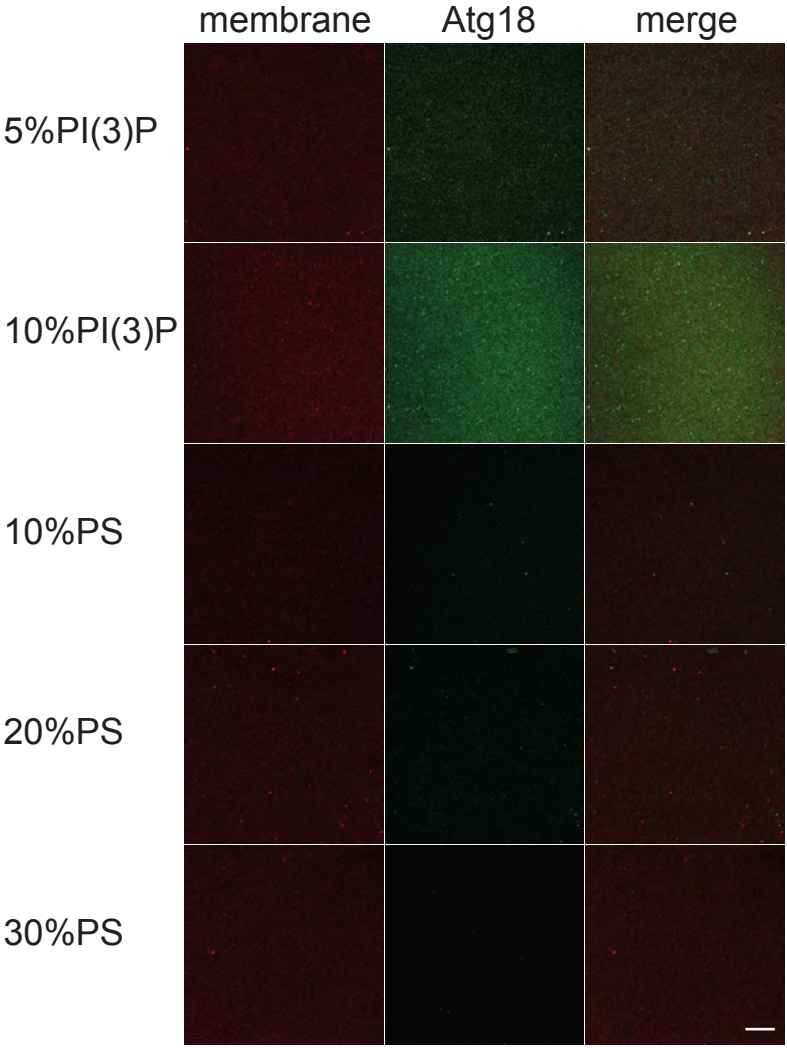

Figure A.3: Atg18 membrane binding specifictiy on SLBS. SLBs containing different PI(3)P concentrations or no PI(3)P but PS as indicated were prepared on plasma-cleanded glass. To test for charge-dependent binding $Atg18^{Alexa488}$ (0.5 μM) was incubated SLBs. Binding was examined by confocal fluorescence microscopy. Atg18 bound to membranes containing PI(3)P in a concentration-dependent manner. Charge replacement by PS did not result in binding. Atg18 binds specifically to PIPs. Scale bar = 10 μm

Table A.4: R^2 and recovery times of Atg8 in FRAP experiments

Atg18	**R^2**	**$\tau_{1/2}$ (s)**	**mean $\tau_{1/2}$ (s)**	**stdev of means $\tau_{1/2}$ (s)**
- Atg18	0.93	27 ± 4	90	70
	0.71	200 ± 500		
	0.98	60 ± 10		
	0.89	70 ± 30		
+ Atg18	0.89	19 ± 3	40	30
	0.99	18.4 ± 0.6		
	0.77	100 ± 100		
	0.99	29 ± 2		
	0.96	26 ± 3		
	0.99	48 ± 3		

Table A.5: R^2 and recovery times of membrane in FRAP experiments

Atg18	**R^2**	**$\tau_{1/2}$ (s)**	**mean $\tau_{1/2}$ (s)**	**stdev of means $\tau_{1/2}$ (s)**
- Atg18	0.97	13.0 ± 0.8	8	4
	0.98	6.5 ± 0.3		
	0.98	3.8 ± 0.1		
	0.77	13 ± 2.0		
+ Atg18	0.82	4.0 ± 0.6	4	1
	0.99	6.7 ± 0.2		
	0.98	4.5 ± 0.2		
	0.94	3.4 ± 0.3		
	0.98	3.8 ± 0.2		
	0.98	3.2 ± 0.1		

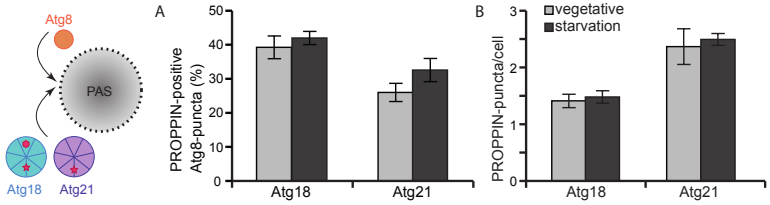

Figure A.4: PROPPINs localize to the PAS and form constant numbers of puncta. As visualized in the cartoon, localization and colocalization of PROPPINs (Atg18 = blue, Atg21 = purple circle) with Atg8 (orange circle) were assessed by confocal fluorescence microscopy under vegetative and starvation conditions. PROPPIN-GFP fusions were expressed from their endogenous locus and 2xmCherry-Atg8 was expressed from a CEN-plasmid under control of a Met25-promoter. (A) PROPPIN-GFP and Atg8-puncta (Figure 3.11 A) and their colocalization were quantified. Both PROPPINs localize to the PAS with similar frequency and the proportion of PROPPIN-positive Atg8 puncta is independent of nutrition conditions. (B) Numbers of Atg18- and Atg21-GFP did not change upon starvation and exceeded numbers of Atg8-puncta per cell (Figure 3.11 B). Scale bar = 5 μm, mean ± SD of N = 3 for all quantifications.

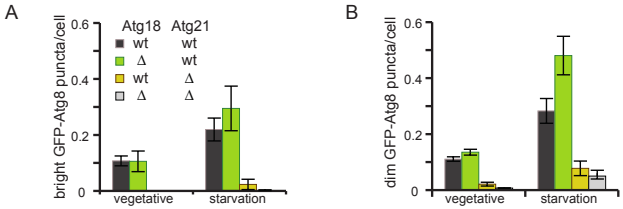

Figure A.5: Atg8-puncta formation *in vivo*. Cells (wt, atg18Δ, atg21Δ and atg18Δatg21Δ) expressing GFP-Atg8 from its endogenous promoter were imaged by confocal fluorescence microscopy in mid-log phase and after 2 h starvation. GFP-Atg8-puncta were quantified for each strain and condition. Since, based on their fluorescence intensity, two populations of GFP-Atg8 puncta were observed they were divided in bright (A) and dim (B) puncta. Bars represent mean ± SD of N = 3 for all quantifications.

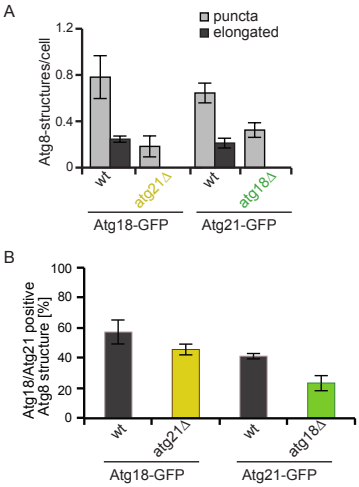

Figure A.6: Quantifications of PROPPIN-localization at giant ApeI. (A) Atg8-structures (crescents and puncta) as observed in Figure 3.15 were quantified. The frequency of Atg8-crescents and puncta is comparable in yeast strains expressing Atg18- or Atg21-GFP. Deletion of either *ATG18* or *ATG21* both prevent formation of elongated Atg8 structures and diminished the number of Atg8-puncta. (B) Colocalization of PROPPIN-GFP fusions with Atg8-puncta were quantified in wildtype cells and in strains deleted for the respective PROPPIN-counterpart. While *ATG21* deletion has no significant effect on Atg18-Atg8 colocalization, the colocalization of Atg21 with Atg8-puncta is reduced by atg18 deletion. mean ± SD of N = 3 for all quantifications.

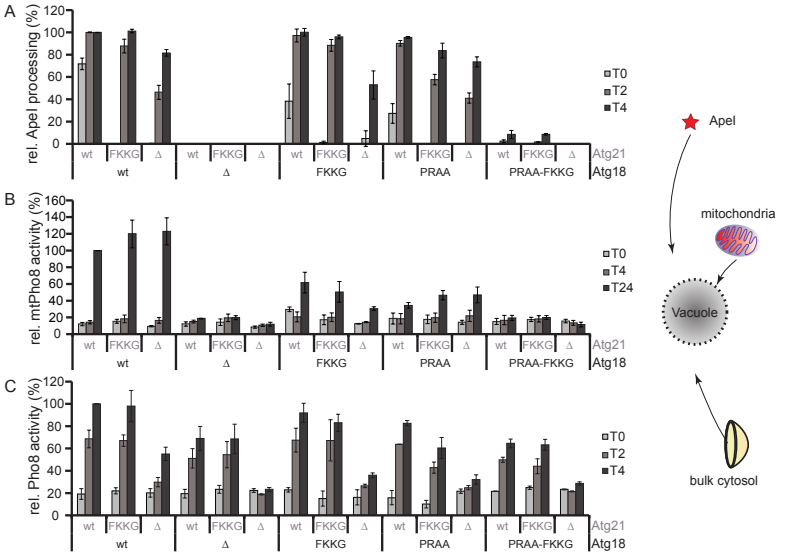

Figure A.7: Comprehensive analysis of PROPPIN-mutants in autophagic processes. *atg18*Δ*atg21*Δ cells were complemented with all possible combinations of plasmids encoding Atg18- and Atg21-variants. FKKG corresponds to ΔPI3P and PRAA to ΔAtg2 in Figure 3.16 C,D). PRAA-FKKG, consequently, is the Atg18 double mutant binding neither PI(3)P nor Atg2. Three different autophagic activities were tested as depicted in the scheme. Cells were grown to mid-log phase (T0) and starved for 2 h (T2), 4 h (T4) or 24 h (T24). (A) ApeI activity was examined by Western Blot and quantification of precursor (pr)ApeI and mature(m)ApeI bands as in Figure 3.16 and in Materials and Methods Chapter 2.11.2. Mitophagy (B) and non-selective autophagy (C) were assessed by the Pho8Δ60 assay as described in Materials and Methods Chapter 2.11.3 using a Pho8Δ60 variant targeted to mitochondria (B) or the cytoplasm (C). mean ± SD of N = 3 independent experiments for all quantifications.

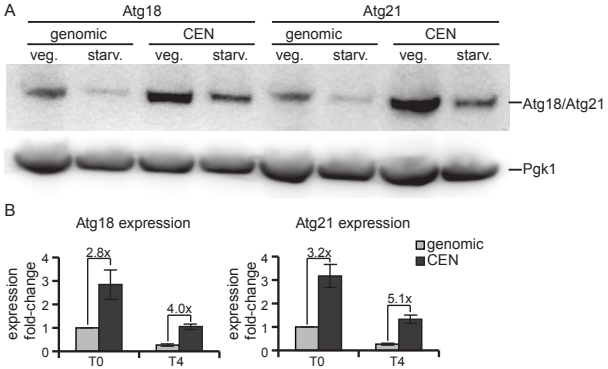

Figure A.8: PROPPIN expression levels. (A) Levels of PROPPINs expressed from their endogenous locus or from a CEN-plasmid under control of a PmaI-promoter were examined by Western Blot. Cells expressing PROPPIN-GFP fusions were grown to mid-log phase and starved for 4 h. Samples were taken as described in Materials and Methods Chapter 2.11.2. After separation on SDS-PAGE gels and transfer to a PVDF membrane, blots were probed by anti-GFP. Membranes were stripped and reprobed with α-Pgk1 as loading control. (B) Band intensities of PROPPIN-GFP fusions and Pgk1 were quantified to obtain a measure for cellular PROPPIN levels. For both PROPPINs levels are decreased under starvation conditions and expression from CEN-plasmids results in 3- to 5-fold enhancement of protein levels. mean $\pm$ SD of N = 3 independent experiments.

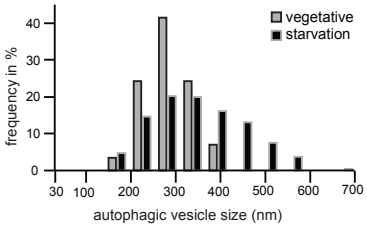

Figure A.9: Change of autophagic vesicle size upon starvation. Cells with a *pep4*Δ background were grown to mid-log phase and starved for 4 h. Cells were harvested and stained as described in Materials and Methods Chapter 2.11.5. The size of autophagic vesicles observed in vacuoles of growing and starving wt cells was quantified and depicted in a histogram. (N = 29 vegetative, N >300 starvation). Vesicles become larger upon starvation.

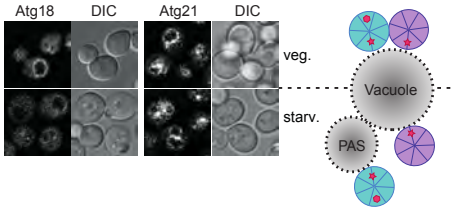

Figure A.10: Atg18 relocalizes from the vacuole to the PAS upon starvation. Yeast cells expressing PROPPIN-GFP fusions were grown to mid-log phase and starved for 2 h. Localization was observed by confocal fluorescence microscopy. While Atg18 relocalizes from the vacuolar rim to the PAS, Atg21 localization is almost unperturbed.

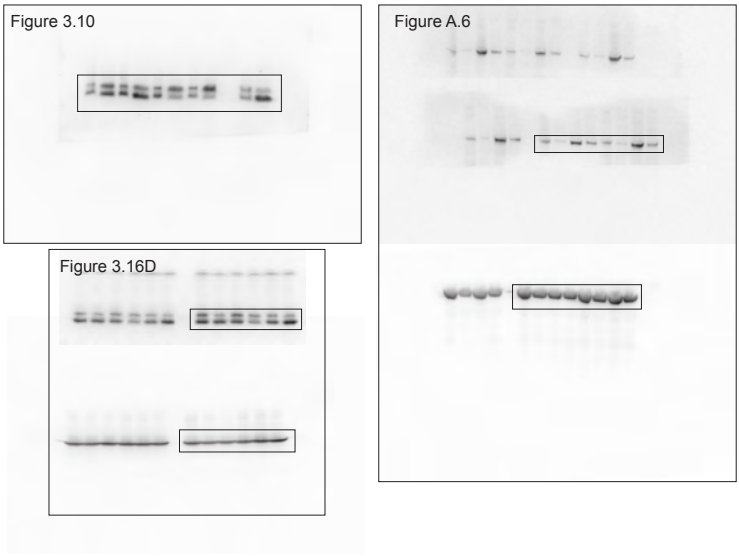

Figure A.11: Full blots. Full blots of those shown throughout the thesis are depicted here.

Acknowledgements

Besonders möchte ich Dr. Thomas Wollert danken für die Möglichkeit meine Dissertation in seiner Arbeitsgruppe durchzuführen. Die Bereitstellung eines interessanten Themas, seine intensive Betreuung und zahlreiche, ausgedehnte Diskussionen haben wesentlich zum Gelingen dieser Arbeit beigetragen. Zudem möchte ich mich für die Durchsicht und die hilfreichen Kommentare zu dieser Dissertation bedanken.

PD Dr. Günther Woehlke danke ich für seine Bereitschaft diese Dissertation als Vertreter der Technischen Universität München zu betreuen und in diesem Zusammenhang als Erstgutachter der Arbeit zu agieren. Zudem möchte ich mich für die Diskussionen im Rahmen des Thesis Advisory Committee sowie für sein großes Engagement bei der Zusammenstellung des Prüfungskommitees danken.

Prof. Dr. Friedrich C. Simmel danke ich für die Übernahme des Zweitgutachtens.

Prof. Dr. Martin Zacharias danke ich für die Bereitschaft den Prüfungsvorsitz zu übernehmen.

Vielen Dank an Dr. Stephan Gruber für seine Teilnahme am Thesis Advisory Committee und seine Diskussionsbeiträge in diesem Rahmen.

Ein großes Dankeschön an Viola Beier für ihre hervorragende Hilfe bei verschiedenen *in vivo* Experimenten, Klonierungen und dergleichen. Vielen Dank auch für die lustige Zeit im Labor.

Zudem möchte ich Anna Kaufmann für die Vorbereitung und Aufnahme der Elektronenmikroskopie Bilder Danken.
Vielen Dank an allen Mitgliedern der AG Wollert für die gute Zusammenarbeit sowie eine angenehme und konstruktive Arbeitsatmosphäre.

Jonas Müksch möchte ich für seine Hilfe und seinen großen Einsatz bei unseren Einzelmolekül-TIRF Messungen danken.

Zudem danke ich Dr. Henri Franquelim für seine Unterstützung und während der AFM Experimente.

Vielen Dank an das gesamte Team der Core Facility, vor allem der Imaging Facility, Dr. Martin Spitaler, Ralf Zenke und Markus Hammerl, die mir immer mit Rat und

Tat zur Mikroskopie zur Seite standen. Elisabeth Weyher-Stingl danke ich für ihre Durchführung und Erklärungen zu Masse Analysen. Vielen Dank an Dr. Stephan Uebel für seine Ratschläge zur Biacore Analyse.

Vielen Dank an Biostruct X für die finanzielle Unterstützung eines ESPRIT screens. Philippe Mas danke ich für seine Betreuung und eine großartige Zeit während einem zweiwöchigen Forschungsaufenthalt am EMBL Grenoble.

Außerdem danke ich meinen "Office-Buddies" Katharina Austen und Anna Kaufmann für lustige, entspannende und aufbauende Gespräche, die wesentlich zur angenehmen Schreib-Atmosphäre beigetragen haben.

Ganz herzlichen Dank an meine Eltern und meine Schwester für ihre kontinuierliche, unermüdliche Unterstützung während meiner gesamten akademischen Ausbildung und besonders während der Doktorarbeit. Ohne Euch wäre das nicht möglich gewesen.

Meiner Freundin danke ich ganz besonders für ihren wunderbaren Optimismus und ihre großartige Unterstützung, die mich immer wieder motiviert und diese Arbeit ermöglicht haben.